Nonlinear Phenomena and Chaos in Periodically Driven Classical Systems

by

Slaven Peleš

A dissertation submitted in partial fulfillment
of the requirements for the degree of

Doctor of Philosophy

University of Manitoba

July 2001

THE UNIVERSITY OF MANITOBA

FACULTY OF GRADUATE STUDIES

*****

COPYRIGHT PERMISSION

NONLINEAR PHENOMENA AND CHAOS IN PERIODICALLY DRIVEN CLASSICAL SYSTEMS

BY

SLAVEN PELEŠ

A Thesis/Practicum submitted to the Faculty of Graduate Studies of The University of Manitoba in partial fulfillment of the requirement of the degree

of

DOCTOR OF PHILOSOPHY

TABLE OF CONTENTS

List of Figures iv

List of Tables ix

Chapter 1: Introduction 1

Chapter 2: The Logistic Map 4

2.1 Prototype Model 4

2.2 Route to Chaos 14

2.3 Lyapunov Exponents 19

2.4 Kolmogorov Entropy 23

2.5 Symbolic Dynamics of a One-Dimensional Map 25

Chapter 3: The Pendulum 34

3.1 Dynamical Flows 34

3.2 Strange Attractors 40

3.3 Basins of Attraction 47

3.4 Bifurcation Graphs 50

3.5 Power Spectra 52

3.6 Lyapunov Exponents 54

3.7 Parametric Resonance 58

3.7.1 Floquet Index 59

3.8 Mathieu Equation 60

3.9 Parametric Resonance Model 64
3.10 Conclusion 66

Chapter 4: The Two Gears and the Rod **67**
4.1 The Equation of Motion 67
4.2 Bifurcation Diagrams 70
4.3 Lyapunov Exponents, Dimensions and Conjectures 77
4.4 Coexisting Attractors and Crisis 81
4.5 Symbolic Dynamics 87
4.6 Partitioning of the Poincaré section 89
4.7 Ordering rules and admissibility conditions 97
4.7.1 Pruning Rules 99
4.8 Unstable periodic orbit sequences 100
4.9 Conclusions 108

Chapter 5: Control Theory **111**
5.1 Lyapunov's Direct Method 111
5.1.1 Discontinuous problems 112
5.2 Application to the Double Pendulum 113
5.3 Conclusion 120

Chapter 6: Conclusion **122**
6.1 Double Pendulum Control Revisited 123
6.2 Future Prospects 127

Bibliography **128**

Appendix A: Source Code for Numerical Experiments **138**
A.1 Note on Numerical Methods 138

A.2 Program for Creating Bifurcation Graphs 138
A.3 Program for Calculating Power Spectrum 141
A.4 Program for Calculating Lyapunov Spectrum 145
A.5 Program for Finding Basins of Attraction 150
A.6 Program for Finding Phase Locked Modes 153
A.7 Program for Calculating Capacity Dimension 156
A.8 Program for Calculating Information Dimension 159
A.9 Program for Calculating Correlation Dimension 162

LIST OF FIGURES

2.1 Cobweb diagram for the logistic map at $\mu = 0.8$. 5

2.2 At $\mu = 2.8$ intersection of diagonal and mapping function is a stable fixed point. 6

2.3 At $\mu = 3.1$ the attractor for the logistic map is a period-2 orbit. . . . 7

2.4 At $\mu = 3.48$ the attractor for the logistic map is a period-4 orbit. . . . 8

2.5 Chaotic logistic map for $\mu = 3.6$ (left) and $\mu = 3.95$ (right). 9

2.6 Bifurcation diagram for the logistic map 10

2.7 Period doubling route to chaos for logistic map 11

2.8 Period-3 window enlarged. 12

2.9 Creation of a period-3 orbit. Mapping function f^3 is plotted for $\mu = 3.825$ (left) and $\mu = 3.841$ (right). 13

2.10 Distances between neighboring bifurcation points 15

2.11 Further magnification of the part of bifurcation diagram 17

2.12 Generating a Cantor set. 18

2.13 Lyapunov exponent for the logistic map 20

2.14 Mapping function for the logistic map at $\mu = 4$. Below are denoted segments of initial conditions which generate itineraries starting with 1-, 2- and 3-letter words. 29

3.1 Trajectory of a damped pendulum in phase space. (a) $\lambda = 0.25$, (b) $\lambda = 0.02$ 38

3.2 Basins of attraction for a damped pendulum. 39

3.3 Trajectory of a driven damped pendulum in phase space. After the initial transient trajectory settles down at the attractor 42
3.4 Attractor for the driven pendulum: (a) limit cycle, (b) after period doubling, (c) after period quadrupling, (d) chaotic attractor. 43
3.5 Projections of pendulum's attractors (Fig. 3.4) in $(\theta, \dot{\theta})$ plane respectively. 43
3.6 Poincaré sections at $\phi = 0$ of pendulum's attractors (Fig. 3.4) respectively. Points representing limit cycles are enlarged for clarity. 44
3.7 Top sheet of a chaotic attractor in Figure (3.6d) enlarged. 45
3.8 Evolution of basins of attraction with change of system's parameter. Two coexisting limit cycles at Q=1.48 (top left). Points representing limit cycles are enlarged for clarity. Two chaotic attractors at the verge of crisis at q=1.555 (top right). Two chaotic attractors conjoin after crisis at Q=1.56 (bottom). 49
3.9 Period doubling cascade of the driven pendulum. 51
3.10 Period doubling cascade seen through power spectra. (a) $Q = 1.48$, (b) $Q = 1.52$, (c) $Q = 1.544$, (d) $Q = 1.56$. 53
3.11 Power spectra of chaotic and quasiperiodic motion. 54
3.12 Phase space trajectory for the Mathieu equation. (a) $A = 2.5$ and $q = 1$, (b) $A = 1$ and $q = 1$. 61
3.13 Exponential growth of the solution for the Mathieu equation. The Floquet exponent is estimated from the slope to be $\mu = 0.453 \pm 0.003$ 62
3.14 Phase space trajectory for the Mathieu equation with appropriate winding condition. The periodic solution (a), $A = 2.5$ and $q = 1$, remains unchanged, while the unstable solution (b), $A = 1$ and $q = 1$, becomes chaotic. 63

3.15 Plot of $\log|\chi|^2$ vs. t shows how the Floquet exponent changes during the time. The average Floquet exponent is estimated from the graph to be $\mu_\chi = 0.0973 \pm 0.0007$. 65
3.16 Phase space projection of the chaotic pseudo-attractor of Eq. (3.25). . 65

4.1 Two gears and the rod 68
4.2 Bifurcation diagrams show that periodic motion is dominant over a range of Q for the choice of parameters (a) $a = 0.7$, $r = 0.6$, (b) $a = 0.7$, $r = 0.9$, (c) $a = 0.9$, $r = 0.6$, (d) $a = 0.9$, $r = 0.9$. 71
4.3 Bifurcation diagrams. Broad chaotic regions are found for (a) $a = 0.9$, $r = 1$,(b) $a = 1$, $r = 0.9$, (c) $a = 1$, $r = 1$, (d) $a = 1.2$, $r = 0.9$. 72
4.4 Bifurcation diagrams for the choice of parameters (a) $a = 1.1$, $r = 1.2$, (b) $a = 1.4$, $r = 1.2$, (c) $a = 1.1$, $r = 1.4$, (d) $a = 1.4$, $r = 1.4$. quasiperiodic behavior is dominant over the range of Q. 73
4.5 Power spectra for different values of quality factor Q: (a) $Q = 0.2$ and (b) $Q = 0.4$, motion is quasiperiodic, (c) $Q = 0.8$, motion is periodic with period one, and (d) $Q = 1.08$, motion is chaotic. $\Theta(\omega)$ is the Fourier transform of $\dot{\theta}(t)$. The frequency on the x–axis is expressed in terms of the virtual drive frequency a. 75
4.6 (a) Enlarged chaotic region of bifurcation diagram 4.3a. (b)Period doubling route to chaos, enlarged from figure a. $a = 0.9$, $r = 1.0$ . . . 76
4.7 (a) Bifurcation graph showing broad chaotic region over segment of Q. $a = 1.2$, $r = 0.9$. (b) Corresponding change of the largest Lyapunov exponent. 77

4.8 (a) Poincaré section of the quasiperiodic attractor is a smooth line. $a = 1.2$, $r = 0.9$, $Q = 0.5$. (b) Poincaré section of the chaotic attractor reveals a kneading sequence. $Q = 1.8$. (c) Higher dimensional chaotic attractor. $Q = 6.5$. 79
4.9 (a) Bifurcation diagram indicating coexisting attractors. Dashed line shows unstable limit cycle. (b) Corresponding plot of average angular velocity. 82
4.10 Poincaré section of the chaotic attractor at the verge of crisis, shown within its basin of attraction. White dots represent a stable, and black dots an unstable, limit cycle. $Q = 1.1$. 83
4.11 (a) Two-dimensional projection of a chaotic attractor at $Q = 1.1$. (b) Two-dimensional projection of the limit cycle at $Q = 1.2$ along with its transient. Both simulations were done for 200 time units. 84
4.12 Bifurcation diagram shows creation of coexisting attractors. 85
4.13 Three coexisting attractors. Period-three limit cycle (black points) and period-one limit cycle (white point) are enlarged for clarity. $Q = 3.515$. 86
4.14 Basin of attraction for $Q = 5.3$. 87
4.15 Bifurcation graph taken against parameter Q with parameter a varying as $a = 0.8 + 0.3Q$. 88
4.16 Attractors shown in the $x - y$, $x_n - x_{n+1}$, and $\mu - \nu$ planes at $Q = 0.57, 0.76, 1.2577, 1.68$, and 2.0 from top to bottom for $r = 1.088$, and $a = 0.8 + 0.3Q$. 90
4.17 Attractor (dots) and forward foliations (dash curves) for $Q = 0.57$. . . 91
4.18 The Poincaré map (dots) and forward foliations (dash curves) at $Q = 0.76$. The primary partition lines •B, •C, and the pre-image •A of •B divide the attractor into three parts labeled by the letters L, R and N. 93

4.19 The $x_{n+1} - x_n$ first return map at $Q = 0.76$. 94
4.20 The chaotic attractor (dots), forward foliations (dashed lines), and partition lines •A, •B, and •C at $Q = 1.2577$. 95
4.21 The $x_{n+1} - x_n$ first return map constructed from Fig. 4.20. 96
4.22 The symbolic plane at $Q = 0.76$. 10000 points of real orbits generated from the Poincaré map are also shown together with the FFZ in which no point falls. 101
4.23 The symbolic plane at $Q = 1.2577$. Together with the FFZ, 10000 points representing real orbits are drawn. None of them falls inside the FFZ. 102
4.24 A blow-up of the symbolic plane Fig. 4.23 in the intervals $\alpha = [0.8794, 0.87965]$ and $\beta = [0, 0.65]$. 103

5.1 An inverted double pendulum. Base point moves with acceleration $f(t)$ horizontally and $g(t)$ vertically. 114
5.2 Leading Lyapunov exponent plotted against control parameters α_1 and α_2. 117
5.3 Position of lower link (left), and control torque exerted upon it (right) for discontinuous and smooth controller, respectively. 118
5.4 Position of upper link (left), and control torque exerted upon it (right) for discontinuous and smooth controller, respectively. 118

6.1 Leading Lyapunov exponent plotted against control parameters k_{p1} and α_{p2}. 124
6.2 Phase plane projections for lower and upper link respectively at $k_{p1} =$ 900 $k_{p1} = 260$, (a) and (b); $k_{p1} = 1050$ $k_{p1} = 270$, (c) and (d); $k_{p1} =$ 3000 $k_{p1} = 800$, (e) and (f). 126

LIST OF TABLES

4.1 Various dimensions of the attractors. 81

4.2 Allowed unstable periods up to 8 for $Q = 0.76$. Only non–repeating strings of the sequences are given. P denotes the period and W the rotation number. 107

4.3 Allowed unstable periods up to 7 for $Q = 1.2577$ in the 1D case; those with an asterisk are forbidden by 2D tangency T_5. 109

4.4 Table 4.3 cont'd. 110

ACKNOWLEDGMENTS

I want to thank my advisor, Dr. Randy Kobes, for his support and guidance, and my committee members Dr. John Dixon, Dr. Gabor Kunstatter, Dr. Tom Osborn and Dr. James Peters. I also want to thank our collaborator Dr. Jun-Xian Liu of University of Toronto, who introduced us to symbolic dynamics techniques, as well as our collaborators from the Department of Mechanical and Industrial Engineering Pooya Sekhavat, Dr. Nariman Sepehri and Dr. Christine Wu. Finally I want to thank my wife Amra and my son Ivor for their love and support. Without their help and understanding this work would not be possible.

University of Manitoba

Abstract

Nonlinear Phenomena and Chaos in Periodically Driven Classical Systems

by Slaven Peleš

Chairperson of Supervisory Committee: Dr. Randal Kobes

Department of Physics and Astronomy

We study in this thesis the behavior of a periodically driven nonlinear mechanical system. Bifurcation diagrams are found which locate regions of quasiperiodic, periodic and chaotic behavior within the parameter space of the system. We also conduct a symbolic analysis of the model, which demonstrates that the symbolic dynamics of two-dimensional maps can be applied effectively to the study of ordinary differential equations in order to gain global knowledge about them. We also study some aspects of nonlinear system control. We show how one can utilize some of the methods developed in recent years for the study of nonlinear equations of motion to improve some aspects of traditional control design. We demonstrate these ideas for the case of an inverted double pendulum, which is a commonly used model in robotics, and compare the results to those found with traditional methods.

Chapter 1

INTRODUCTION

Although most phenomena occurring in the physical world are nonlinear in their nature, contemporary science still has very limited success in providing a mathematical description of them. Physical processes are usually described by differential equations. Except for some special cases, there are no exact analytical methods for obtaining general solutions of nonlinear differential equations. Analytical solutions for nonlinear problems are usually obtained using perturbation methods, i.e. in the way that nonlinear terms in the equation are treated as a perturbation to the solution of an otherwise linear equation. This approach is valid only if the linear part of the equation is dominant, which may not always be the case. Also, some purely nonlinear phenomena may be lost in a perturbative model. The other way of solving nonlinear problems are numerical methods. In these methods differential equations are reduced to a discrete map such that iterations of the map stay close enough to the trajectory of the solution. Numerical methods can be successfully used for solving a variety of nonlinear problems, however they usually require a lot of time consuming calculations before they give convergent results.

Rapid development of information technologies over the last 20 years reduced computation time for numerical methods significantly. More sophisticated and more accurate techniques have been implemented, and, as a result, many new features of nonlinear systems were discovered.

One of the most interesting nonlinear phenomena is deterministic chaos. It man-

ifests itself as a high sensitivity to a change in initial conditions. For chaotic systems arbitrary small changes in initial conditions will result in a large difference in the solution after some finite amount of time, thus making any long term prediction about a system's behavior impossible. This is popularly called a butterfly effect – a flip of butterfly's wings at one place may cause a hurricane at the other side of the Globe. The fact that the solution of the equation of motion of a deterministic system may still not allow long term prediction of its future behavior came as a bit of a surprise. The concept of a single orbit solution, which suited linear systems very well, became insufficient to describe behavior of nonlinear ones. Instead, the distribution of orbits and invariant limit sets in a system's phase space has to be studied.

In our research we studied periodically driven nonlinear systems, and we analyzed their chaotic behavior. In Chapter 2 we study the logistic map, which is a simple one-dimensional model that exhibits chaos. We use it to introduce some basic concepts of chaos and nonlinear dynamics, and to define terminology we are to use throughout this thesis.

In Chapter 3 we discuss chaos in dynamical flows using the example of a simple pendulum. We also elaborate the difference between chaotic and simply divergent systems. Both are characterized by exponential divergence of two nearby trajectories in phase space; however chaotic systems are bounded.

The focus of our research was a propulsion device [49, 73], which consists of two gears and a rod (Chapter 4). We detect chaotic behavior in the system and locate regions in the parameter space where the system is chaotic, periodic and quasiperiodic. Since the system we study is dissipative, most of the information about its dynamics is obtained by studying its attractor. We analyze the geometry of the system's attractor for different values of the system's parameters and we calculate the attractor's dimensions. We also observe creation of coexisting attractors and crisis phenomena in our system. The most interesting feature we obtained was coexistence of the chaotic attractor and a limit cycle in the phase space, meaning that the system

would exhibit chaotic or periodic behavior, respectively, depending on the choice of initial conditions.

We extend our study by developing a symbolic dynamic analysis for our model. Such an analysis provides almost the only rigorous approach to study chaotic motion of dynamical systems, as it enables one to find and count all ingredients of chaos – unstable periodic orbits embedded in a chaotic attractor. Up until recently chaos has been treated in a similar fashion as a random noise, and it was considered as an undesirable physical behavior. With symbolic dynamics we can study chaotic behavior in detail and use some of its properties. Applying this concept we may, for example, reformulate some aspects of statistical mechanics without any probabilistic assumptions, and calculate thermodynamic averages with high accuracy. So far, symbolic dynamics analysis techniques have been developed for 1- and 2-dimensional maps only, and so we reduced our system to a 2-dimensional map by suitable choice of the Poincaré section.

We have also looked into some problems related to automatic control of robotic systems. In particular, in this thesis we discuss the problem of stabilizing an inverted double pendulum with perturbed base point around its upright position. This model has been studied extensively in robotics engineering literature as it is used to model a human walk. We showed that some of the above mentioned techniques may be used for optimization of controllers designed for this model using Lyapunov's Direct Method, which is the standard method in control theory. In chapter 5 we show the results which we obtained working with our collaborators from the Department of Mechanical and Industrial Engineering at the University of Manitoba, when we used calculation of the Lyapunov exponents to fine-tune control parameters of a double pendulum system [87].

In the Conclusions we discuss prospects for some more sophisticated applications of chaotic dynamics in control theory.

Chapter 2

THE LOGISTIC MAP

2.1 Prototype Model

The logistic map is maybe the simplest model that exhibits chaotic behavior. Therefore, it is very convenient for illustrating some general chaotic features, and is often called a prototype model of chaos. We will use it to define certain terms and to describe some tools that are used in chaotic dynamics.

The logistic map was first used in biology for estimation of a population growth in a closed environment. According to this model, the number of species, p_{n+1}, in year $n+1$ is proportional to their number, p_n, in the year before n and to the amount of free space. Specifically, this is defined as the difference between maximum number of species that can coexist in the closed environment, P, and their current number p_n. If we introduce some constant of proportionality m, that depends on, say, the fertility of the population we can write it altogether as a logistic equation:

$$p_{n+1} = mp_n(P - p_n) \tag{2.1}$$

For our calculation it is more convenient to use another form of the equation where the maximum number of species is normalized to unity:

$$x_{n+1} = \mu x_n(1 - x_n) \tag{2.2}$$

Here $x_n = p_n/P$, and $\mu = mP$. The logistic equation (2.2) is defined for $x \in [0, 1]$, as the number of species is expressed as a fraction of their maximal number in given environment.

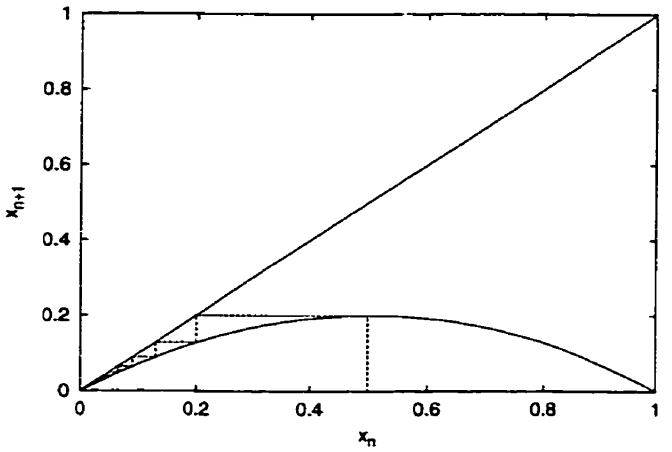

Figure 2.1: Cobweb diagram for the logistic map at $\mu = 0.8$.

Assuming that the logistic map is a good enough approximation for certain biological systems, e.g. the number of fish in a lake, we would believe that with knowing the initial number of fish x_0, and parameter μ, we could estimate the number of fish after an arbitrarily long period of time. We will show that this is not always the case. Although it is described by a simple mathematical relation, the logistic map exhibits fairly complex behavior, and for certain values of μ long-term prediction is impossible.

For $\mu \leq 1$, x_n would tend to zero after a sufficient number of iterations (usually, it is just a few of them) for any initial condition $x_0 \in [0, 1]$. We say that the segment $[0, 1]$ is mapped to zero. The solution to the logistic map can be very vividly described graphically, using the cobweb plot (Fig. 2.1). Once the logistic map is found at a point $x_n = 0$ it remains there for all subsequent iterations. This is something that we would expect from the real biological system – there is no more natural growth of a population after its extinction. We say the point zero is a fixed point of the logistic map. More generally, for any one-dimensional map

$$x_{n+1} = f(x_n) \tag{2.3}$$

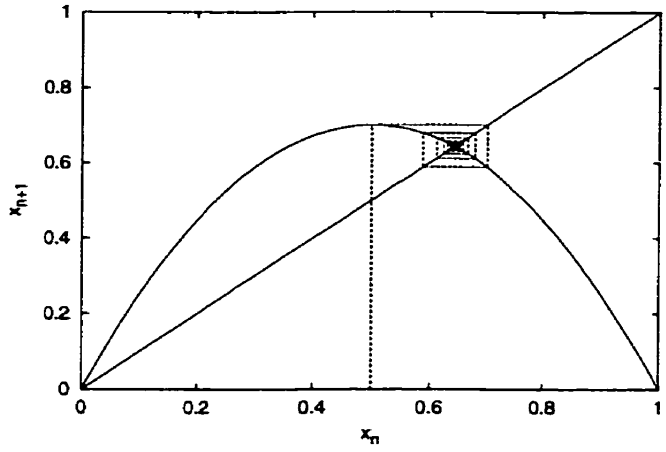

Figure 2.2: At $\mu = 2.8$ intersection of diagonal and mapping function is a stable fixed point.

every point x_e for which $x_e = f(x_e)$ is called a fixed or equilibrium point. For one-dimensional systems there are two types of equilibrium points: stable equilibrium points, or sinks, which attract all orbits starting in their vicinity; and unstable equilibrium points or sources, which repel all orbits in their vicinity. In our case zero is a point of stable equilibrium. Iterations starting from any initial condition $x_0 \in [0, 1]$ will eventually end up in $x_n = 0$. We say that the point zero is the attractor and segment $[0, 1]$ is its basin of attraction. We denote the attractor by $x_a = 0$. Generally, stability of a fixed point for a one-dimensional map is determined from the derivative of the mapping function $f(x)$ [2]. If x_e is a fixed point and $|f'(x_e)| < 1$, then x_e is a stable equilibrium point or sink. In cases when $|f'(x_e)| = 0$, the equilibrium point is called superstable. If $|f'(x_e)| > 1$, then x_e is an unstable equilibrium point or source. Finally, in a special case when $|f'(x_e)| = 1$, the equilibrium point is said to be marginally stable.

As we increase the parameter μ from 1 up to 3 we obtain a similar situation. The attractor of the map is still a fixed-point, only it is shifted from zero to $x_a = 1 - 1/\mu$ (Fig. 2.2). The basin of attraction is the interval $(0, 1)$ rather than the segment

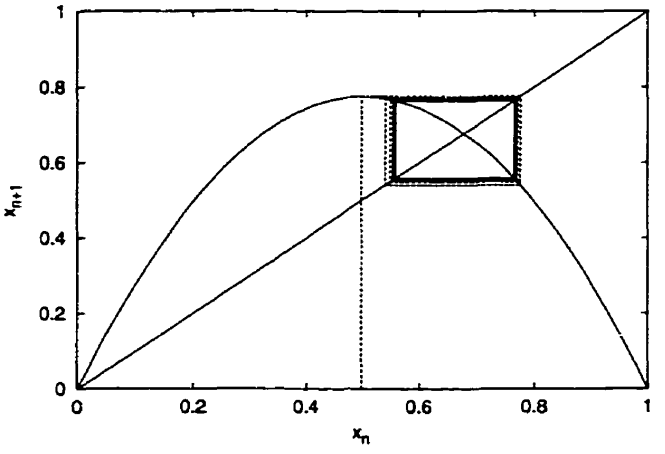

Figure 2.3: At $\mu = 3.1$ the attractor for the logistic map is a period-2 orbit.

$[0, 1]$. The point $x = 0$ is still a fixed point itself, however it is now unstable, since $|f'(0)| = \mu$. The point $x = 1$ is mapped to zero by a single iteration, and it is called a pre-image of the unstable fixed point $x = 0$.

So far, behavior of the logistic map was quite predictable. It was sufficient to know only the parameter μ in order to predict value of x_n, for n large enough. Since $f'(1-1/\mu) = 2-\mu$, the fixed point $x_e = 1-1/\mu$ becomes unstable as μ increases over 3. Iterates x_n do not tend to a single value any more, but rather alternate between two values x_{a1} and x_{a2} when n is large enough (Fig.2.3).

The attractor now consists of these two points, and we say that attractor is stable period-2 orbit. This means that certain values will occur every second instead of every single iteration. This is called period doubling. The previous attractor loses its stability and becomes a repeller, which we will denote as x_r. The numerical value of the repeller point is always in between those of attraction points $x_{a1} < x_r < x_{a2}$. Therefore, period doubling is a consequence of an increase of a system's parameter, resulting in creation of a period-2 orbit attractor and an unstable fixed-point. This phenomenon is also called a pitchfork bifurcation.

Stability of a periodic orbit can be straightforwardly derived from the fixed point

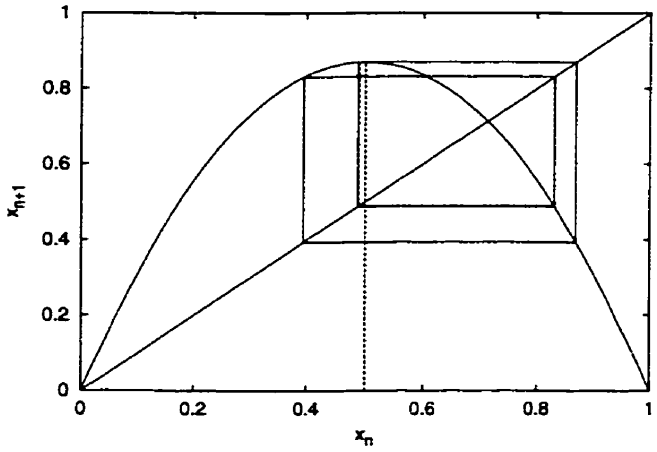

Figure 2.4: At $\mu = 3.48$ the attractor for the logistic map is a period-4 orbit.

stability criteria. Every point x_{pi} of a period-n orbit of a map (2.3) is a fixed point of a map

$$x_{k+1} = f^n(x_k) \tag{2.4}$$

where f^n is a composition of n mapping functions (2.3)

$$f^n(x) = \underbrace{f(f(f(\cdots f}_{n}(x)\cdots))), \tag{2.5}$$

or written in more convenient notation

$$f^n = \underbrace{f \circ f \circ f \circ \cdots \circ f}_{n}. \tag{2.6}$$

Therefore, the periodic orbit $x_{p1}, \ldots, x_{pn}$ of a map (2.3) is stable if any point of that orbit x_{pi} is a stable fixed point of the map (2.4):

$$\left| \frac{d}{dx} f^n(x) \right|_{x=x_{pi}} < 1 \tag{2.7}$$

Applying the chain rule for the derivatives we obtain the stability criteria for a periodic orbit to be:

$$|f'(x_{p1})| \cdot |f'(x_{p2})| \cdots |f'(x_{pn})| < 1 \tag{2.8}$$

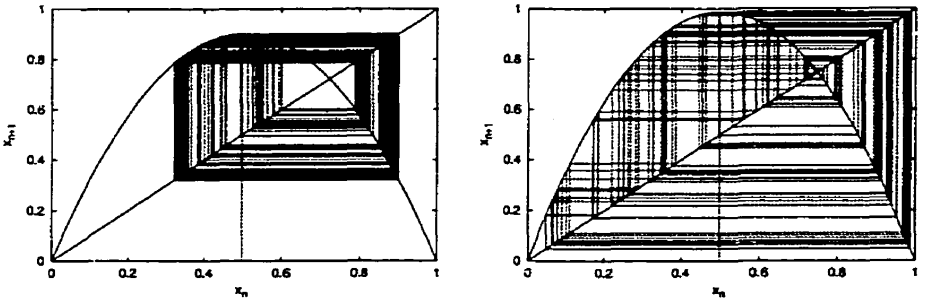

Figure 2.5: Chaotic logistic map for $\mu = 3.6$ (left) and $\mu = 3.95$ (right).

Superstable and unstable orbits are defined accordingly.

As for the single-point attractor, a change in initial condition x_0 will not change points x_{a1} and x_{a2}. A change in the initial condition may actually reverse the order of appearance of these two values during consecutive iterations. For example, a change in the initial condition may cause x_n to be found in x_{a1} for every odd instead of every even iteration, for sufficiently large n. Information about this we obtain from the initial condition. There are two regions within the basin of attraction that would lead to one or another order, separated by repeller x_r. In order to predict the future state of the system x_n, we still do not need to know the exact initial value x_0, but only which part of the basin of attraction it belongs to.

For $\mu = 3.4494\ldots$ another period doubling occurs, so x_n now goes through a cycle of four different values, i.e. the attractor is now stable period-4 orbit (Fig. 2.4). The period-2 orbit becomes unstable, and along with the period-one orbit divides the basin of attraction into four subintervals. In order to make a prediction we have to locate the initial condition for one of them. The next period doubling occurs at $\mu = 3.5440\ldots$, then at $\mu = 3.5644\ldots$, and so forth. Finally, at $\mu = \mu_\infty = 3.5699456\ldots$ we reach an infinite number of period doublings, and the system becomes chaotic. The attractor is now an infinite set of points, within the basin of attraction. With every iteration x_n is found in a different point at the attractor, and since there is an infinite number

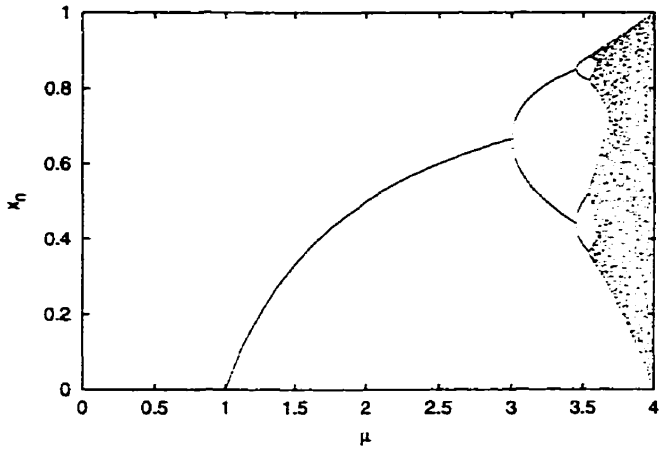

Figure 2.6: Bifurcation diagram for the logistic map

of these points, behavior of the system is not periodic any more. Furthermore, all unstable orbits generated by period doublings are still embedded in the attractor. Such an object is called a chaotic attractor. Unstable orbits divide chaotic attractor, and therefore the basin of attraction as well, into an infinite number of subintervals, each containing initial conditions which leads to a different pattern of going over the attractor. Obviously, arbitrarily small changes in the initial condition x_0 would place it in another subinterval, which will cause the system to be found in a quite different point x_n, after a sufficiently large number of iterations n. Hence, in order to make predictions it is necessary to determine initial condition with absolute precision.

If we stick to the fish example, though, prediction still seems possible, because we simply count the fish in the lake, and we have a sharp initial condition for our model. The problem occurs when we do calculations. In order to make a long term prediction we have to keep an infinite number of digits. The smallest round off error would shift us onto another orbit, leading us to a quite different result after a finite number of iterations. In other words, long-term prediction is inherently impossible for a chaotic system.

It is important to note that although this behavior is unpredictable it is still

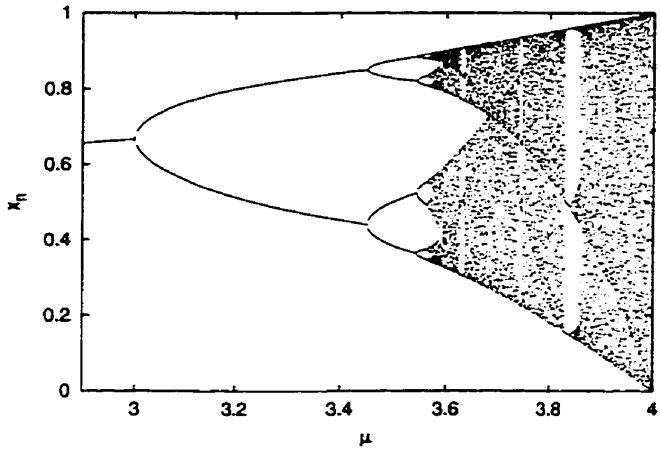

Figure 2.7: Period doubling route to chaos for logistic map

deterministic, because it is completely described by the logistic equation (2.2).

We can summarize the previous discussion in diagram 2.6. This diagram shows possible values of x_n (for n large) where the system can be found for particular μ, and is called a bifurcation graph. It actually describes evolution of the logistic map's attractor with change of parameter μ. Bifurcation diagrams are an important tool for examining chaotic properties of dynamical systems, and are often used to locate chaotic regions within the parameter space. Obviously, the name comes from the fact that curve x_n vs. μ bifurcates for every period doubling. The bifurcation that corresponds to a period doubling is called a pitchfork bifurcation.

We will now use the bifurcation diagram to show the behavior of the logistic map when $\mu > \mu_\infty$. Beyond pitchfork chaos the system suddenly becomes periodic again for certain values of μ, with a period n which is different from any power of two. The chaotic attractor is then replaced with a non-chaotic one. This phenomenon is called subduction [29]. As μ increases further, the system will get back to chaos through another sequence of period doublings, similar to the initial one. At the bifurcation diagram subductions are observed as narrow "windows" of periodic behavior within an otherwise chaotic region. Periodic windows starting with 3-, 5-, 6-, and 7-point

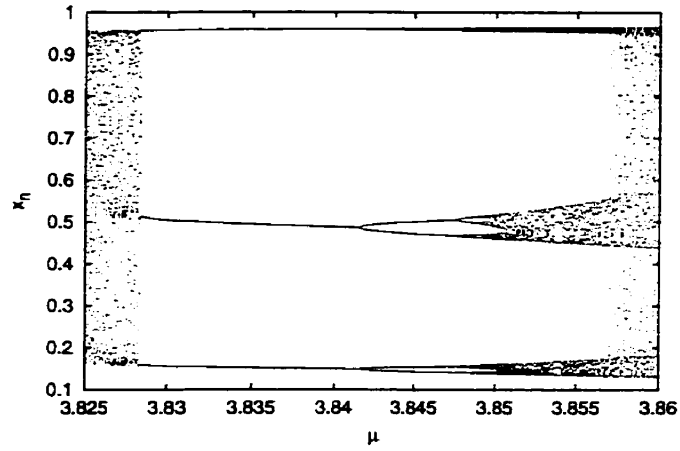

Figure 2.8: Period-3 window enlarged.

cycles are clearly visible in figure 2.7. Subduction occurs as a consequence of a tangent bifurcation, which is preceded by intermittent chaos or intermittency [62].

Tangent bifurcation [1] creates a pair of stable and unstable period-n orbits. As we further increase the parameter μ the stable orbit goes through a cascade of period doublings, similar to the initial pitchfork cascade, leading back toward chaos, and stable orbits of period 2n, 4n, 8n, etc. subsequently occur (fig. 2.8).

To understand this phenomenon, let us observe creation of a period-3 stable-unstable orbit pair. We plot the f^3 function (2.4) of a logistic map for μ (Fig. 2.9). We notice that as we increase μ the curve touches the diagonal $x_{n+1} = x_n$ at three points, creating in that way a marginally stable period-3 orbit, as $f^3(x)' = 1$ at tangent points. With a further increase in μ, the curve crosses the diagonal thus creating stable-unstable pair of orbits (Fig 2.9). Similar analysis can be done for any

[1] A caution in the use of terminology is needed here. The word bifurcation refers to a doubling of the stable orbit at the pitchfork bifurcation, while at tangent bifurcation refers to creation of a stable-unstable pair of orbits. In that regard, a tangent bifurcation that results in a period triplication is called "trifurcation" in some articles (e.g. [11]), or in more general case, when it results in n-point orbit, "n-furcation".

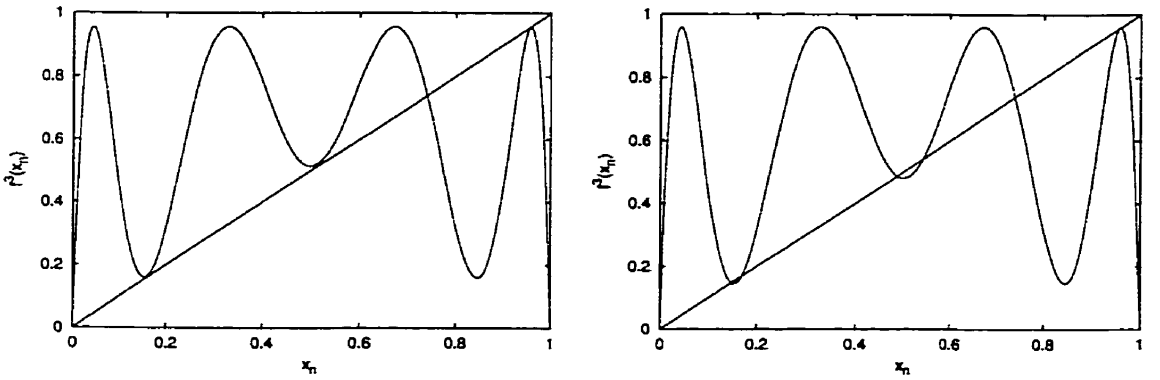

Figure 2.9: Creation of a period-3 orbit. Mapping function f^3 is plotted for $\mu = 3.825$ (left) and $\mu = 3.841$ (right).

other odd order tangent bifurcation.

It should be noted here that chaos is not merely a limit case of period-2^k orbit when $k \to \infty$. Every tangent bifurcation creates a new infinite set of unstable orbits that are embedded within a chaotic attractor. There occurs infinitely many tangent bifurcations when μ changes from μ_∞ to 4, so every value of μ at that interval corresponds to a different "kind" of chaos. The order at which unstable periodic orbits occur in a logistic map is prescribed by the theorem of A. N. Sharkovskii [70, 77, 78]. With the decrease of μ orbits are ordered as:

$$3 \prec 5 \prec 7 \prec 9 \prec \ldots \prec 3 \cdot 2 \prec 5 \cdot 2 \prec 7 \cdot 2 \prec \ldots \prec 3 \cdot 2^2 \prec 5 \cdot 2^2 \prec 7 \cdot 2^2 \prec \ldots$$
$$\prec 3 \cdot 2^n \prec 5 \cdot 2^n \prec 7 \cdot 2^n \ldots \prec 2^n \prec \ldots \prec 2^3 \prec 2^2 \prec 2 \prec 1$$

Sharkovskii's theorem is actually valid not only for a logistic map, but for any unimodal map, i.e. any map on a unit interval which mapping function has a single supremum value on that interval.

For $\mu \geq 4$ the size of attractor exceeds that of the basin of attraction, and the attractor, along with its basin, suddenly disappears. Almost any initial value x_0, either in or out of the former basin, is then mapped toward $-\infty$. We say that the system has come to crisis at $\mu = 4$ [28]. Such a phenomenon is called a boundary

crisis and it occurs when an attractor "collides" with boundaries of its basin. The geometrical structure, made of an infinite number of periodic orbits, is still there, though it does not act as an attracting set. Apart from a boundary crisis, there is another type of crisis that is observed - the interior crisis. An interior crisis results in a sudden change in the size of an attractor, and it occurs when an attractor collides with an unstable orbit. Most of the periodic windows end by an interior crisis when period doubling cascade collides with its respective repeller. For example, at $\mu = 3.855$ the logistic map exhibits chaos, and its attractor is contained within three finite segments in its basin of attraction (fig. 2.8). At $\mu = 3.857$ the attractor collides with unstable period-3 orbits and suddenly increases in size, occupying the most of the basin of attraction.

The "direction" of evolution of the logistic map's attractor is here chosen quite arbitrarily, and it depends only on how we define the system's parameter. Therefore, a period doubling sequence leading to chaos is equivalent to a period halving sequence leading from chaos to periodicity. Also, it is equally legitimate to state that intermittent chaos occurs for $\mu = 3.828$, (fig. 2.8) where stable and unstable period-3 orbits annihilate, as to say that a tangent bifurcation converts a chaotic attractor into stable-unstable period-3 orbit pair. In more complex systems that we are going to describe these transitions occur in both directions within the same bifurcation diagram.

2.2 Route to Chaos

Period doubling as observed at the logistic map model is at present the most commonly known route to chaos. With the increase of the parameter μ the logistic map goes through a sequence of period doublings before it becomes chaotic. Points μ_i for which bifurcations occur make an array $\{\mu_i\}$ that converge to some finite accumulation point μ_∞.

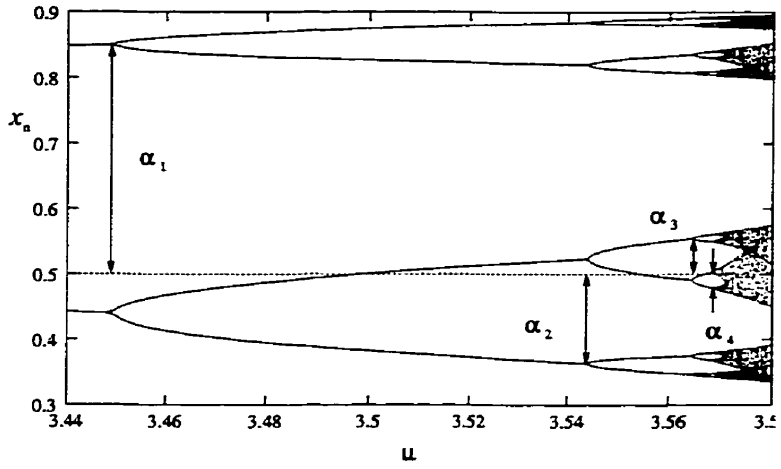

Figure 2.10: Distances between neighboring bifurcation points

Physicist Mitchell J. Feigenbaum set certain rules that characterize this route to chaos. As well, he showed that these rules have a universal nature and do not depend on properties of a particular map. According to Feigenbaum, a bifurcation route to chaos occurs for a map

$$x_{n+1} = \mu f(x_n) \tag{2.9}$$

defined over the segment $[0, 1]$, when $f(x)$ has a single differentiable maximum x_{max} on that segment [18]. This is a weak condition, and a large number of functions satisfy it with proper scaling. Feigenbaum further showed that the route to chaos is characterized by two constants - the scaling ratio α, and the convergence ratio δ, which are also called Feigenbaum numbers, or in some literature Feigenvalues [41]. The scaling ratio is defined by:

$$\alpha = \lim_{n\to\infty} \frac{d_{n-1}}{d_n} \tag{2.10}$$

where d_n is the vertical distance between a bifurcation point and the maximum point of the mapping function at μ_n (Fig. 2.10). The convergence ratio δ describes the convergence of the array $\{\mu_i\}$, and it is defined by:

$$\delta = \lim_{n\to\infty} \frac{\mu_{n-1} - \mu_{n-2}}{\mu_n - \mu_{n-1}} \tag{2.11}$$

Feigenbaum numbers for a logistic map are calculated to be

$$\alpha = 2.5029... \quad \delta = 4.6692... \tag{2.12}$$

These numbers are the same for any other one-dimensional map (2.9) when the function x_{max} has a simple quadratic maximum on $[0, 1]$, i.e. when $f'(x_{max}) = 0$ and $f''(x_{max}) < 0$. Feigenbaum defined whole classes of maps characterized by the same α and δ. All maps defined by (2.9) whose mapping functions satisfy

$$f(x_{max}) - f(x) \sim |x - x_{max}|^z, \quad z > 1 \tag{2.13}$$

belong to the same class which is determined only by z [18]. Obviously, for the logistic map $z = 2$.

This means that the Feigenbaum numbers depend only on the behavior of the mapping function around the maximum point, and not on any other particular properties of the function. Hence, the mapping function $f(x)$ will determine only local scaling, while a period doubling transition to chaos in a qualitative sense will be governed by some universal function. Every function from class 2.13 renormalized by α would then resemble a universal function in a vicinity of x_{max} [19].

A period doubling sequence starting off from a tangent bifurcation inside a window of periodic behavior will be described by different Feigenbaum numbers, depending on the particular period multiplication pattern in it. For example, Feigenbaum numbers in windows that contain period triplication routes are calculated to be $\alpha = 9.277$ and $\delta = 55.26$ [11].

At this point a digression is necessary in order to introduce the concept of fractals. Fractals are geometrical forms generated by replicating a certain pattern infinitely to a smaller and smaller scale. Therefore, an arbitrarily small part of a fractal magnified would resemble the shape of a whole fractal. This is called self-similarity. As a consequence, fractals are non-differentiable at every point. The main feature of fractals and the reason they got their name is that their dimension is a fractional number.

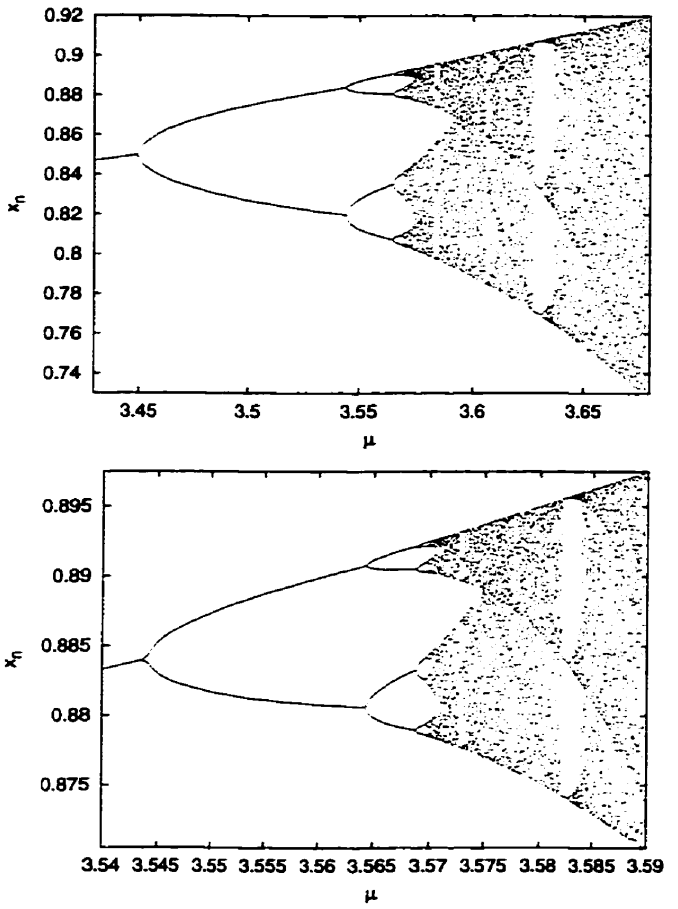

Figure 2.11: Further magnification of the part of bifurcation diagram

Figure 2.12: Generating a Cantor set.

The Cantor set is an illustrative example of a fractal. It is generated from a straight line of finite length. First, the middle third of the line is erased, so that we are left with two new, shorter lines. Then the middle thirds of these new lines are erased, and we are left with four even shorter lines. As we proceed we are left with more lines of lesser length after every step. If we repeat this pattern infinitely, the final result will be an infinite set of dimensionless points. This is the Cantor set. We can immediately see that its dimension is greater than 0, and less than 1. In order to estimate an exact numerical value for the fractal dimension of the Cantor set we have to generalize the concept of Euclidian dimension, which considers only nonegative integer values. For example, we might use the definition of capacity fractal dimension as given in Ref. [4].

If we cover a fractal with a grid of hypercubes of size ϵ, which are volume elements of the space in which the fractal lies, and if the number of hypercubes needed to cover the whole attractor, $N(\epsilon)$, grows like

$$N(\epsilon) \propto \epsilon^{-D} \tag{2.14}$$

when $\epsilon \to 0$, then the number D is called the capacity fractal dimension.

Using this definition we can calculate the fractal dimension as

$$D = \lim_{\epsilon \to 0} \frac{N(\epsilon)}{1/\epsilon} \tag{2.15}$$

Substituting values for a Cantor set we obtain $D = \log 2/\log 3$. One should note that the capacity dimension of a non fractal object equals its Euclidian dimension. For example, the capacity dimension of a straight line is $D = 1$, and for a finite set of disconnected points (2.15) becomes zero. However, the generalization of the Euclidian dimension is not unique. Apart from the capacity dimension, there are several other fractal dimensions defined [14, 16, 17, 24, 25, 26], and their numerical values may differ for certain fractals.

The way how a chaotic attractor for the logistic map at the onset of chaos is created indicates that this attractor has a fractal nature as well. An infinite sequence of bifurcations, which become self-similar after a large number of iterations, generates a Cantor-like fractal. Its dimension D is estimated to be $0.53763 < D < 0.53854$ [23]. The attractor is called a strange attractor because of its fractal properties. Furthermore, the bifurcation graph also has a fractal form, and self-similarity is observed (Fig. 2.11). The fractal geometry of the bifurcation diagram for the logistic map is simply a reflection of the existence of Feigenbaum numbers. This is one example why fractals are so convenient for describing chaotic systems. Most chaotic attractors have a fractal structure, and exploring their geometrical properties helps us obtain important information about the system's dynamics. However, not all chaotic attractors are strange and vice versa. The chaotic logistic map attractor for certain values of μ consists of a finite number of disjoint intervals [45] within the basin of attraction, i.e. it is not strange. In Ref. [30] examples of strange attractors that are not chaotic are given.

2.3 Lyapunov Exponents

Lyapunov characteristic exponents are quantitative measure of chaos. Lyapunov exponents help us describe behavior of a system when it becomes chaotic, and also helps us distinguish chaotic from random motion. The number of exponents corresponds

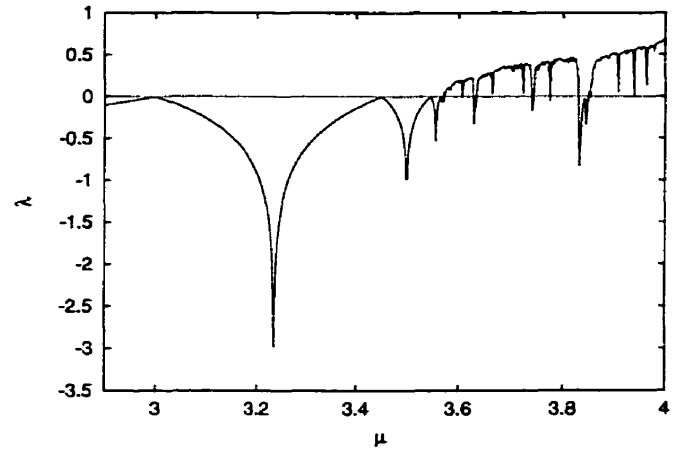

Figure 2.13: Lyapunov exponent for the logistic map

to the number of independent variables necessary to uniquely define the state of the system. Calculating Lyapunov exponents is a complex task, however it is fairly simple to estimate a Lyapunov exponent for systems that have only one, like it is the case for the logistic map. For any one-dimensional map (2.3) the state is determined by a variable x, and the corresponding Lyapunov exponent is defined as an average stability of an orbit when the number of iterations goes to infinity.

$$\lambda = \lim_{n\to\infty} \frac{1}{n} \sum_{i=1}^{n} \ln \left| \frac{df(x)}{dx} \right|_{x=x_i} \tag{2.16}$$

Particularly, for the logistic map it is:

$$\lambda = \frac{1}{n} \sum_{i=1}^{n} \ln |\mu(1-2x_i)| \tag{2.17}$$

Here we take logarithms of mapping function derivatives just to get more convenient numerical values. Alternatively, we can drop logarithm and define equally useful dynamical average, *Lyapunov numbers*, as:

$$L = \lim_{n\to\infty} \left(\prod_{i=1}^{n} \left| \frac{df(x)}{dx} \right|_{x=x_i} \right)^{\frac{1}{n}} \tag{2.18}$$

For a periodic orbit a Lyapunov exponent can be estimated after a finite number of steps. Obviously, for a period-N orbit limit (2.16) becomes

$$\lambda = \frac{1}{N}\sum_{i=1}^{N} \ln \left| \frac{df(x)}{dx} \right|_{x=x_{pi}} \tag{2.19}$$

For a stable periodic orbit the value of Lyapunov exponent is the same for any initial condition from its basin of attraction, because contribution from transient iterations in average (2.16) becomes negligible as $n \to \infty$. Transient iterations does not affect value of the Lyapunov exponent when the motion is chaotic, either. Therefore, although it is estimated for an orbit starting from a particular initial condition Lyapunov exponent can be understood as a property of the phase space, rather than the orbit itself. Its value depends on geometrical properties of the attractor for the system, and in most cases we can obtain a good enough approximation after finite number of iterations.

The average Lyapunov exponent characterizes the separation rate for two orbits starting from infinitesimally close initial conditions x_0 and $x_0 + \epsilon_0$, which are after a large number of iterations found in x_n and $x_n + \epsilon_n$ respectively. Hence, we may alternatively define λ as:

$$\lambda = \lim_{n\to\infty} \frac{1}{n} \ln \frac{\epsilon_n}{\epsilon_0} \tag{2.20}$$

As long as the limit above exists, λ does characterize sensitivity to the initial conditions of a one-dimensional map. From (2.20) it follows that for positive Lyapunov exponent iterations starting from two infinitesimally close initial conditions would diverge exponentially. For a large number of iterations n, the separation ϵ_n will grow approximately like:

$$\epsilon_n \approx \epsilon_0 e^{\lambda n} \tag{2.21}$$

That means no matter how small the separation between two initial conditions is, it will become finitely large after sufficient number of iterations. Therefore, the system is chaotic. In the limit case $\lambda \to \infty$ the system becomes random. For $\lambda < 0$ iterations

converge and the system exhibits regular behavior. It is easy to show that definitions (2.16) and (2.20) are equivalent. We may write ϵ_n as

$$\epsilon_n = f^n(x + \epsilon_0) - f^n(x), \tag{2.22}$$

where f^n denotes the n^{th} iteration of the mapping function f. If we substitute (2.22) in (2.20) and, since ϵ_0 is defined as an arbitrary small value, take the limit $\epsilon_0 \to 0$ we get:

$$\lambda = \lim_{n\to\infty} \lim_{\epsilon_0 \to 0} \frac{1}{n} \ln \left[\frac{f^n(x+\epsilon_0) - f^n(x)}{\epsilon_0} \right] = \lim_{n\to\infty} \frac{1}{n} \ln \left| \frac{df^n}{dx} \right|. \tag{2.23}$$

Applying the chain rule for the derivative we finally obtain

$$\lambda = \lim_{n\to\infty} \frac{1}{n} \sum_{i=1}^{n} \ln |f'(x_i)| \tag{2.24}$$

which is equivalent to the expression (2.16). Definition (2.16) is used when the mapping function f is known, while (2.20) is more suitable for estimating Lyapunov exponents from experimental data.

Since the attractor for the logistic map lies in a bounded region, i.e. within segment $[0, 1]$, it is obvious that besides stretching of the distance between two nearby initial conditions ϵ_0, some other process must take place. It appears that the distance ϵ_n will be reset to some smaller value before it exceeds the size of attractor. Actually, the orbit of the logistic map folds whenever value of x_n crosses over the critical point $x_c = 0.5$ [85]. Separation between nearby orbits then keeps stretching, but in the opposite direction. Therefore relation (2.21) holds only for as long as the orbit is not folded, and ϵ_n is much smaller than size of the attractor. Stretching and folding patterns are characteristic of any chaotic motion, and it is more emphasized for systems with more than one dimension. Lyapunov exponents, however, contain information about stretching only, and for their estimation it is necessary to circumvent folding effects.

If we plot the Lyapunov exponent for the logistic map versus the parameter μ (Fig. 2.13) we find that for $\mu > \mu_\infty$ λ increases smoothly with μ [43], apart from the

interceptions due to the windows of periodic behavior. It can be shown that in that region

$$\lambda(\mu) = \lambda_o(\mu - \mu_\infty)^{\frac{\ln 2}{\ln \delta}} \tag{2.25}$$

where λ_0 is constant, and δ is the Feigenbaum number for a quadratic map. This result tells us that chaotic behavior has certain universal properties, and indicates that the bifurcation route to chaos contains information about the system's behavior once it becomes chaotic. On the other hand, in a deterministic non-chaotic region in parameter space ($\mu < \mu_\infty$) the system is unstable at the bifurcation points, and the Lyapunov exponent there is zero, unlike the rest of the region where it is negative.

2.4 Kolmogorov Entropy

For deterministic periodic systems, we are able to predict their future behavior if given initial conditions. On the other hand, when the system becomes chaotic we are not able any more to predict its behavior after a certain period of time. In other words, the information about system's behavior is lost when it becomes chaotic. Loss of information is generally characterized by entropy, so it seems reasonable to introduce entropy to measure loss of information due to chaotic behavior. In analogy with statistics we define the information entropy to be

$$S = -\sum_i p_i \ln p_i, \tag{2.26}$$

where the summation is done over all possible states i where the system can be found. p_i is the probability of finding the system in the i^{th} state when we know its equation of motion but not the initial condition(s) [16, 24]. For the logistic map, when the attractor is a single point, the state in which the system is found after several iterations can be predicted regardless of the initial condition x_0, so the information entropy $S = 0$. After period doubling, when the attractor consists of two points, the system can be found in any of these with equal probability, and hence $S = \ln 2$. This

is the amount of information that we would obtain with the initial condition. For random motion all states are accessible with equal probability, and the entropy has its maximal value $S = \ln N$ where N is number of states. This number is infinite if the system is defined over a continuous segment like the logistic map is.

Similar to the random systems the number of states in which a chaotic system can be found is generally infinite so in (2.26) we have to circumvent somehow the problem of an infinite summation. Therefore, in order to calculate entropy for one-dimensional iterated maps we usually first divide the basin of attraction of the system in N small subintervals of size ϵ. Then we count n of those subintervals in which the system can be found, and assuming they are equally probable assign them probability $p = 1/n$. Other subintervals obviously have zero probability. This assumption is valid for the limiting case $\epsilon \to 0$, $N \to \infty$, when the subintervals approximate well states in which the system can be found. The entropy then takes the simple form:

$$S = \lim_{\epsilon \to 0} \ln n(\epsilon) \tag{2.27}$$

Information entropy, however, is not the best tool for describing chaotic systems. For example, entropy of an n-periodic system initially acquires its maximum value $S \sim \ln n$, and remains constant thereafter. On the other hand, entropy of a chaotic system will increase with every iteration, because every time the system will be found in a new state. Therefore it seems more reasonable to use the change in entropy, rather than entropy itself, for describing chaotic systems. That is why the Kolmogorov entropy is introduced. For iterated maps the Kolmogorov entropy is defined as an average change in statistical entropy over a large number of iterations:

$$K = \lim_{I \to \infty} \frac{S_I - S_0}{I} \tag{2.28}$$

In the last equation S_0 and S_I are the initial entropy and entropy after I iterations, respectively, and ϵ is the size of subintervals dividing the basin of attraction. The number of iterations should be chosen so that the whole attractor is covered. Apparently $K = 0$ for any periodic motion, $K > 0$ for a chaotic motion. For a random

system for any given initial condition all states are equally probable already with a next iteration, therefore, $K \to \infty$.

Let us estimate now the K-entropy for a chaotic system. If we assume that the size of of subintervals within the basin of attraction is some very small value ϵ_o, then according to (2.21) its size would after I iterations expand to $\epsilon_o\, e^{\lambda I}$, where λ is the Lyapunov exponent for the map, and $\lambda > 0$. Since the size of the subinterval is proportional to the number of states within it, we conclude that if initially the system is found in n_0 states, after I iterations the system may be found in $n_0\, e^{\lambda I}$ different states. For a large number of iterations we may estimate the K-entropy using (2.27) to be

$$K = \lim_{\epsilon \to 0} \lim_{I \to \infty} \frac{\ln(n_0\, e^{\lambda I}) - \ln n_0}{I} = \lambda \tag{2.29}$$

so, when the logistic map exhibits chaotic behavior its Kolmogorov entropy equals its Lyapunov exponent, which is positive in that case. For the system with multidimensional phase space, K-entropy approximately equals the sum of all positive Lyapunov exponents. Therefore, positive Lyapunov exponents describe information loss rate for a chaotic system.

Equation (2.29) tells us that maps exhibits chaos only if two iterations starting from nearby points diverge exponentially. Otherwise, the K-entropy equals zero in the limit $I \to \infty$. Especially interesting is the case when the iterations diverge, but slower than exponentially. The behavior is not periodic, but we are able, at least in theory, to make predictions since the Kolmogorov entropy vanishes for a large number of iterations. Such a behavior is called quasiperiodic, and it will be discussed later in Chapter 3.

2.5 Symbolic Dynamics of a One-Dimensional Map

For a long time chaotic motion was considered to be undesirable in dynamical systems, and chaos was treated in a similar manner as a random noise. The reason for that was

that up to recently there were no tools for a general analysis of chaotic motion. On the other hand, Sharkovskii showed that with the change of parameter μ in any unimodal map (2.3) periodic orbits occur in a certain sequence. Therefore it is possible to count all periodic orbits that exist in the phase space of an unimodal map, even if there are infinitely many of them, like it is the case in chaos.

Symbolic dynamics provides a general framework for finding periodic orbits in phase space, which are the main "ingredients" of chaos. The characteristic of chaotic dynamics is high sensitivity to change in initial conditions. It is, therefore, very difficult to characterize chaotic trajectories numerically, since small errors in calculation may shift our results from one trajectory to another. The idea behind symbolic dynamics is to make a suitable partition of phase space into a finite number of subspaces, and follow the motion of the system not by numerical values of its phase space coordinates, but by the sequence at which a trajectory visits different partitions. Each partition is assigned a character, and subsequently any trajectory is encoded by a sequence of characters, or itinerary, which describes the order in which a trajectory visits different partitions. If the partitioning is done properly, every periodic orbit is uniquely defined by a finite number of letters or a word. Furthermore, by observing sequences starting from partition lines we may derive pruning rules, which tell us what are the admissible and what are inadmissible words. In this way we may determine and count all unstable periodic orbits embedded in a chaotic attractor. Symbolic dynamic analysis may also help us find parameter locations of periodic windows. We shall describe these ideas using the example of a logistic map.

The first step of symbolic analysis of a dynamical system is to partition the phase space properly. We can intuitively conclude that the phase space of a logistic map can be divided in two partitions, separated by the maximum or critical point of the mapping function, since it is the only "special" point in the phase space. It is also called a critical point of the logistic map. In fact, the general rule for partitioning the phase space of 1-D maps is to split it into regions where the mapping function is

monotonic. The two regions of an unimodal map are usually denoted with letters L and R, which stand for left and right of the critical point, respectively. We, hence, encode a trajectory of a logistic map with a binary sequence of letters L and R.

$$.s_0 s_1 s_2 s_3 \ldots, \quad s_i = L, R \tag{2.30}$$

We denote the critical point with letter C. Every orbit of a logistic map is determined by the initial condition x_0. We can order itineraries by the numerical value of the initial condition. Obviously, for one letter sequences it is:

$$L < C < R \tag{2.31}$$

We can also immediately see that L^∞ is the smallest itinerary as it corresponds to $x_0 = 0$, and RL^∞ is the largest as it starts from $x_0 = 1$. Analyzing itineraries further, we find that $LL < LR$, but $RL > RR$ because the second iteration is mapped from a monotonically decreasing function. In order to make this point clear, let us recall here some properties of monotonic functions.

- A monotonically decreasing function $g(x)$ inverts the order of its arguments such that $x_1 < x_2 \Leftrightarrow g(x_1) > g(x_2)$, while a monotonically increasing function function preserves the order of its arguments so it is $x_1 < x_2 \Leftrightarrow g(x_1) < g(x_2)$.

- The inverse of a monotonically increasing (decreasing) function is also a monotonically increasing (decreasing) function.

- A composition of n monotonic functions is monotonically increasing (decreasing) if there is an even (odd) number of monotonically decreasing functions in the composition

Now, let us observe two iterations starting from two initial conditions x_0 and x_0', which belong to the same monotonic segment of mapping function f:

$$\begin{aligned} x_0 &\to x_1 = f(x_0) \\ x_0' &\to x_1' = f(x_0') \end{aligned} \tag{2.32}$$

In other words both x_0 and x_0' are denoted with the same symbol s_0. Now we take the inverse f^{-1} on both sides of (2.32) to obtain:

$$\begin{aligned} x_0 &= f_{s_0}^{-1}(x_1) \\ x_0' &= f_{s_0}^{-1}(x_1') \end{aligned} \tag{2.33}$$

The inverse function f^{-1} is not uniquely defined unless we know whether x_0 is left or right of the critical point. Therefore, we put a lower index s_0 to f^{-1} in order to avoid ambiguity. If $s_0 = L$, then the inverse function is monotonically increasing, since the original function $f(x)$ is monotonically increasing for those values of x. If $s_0 = R$, the inverse function is monotonically decreasing. If we take $x_1 \to L$ and $x_1' \to R$, so that $x_1 < x_1'$, knowing properties of monotonic functions, we conclude that

$$\begin{aligned} f_L^{-1}(x_1) &< f_L^{-1}(x_1') \\ f_R^{-1}(x_1) &> f_R^{-1}(x_1') \end{aligned} \tag{2.34}$$

or, in other words, $LL < LR < RR < RL$. We can expand this reasoning to an itinerary of an arbitrary length. Let us take two points x_0 and x_0' that would lead to two itineraries of length n with first $n-1$ letter same:

$$\begin{aligned} x_0 \to x_n &= f^n(x_0) \\ x_0' \to x_n' &= f^n(x_0') \end{aligned} \tag{2.35}$$

Taking the inverse function f^{-1} on both sides of (2.34) n times we get:

$$\begin{aligned} x_0 &= f_{s_0}^{-1} \circ f_{s_1}^{-1} \circ \cdots \circ f_{s_{n-1}}^{-1}(x_n) \\ x_0' &= f_{s_0}^{-1} \circ f_{s_1}^{-1} \circ \cdots \circ f_{s_{n-1}}^{-1}(x_n') \end{aligned} \tag{2.36}$$

where $s_i = L, R$. If there is an odd number of letters R within the itinerary $s_0 s_1 s_2 \ldots s_{n-1}$, then the composite function on the right hand sides of equations (2.36) is monotonically decreasing. Otherwise, it is monotonically increasing. Therefore, if we assigning again $x_n \to L$ and $x_n' \to R$ so that $x_n < x_n'$, then $x_0 > x_0'$ for odd number of letters R, and $x_0 < x_0'$ otherwise.

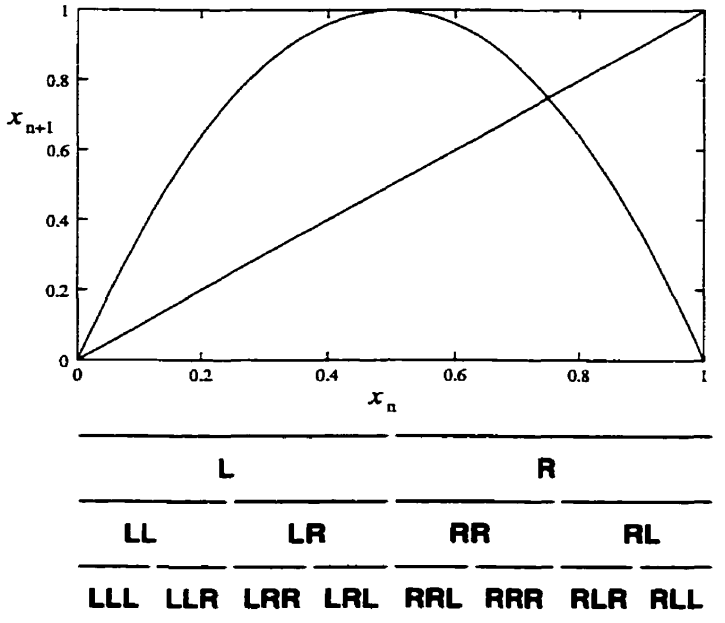

Figure 2.14: Mapping function for the logistic map at $\mu = 4$. Below are denoted segments of initial conditions which generate itineraries starting with 1-, 2- and 3-letter words.

We may define, hence, a general rule for ordering itineraries for a unimodal map: Let us have two itineraries W_1 and W_2 which have a common part $W = s_0 s_1 s_2 \dots s_{n-1}$ such that:

$$\begin{aligned} W_1 &= W s_n s_{n+2} s_{n+2} \dots \\ W_2 &= W t_n t_{n+1} t_{n+2} \dots \end{aligned} \tag{2.37}$$

Then, if W contains an even number of Rs $W_1 < W_2$ if $s_1 < t_1$. If W contains odd number of Rs $W_1 > W_2$ if $s_1 < t_1$.

It is convenient to define a parameter α which describes the order of the symbolic sequence. We may interpret characters R and L as binary digits of a number $0 \leq \alpha < 1$ in such a way that $\alpha(W_1) < \alpha(W_2)$ whenever $W_1 < W_2$, and vice versa. Thus for itinerary (2.30) we define a binary number

$$\alpha = 0.\alpha_1 \alpha_2 \alpha_3 \dots \tag{2.38}$$

where $\alpha_i,\ i = 1, 2, 3, \dots$ are binary digits determined as

$$\alpha_i = \begin{cases} 0 \\ 1 \end{cases} \quad \text{for} \quad s_i = \begin{cases} L \\ R \end{cases} \quad \text{and} \quad \prod_{j=1}^{i-1} \epsilon_j = 1, \tag{2.39}$$

and

$$\alpha_i = \begin{cases} 1 \\ 0 \end{cases} \quad \text{for} \quad s_i = \begin{cases} L \\ R \end{cases} \quad \text{and} \quad \prod_{j=1}^{i-1} \epsilon_j = -1, \tag{2.40}$$

Here ϵ_i is an auxiliary parameter, which has value $\epsilon_i = 1$ for $s_i = L$, and $\epsilon_i = -1$ for $s_i = R$.

In Figure 2.14 are shown segments of initial conditions that generate itineraries which start with a certain string of letters. As the string gets longer, the segments become smaller and smaller, until they become points in the limit case. Therefore, itineraries of infinite length describe uniquely a single orbit. More importantly, periodic orbits are uniquely described by words of finite length. A periodic orbit can be described by any cyclic permutation of its letters. As a representative word for a periodic orbit we choose the maximal word. For example a period-3 orbit $(RLR)^\infty$

can be written as $(RRL)^\infty$ or $(LRR)^\infty$. Since $RLR > RRL > LRR$, we use the first word to describe the orbit.

The next question is whether any combination of these letters makes an admissible word or there are some pruning rules that explicitly forbid certain words. We can see that the critical point x_c is mapped to the largest, or if one prefers the leftmost, value of x that logistic map can reach. The itinerary starting off with the critical point is called a kneading sequence, and for the logistic map (except for dynamically uninteresting case when $\mu \leq 2$) it looks like:

$$.CRLs_3s_4s_5\ldots, \quad s_i = L, R \tag{2.41}$$

Since R in the expression above corresponds to the largest value of x for the map, no periodic orbit may contain point beyond that value. Therefore we obtain a pruning rule [10, 36, 66]:

$$(t_1t_2\ldots t_n)^\infty < RLs_3s_4s_5\ldots \tag{2.42}$$

Now it becomes more clear why we represent orbits by their maximal words. A cyclic permutation of the maximal word may satisfy the pruning rule and still contain a point which cannot be reached by the map for given μ. Rigorous mathematical proof of the pruning rule for a unimodal map is first presented in 1973 by Metropolis at al. [66].

We shall illustrate usefulness of the symbolic dynamics in analysis of a dynamical system on a simple example. Let us first state the periodic windows theorem [37].

Theorem. If ΣC, where $\Sigma = s_1s_2\ldots s_{n-1}$, and $s_i = L, R$, is a maximal word describing a superstable orbit, then both, ΣL and ΣR, are maximal words too.

Superstable periodic orbits are obtained from the kneading sequence, and they represent periodic windows in bifurcation diagrams. We use superstable orbits in order to find all admissible words of certain length. For example, there is only one period-3 orbit which contains the critical point: RLC, and three period-5 orbits $RLLLC$, $RLLRC$ and $RLRRC$. All the other combinations of characters do not

make an admissible word. We obtain all possible orbits by changing the last letter $L \to C \to R$. Let us check which of these orbits are embedded in the chaotic attractor of a logistic map for $\mu = 3.8$. The kneading sequence for this attractor is:

$$.CRLRRLRRRRLRRLRRRRRLR\ldots \tag{2.43}$$

Period three orbits are larger than the kneading sequence, as well as $RLLLR$ and $RLLRL$. Two period-5 orbits $RLRRR$ and $RLRRL$ are embedded in the attractor.

We check this result by calculating values of μ at which periodic orbits occur. Let us substitute values for superstable period-3 and period-5 orbits into equation (2.36), and write for simplicity $f_{s_i}^{-1}(x) \equiv s_i(x)$. For period-3 orbit we get:

$$x_c = R \circ L(x_c) \tag{2.44}$$

By taking the inverse of the mapping function $f(x)$ for the logistic map we obtain

$$L(x) = \frac{1}{2} - \sqrt{\frac{1}{4} - \frac{x}{\mu}} \tag{2.45}$$

$$R(x) = \frac{1}{2} + \sqrt{\frac{1}{4} - \frac{x}{\mu}} \tag{2.46}$$

and further

$$R \circ L(x) = 1 - \sqrt{\frac{1}{4} - \frac{1}{\mu}\left(1 + \sqrt{\frac{1}{4} - \frac{x}{\mu}}\right)} \tag{2.47}$$

We put (2.47) into (2.44) and substitute $x_c = 0.5$, so we get:

$$\mu = 4\left(\frac{1}{2} - \sqrt{\frac{1}{4} - \frac{1}{2\mu}}\right) \tag{2.48}$$

As suggested in Ref. [37] we solve this equation by iteration as

$$\mu_{n+1} = 4\left(\frac{1}{2} - \sqrt{\frac{1}{4} - \frac{1}{2\mu_n}}\right) \tag{2.49}$$

where μ_0 can be any value from interval $(3.5, 4)$. This gives us the value for $\mu_{RLC} = 3.8323\ldots$. Similarly, we get $\mu_{RLLLC} = 3.7524\ldots$, $\mu_{RLLRC} = 3.8706\ldots$, and $\mu_{RLRRC} =$

3.9854.... Only the last periodic window occurs before $\mu = 3.8$, therefore we confirm that only $RLRRR$ and $RLRRL$ orbits are present at that value of parameter μ.

Symbolic dynamics can be used to rigorously prove some mathematical properties of unimodal maps, such as Sharkovskii's theorem and Feigenbaum universality. Here we presented just a simple example in order to introduce some basic concepts of symbolic dynamics analysis.

Chapter 3

THE PENDULUM

3.1 Dynamical Flows

Chaotic behavior is a characteristic of non-linear dynamical systems, i.e. systems that may be described by non-linear equations of motion. There are many different types of such systems, which are not necessarily physical, and different methods are employed for describing their behavior. The logistic map was one example. From now on we will limit our discussion to chaotic systems in classical dynamics, and use the basic example of a pendulum to describe some tools and techniques employed.

When we speak about dynamical systems that exhibit chaos we may generally divide them in two groups - conservative and dissipative systems. The former are characterized by some physical value - usually the energy - that is conserved throughout the motion. According to the principle of classical determinism the state of the system is determined by its position and velocity. The state of a conservative system may be described by Lagrange's function, or Lagrangian $L = L(q, \dot{q}, t)$, which is defined as the difference between the system's kinetic and potential energy. The variable q stands for a set of s generalized coordinates $q_1(t), ..., q_s(t)$, where s is number of degrees of freedom of the system. The motion of the system is determined by the Euler-Lagrange equations, which are the mathematical equivalent of the principle of least action, the fundamental principle of classical mechanics [53]. These equations are written as:

$$\frac{d}{dt}\frac{\partial L}{\partial \dot{q}_\alpha} - \frac{\partial L}{\partial q_\alpha} = 0, \quad \alpha = 1, ..., s \tag{3.1}$$

Solving these equations for some initial conditions $q_\alpha(0)$ and $\dot{q}_\alpha(0)$ gives us solutions

$q_\alpha(t)$ and $\dot{q}_\alpha(t)$ that represent trajectories of the system's motion in time.

An equivalent way to express the equations of motion for a conservative system is through Hamilton's formalism. If we define generalized momenta and Hamilton's function as:

$$p_\alpha = \frac{\partial L}{\partial \dot{q}_\alpha}\ , \quad H(p,q,t) = \sum_{\alpha=1}^{s} p_\alpha \dot{q}_\alpha - L(p,q,t) \tag{3.2}$$

respectively, we may write instead of s second-order differential equations (3.1) s pairs of first-order Hamilton's equations:

$$\dot{p} = \frac{\partial H}{\partial q_\alpha}, \quad \dot{q} = -\frac{\partial H}{\partial p_\alpha}, \quad \alpha = 1, ..., s \tag{3.3}$$

Hamilton's function, or the Hamiltonian, equals the total energy of the system. When it is constant in time, i.e. $dH/dt = 0$, energy is conserved. By taking the total time derivative of $H(p,q,t)$ and substituting (3.3) in it we get $dH/dt = \partial H/\partial t$. Therefore, the energy is conserved whenever the Hamiltonian does not depend explicitly on time. Since conservative systems can be fully described by Hamilton's formalism they are frequently called Hamiltonian systems.

Dissipative systems are those which interact with their environment in a way that they give up their energy to it. This energy is converted into some other form and is permanently lost for the system. The motion of a dissipative systems may be described by the slightly modified equation (3.1):

$$\frac{d}{dt}\frac{\partial L}{\partial \dot{q}_\alpha} - \frac{\partial L}{\partial q_\alpha} = Q_\alpha, \quad \alpha = 1, ..., s \tag{3.4}$$

Here L is the Lagrangian of the system without dissipation, and Q_α are generalized dissipative forces [22]. Dissipative forces in this context characterize energy loss rate, rather than describe the interaction of the system with its environment.

It is convenient to define a state space for a particular system where every state can be represented by one point. For the logistic map the state space was one-dimensional, and the state of the system was determined only by the dimensionless variable x that stands for a number of species in a closed environment. As we mentioned before, the

state of the classical system is fully determined by its space coordinates and their first derivatives. Therefore, we can define the phase space as having coordinates $q_\alpha(t)$ and $\dot{q}_\alpha(t)$, although an equally good choice of coordinates are $q_\alpha(t)$ and $p_\alpha(t)$. Solutions of the equations (3.1) or (3.3) then can be comprehensively described by a trajectory in the phase space. The dimension of a phase space appears to be $2s$. Nevertheless, in classical dynamics we sometimes do not take into consideration coordinates which correspond to variables that are constant or change trivially in time, so for a phase space we may choose a system with dimension smaller than $2s$. Analysing trajectories of a system's motion in a phase space proves to be a very convenient method for exploring properties of the system, and this is even more true when the system exhibits chaotic behavior.

According to Liouville's theorem, for conservative systems the volume element in the phase space is conserved during the motion. As a consequence, all trajectories will lie on "surfaces" within the phase space characterized by a constant of motion. If Hamilton's function $H(p, q)$ does not depend on time explicitly, then the energy E is a constant of motion, and all paths in the phase space will lie on a constant-energy "surface" $H(p, q) = E$. The term "surface" should not be taken too literally, because its dimension is $2s - 1$, and is often different than two.

Trajectories of a dissipative system in a phase space will converge toward the attractor(s) of the system. Therefore, a volume element in the phase space will not be conserved, but rather will shrink in time. A dissipative force actually determines the rate at which the volume element shrinks or, equivalently, the rate at which a trajectory leaves the initial-energy "surface" $H(p, q) = E_0$ and approaches the attractor. For larger Q the trajectory will reach the attractor sooner. In the limiting case $Q \to 0$ the trajectory will remain in the vicinity of the surface $H(p, q) = E_0$ for an infinitely long time.

Most of information that we can infer about a chaotic dissipative system we obtain by investigating geometrical properties of a system's attractor. In this way, instead

of analysing trajectories in a multi-dimensional phase space, we reduce our task to exploring properties of a lower dimensional fractal. Even infinite dimensional dynamical systems, i.e. those described by partial differential equations, may have a finite dimensional attractor. Similarly to the logistic map, for most cases periodic systems will have integer–dimensional attractors, while attractors of chaotic systems will be fractal structures. In this work we will focus ourselves primarily on the topic of dissipative systems.

Let us take the simple pendulum as an example of conservative system. The pendulum has only one degree of freedom, so its dynamical state will be characterized by only one coordinate and its respective derivative. It is convenient to choose for this coordinate the angle of inclination from the equilibrium position θ. Therefore, states of the pendulum can be represented in a 2-dimensional phase space $(\theta, \dot{\theta})$. The pendulum's Lagrangian, which is defined as the difference between its kinetic and potential energy, is then $L = \frac{1}{2}ml^2\dot{\theta}^2 + mgl\cos\theta$. Substituting $L(\theta, \dot{\theta})$ in (3.1) gives us the equation of motion for pendulum

$$\ddot{\theta} + \omega_0^2 \sin\theta = 0, \quad \omega_0^2 = g/l \tag{3.5}$$

which has periodic solutions $\theta(t)$ and $\dot{\theta}(t)$. The Lagrangian, and hence the Hamiltonian, of the pendulum is not dependent on time explicitly, so the pendulum's energy is conserved. The pendulum will perform motion along a closed curve $\frac{1}{2}ml^2\dot{\theta}^2 + mgl\cos\theta = E$ in phase space, i.e. the motion of the pendulum will be confined to a constant energy path.

In the previous discussion we neglected friction that the pendulum experiences during its motion. Due to friction, part of the pendulum's kinetic energy is transferred to its environment in a form of heat, and oscillations are damped. We may assume that dissipative friction force acts on the pendulum, and we may take it to be simply proportional to the pendulum's velocity $Q \propto \dot{\theta}$. This is a rough approximation, but it is quite sufficient for describing general properties of dissipative systems. The

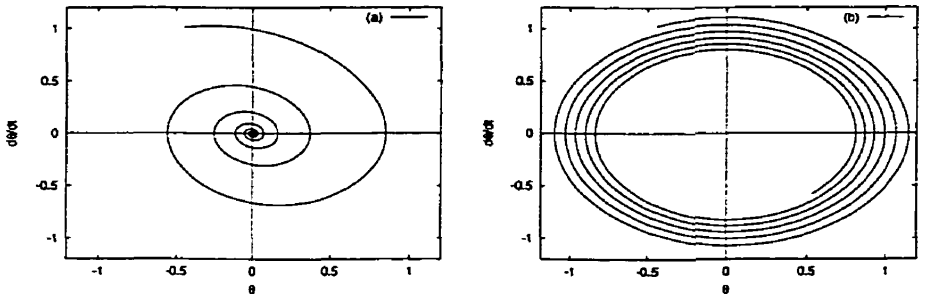

Figure 3.1: Trajectory of a damped pendulum in phase space. (a) $\lambda = 0.25$, (b) $\lambda = 0.02$

dissipative force is then $Q = -\eta\,\dot{\theta}$ ($\eta > 0$), where the minus sign indicates that friction resists the motion (otherwise, the system would acquire energy instead of losing it). If we substitute this into equation (3.4), along with the Lagrangian of the undamped pendulum we will get the equation of motion to be:

$$\ddot{\theta} + \lambda\dot{\theta} + \omega_0^2 \sin\theta = 0, \quad \lambda = \frac{\eta}{ml^2} \tag{3.6}$$

The trajectory in phase space now spirals toward the origin, which is in this case the attractor of the system. The dissipative coefficient λ determines how fast a trajectory will reach the attractor. One can see from fig. (3.1) that for a friction coefficient $\lambda = 0.25$ the trajectory reaches the attractor after just several cycles, while after the same time, for $\lambda = 0.02$, the trajectory is still very close to the path of the undamped pendulum. The motion from the initial condition toward an attractor is called the phase transient. Neither damped nor undamped pendula exhibit chaos.

For the case of a damped pendulum the attractor is a fixed point, as it was for the logistic map when $\mu < 3$. Once the phase-space trajectory gets to a fixed point it stays there for the rest of the motion. Unlike the logistic map there are infinitely many attractors for a pendulum – an equally legitimate attractor for a damped pendulum is any fixed point $(2k\pi, 0)$, where $k = 0, 1, 2, ...$, because the pendulum may perform several full rotations before it settles down to its stable equilibrium position. Each

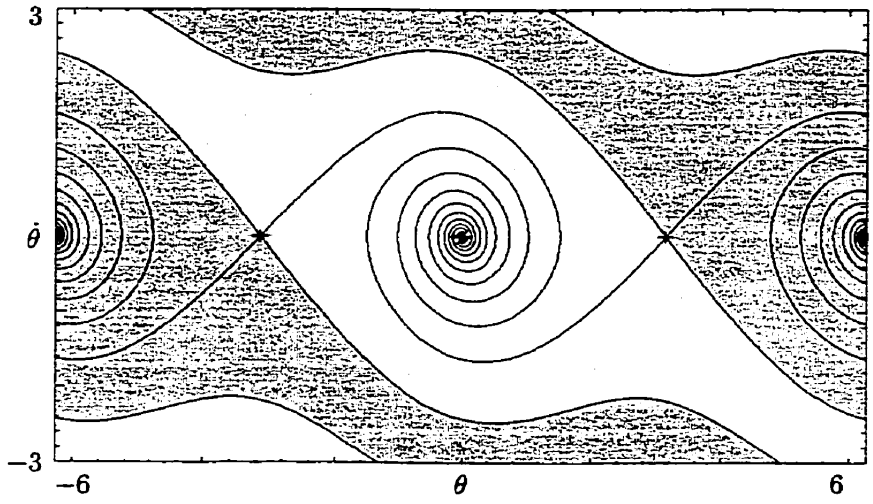

Figure 3.2: Basins of attraction for a damped pendulum.

of these attractors has its respective basin of attraction. Basins of attraction are invariant manifolds of stable fixed points. Three consecutive attractors along with their basins are presented in figure 3.2.

If we assume that the pendulum is hung on a massless rigid rod we will be able (at least theoretically) to stand upside down in its unstable equilibrium position. Fixed points $((2k+1)\pi, 0)$ that correspond to unstable equilibrium are called saddle points. Saddle points are different from repellers described for logistic map (Sec. 2.1) because there is a set of initial conditions that would bring the system to the saddle point. Such a set represents a stable invariant manifold of that point. The set of initial conditions that would bring a damped pendulum to its upright position forms a curve in the phase space which is called a separatrix. Separatrices are basin boundaries and for a damped pendulum they are smooth curves. Any other point within the basin of attraction, arbitrary close to separatrix will be repelled from it toward the attractor for that basin. Hence, in any one-dimensional section of the phase space the separatrix or saddle point itself will appear as a repeller, similar the to repeller in point zero for a logistic map.

Saddle points have their unstable invariant manifold as well. An unstable manifold is a set of initial conditions that would bring the system to the saddle point when integrated backward in time. In Figure 3.2 unstable manifolds are shown as curves spiraling around stable equilibria. One should note that attractors are part of the unstable manifold.

Because they have both, stable and unstable invariant manifolds saddle points are very important for studying dynamics of a system. Later, in Section 4.5 we shall use them to partition phase space in order to develop two-dimensional symbolic dynamics.

3.2 Strange Attractors

The main characteristic of chaotic systems is a sensitivity to initial conditions. Small changes in the initial conditions will eventually result in significant changes in the system's behavior later on. Therefore, initially close trajectories in a phase space should diverge if a system exhibits chaos. As a rule, trajectories in a phase space are restricted to some bounded region, either a "surface" of constant energy or to an attractor. Trajectories that diverge toward infinity usually do not represent any physical process.

A very important consequence of classical determinism is that trajectories in phase space must not intersect. Otherwise, a dynamical system with initial conditions in an intersection of a trajectory could be found in two or more different states later, so the system would be indeterministic. It should be noted that this is fundamentally different from period doubling as observed for the logistic map. Period doubling is a completely deterministic phenomenon, and lack of predictability is due to the high sensitivity to the initial conditions.

It seems impossible to satisfy all of these conditions in a 2-dimensional phase space. Indeed, the Poincaré-Bendixon's theorem [42] says that the attractor of a dynamical system with a 2-dimensional phase space can be either single point - like

for damped pendulum - or a limit cycle (e.g. figure 3.3). Hence, any motion in the phase plane eventually becomes either stationary or periodic. It appears that the minimal dimension of phase space where chaos can occur is 3.

Let us get back to the pendulum. If we drive a damped pendulum with some harmonic force $F(t) = F_0 \cos \omega_D t$ its equation of motion will take the form:

$$\ddot{\theta} + \lambda\dot{\theta} + \omega_0^2 \sin\theta = \frac{F_0}{ml^2}\cos(\omega_D t) \tag{3.7}$$

This is equivalent to adding a term $\theta F(t)$ to the pendulum's potential energy [53], so now the Lagrangian is explicitly time-dependent. That means that points in phase space $(\theta, \dot{\theta})$ do not uniquely represent states of the system, but rather stand for a number of different states where the system can be found at different times t. In order to define an appropriate phase space we introduce a new generalized coordinate $\phi = \omega_D t$, and substitute it into the Lagrangian. The Lagrangian is now time-independent, and each point of the 3-dimensional phase space $(\theta, \dot{\theta}, \phi)$ represents only one state in which the pendulum can be found. This is not just a mathematical way to write Lagrange's function in a more convenient form. The driven pendulum has to consist of a simple pendulum coupled with some driving device, which has one degree of freedom relevant to the pendulum's motion. Therefore, a driven pendulum has 2 degrees of freedom, and its motion can be described in a 4-dimensional phase space $(\theta, \dot{\theta}, \phi, \dot{\phi})$, where θ and ϕ are position coordinates of a simple pendulum and the driving device respectively. At the beginning we assumed that the motion of the driving device is constant, so trajectories of the system will lie in a phase subspace $\dot{\phi} = \omega_D$, where ω_D is constant. Hence, the 3-dimensional phase space $(\theta, \dot{\theta}, \phi)$ is sufficient and necessary for describing the motion of a driven pendulum. However, projections in $(\theta, \dot{\theta})$ plane still remain a useful tool for exploring its properties.

Equation (3.7) is a non-linear second-order differential equation, that has to be solved numerically. Therefore, we may want to write this equation in a dimensionless form, which is more suitable for numerical calculation. If we express time in units

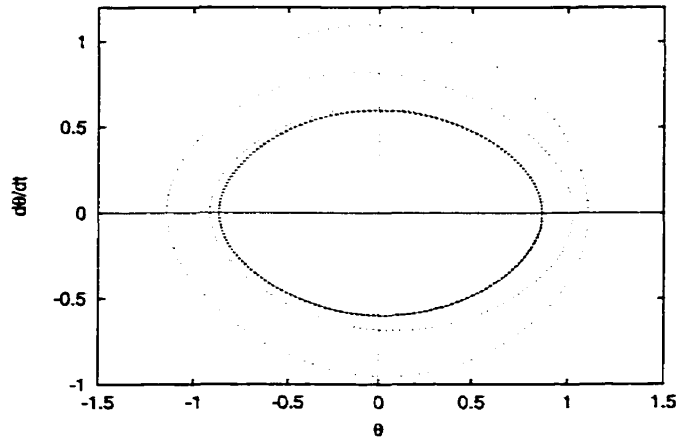

Figure 3.3: Trajectory of a driven damped pendulum in phase space. After the initial transient trajectory settles down at the attractor

$1/\omega_0$, and introduce a dimensionless time-variable $\tau = \omega_0 t$, (3.7) will take the form:

$$\ddot{\theta} + \frac{1}{Q}\dot{\theta} + \sin\theta = f\cos(\omega_d \tau), \tag{3.8}$$

where $Q = \omega_0/\lambda$, $f = F_0/(ml^2\omega_0^2)$, and $\omega_d = \omega_D/\omega_0$ are three dimensionless parameters that correspond to the friction coefficient, drive force amplitude, and drive force frequency, respectively. Of course, it is a mere coincidence that the parameter space for this driven pendulum has the same dimension as its phase space.

Let us choose parameters to be $Q = 1.48$,$f = 1.72$, and $\omega_d = 2/3$. The trajectory of the driven pendulum in phase space $(\theta, \dot{\theta})$ spirals towards and asymptotically reaches the attractor (fig.3.3), like for the case of a damped pendulum (fig.3.1). The difference is that now the attractor is a limit cycle, not a single point. The limit cycle is actually a closed curve in a 3-dimensional phase space, as is shown in figure (3.4a). It takes some imagination though to see this figure as a closed curve. One has to bear in mind that the phase space from $\phi = 2\pi$ continues in $\phi = 0$, and from $\theta = \pi/2$ in $\theta = -\pi/2$.

For a finite value of Q the trajectory will get arbitrarily close to the attractor after

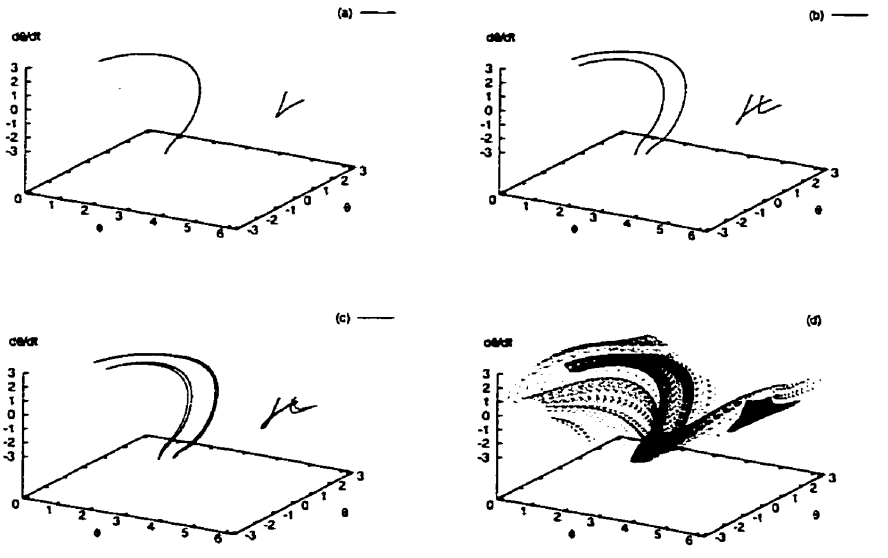

Figure 3.4: Attractor for the driven pendulum: (a) limit cycle, (b) after period doubling, (c) after period quadrupling, (d) chaotic attractor.

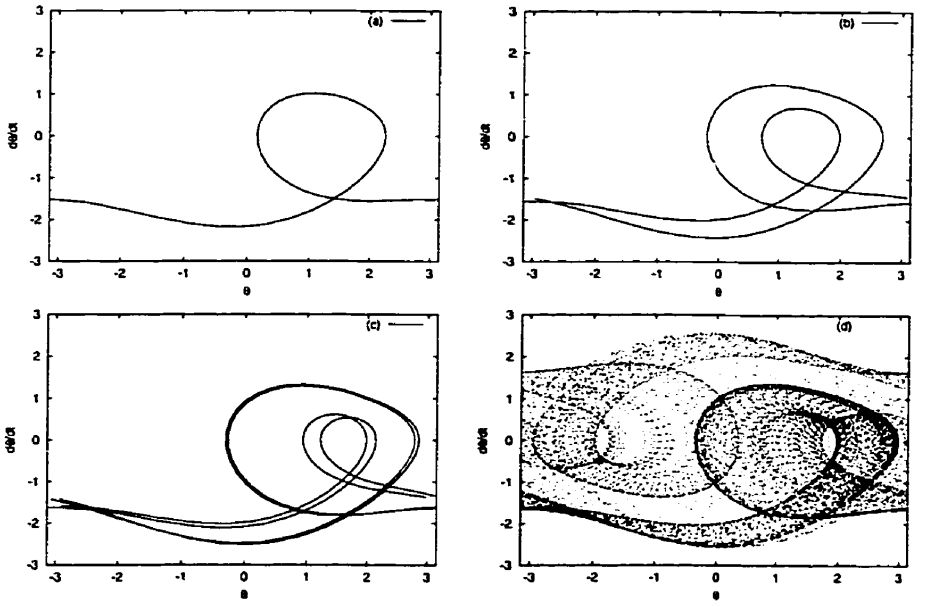

Figure 3.5: Projections of pendulum's attractors (Fig. 3.4) in $(\theta, \dot{\theta})$ plane respectively.

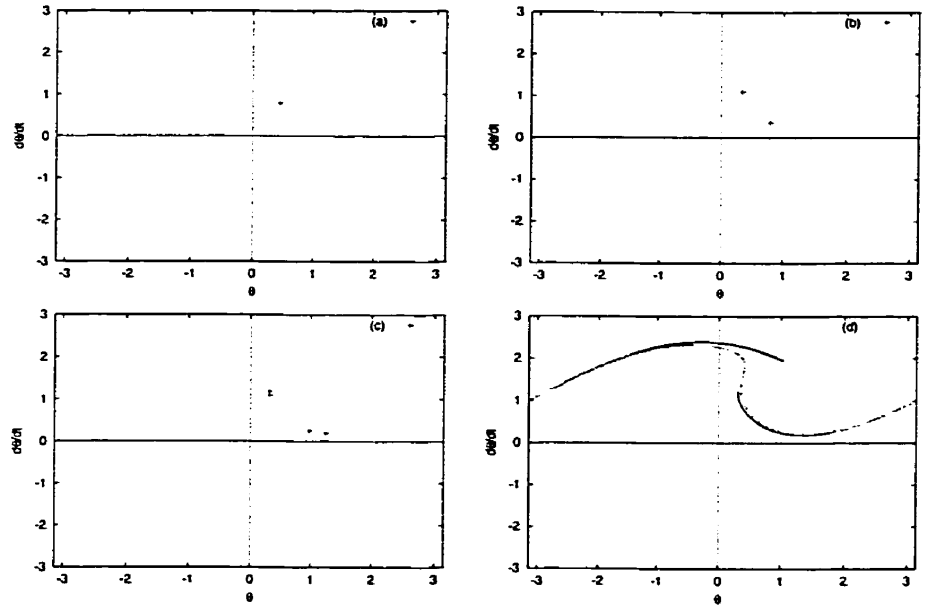

Figure 3.6: Poincaré sections at $\phi = 0$ of pendulum's attractors (Fig. 3.4) respectively. Points representing limit cycles are enlarged for clarity.

a sufficiently long time. In practical numerical calculations the trajectory usually reaches the attractor within the limits of uncertainty after just several drive cycles. We may therefore assume that the motion will be performed along the attractor. For our choice of parameters it means that pendulum's trajectory eventually "gets caught" at the attractor and retracts itself every drive cycle. The pendulum hence exhibits periodic motion in time with period $2\pi/\omega_d$.

Now, if we increase the dissipative parameter to $q = 1.52$ the attractor changes its shape (figures 3.4b and 3.5b) so that the limit cycle is closed after two drive cycles instead of one, i.e. the trajectory now retracts itself every second drive cycle. The motion is still periodic, but its period has doubled to $4\pi/\omega_d$. For $q = 1.544$ there is another period doubling (figures 3.4c, 3.5c), and the period of the limit cycle is now $8\pi/\omega_d$. Indeed, here we observe a period doubling route to chaos for a driven pendulum that is the analog to the period doubling route for a logistic map.

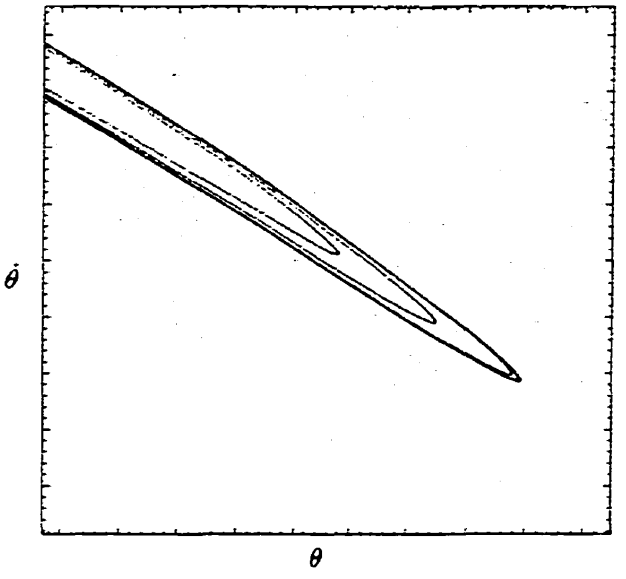

Figure 3.7: Top sheet of a chaotic attractor in Figure (3.6d) enlarged.

Finally, at $q = 1.56$ the system is chaotic. Regardless of the initial conditions the pendulum's trajectory asymptotically reaches a bounded region in the phase space and goes along it continuously, never repeating itself. The bounded region is called the chaotic attractor. The trajectory will pass through any point of the attractor after a sufficiently long time. In other words, for an infinitely long period of time the trajectory will cover the whole attractor. This fact has great practical importance, because plotting the trajectory in the phase space for a long time will give us the shape of the attractor. However, neither its 3-dimensional picture (Fig. 3.4d), nor its 2-dimensional projection (Fig. 3.5d) gives us a lot of information about the attractor's geometry. Apparently, the chaotic attractor has a fairly complex structure, and it is due to the demanding conditions the attractor has to satisfy.

Since the system is dissipative, a volume element in phase space is not conserved during the motion, and in fact vanishes after a very long time. Therefore the volume of the attractor has to be zero, or in other words its dimension has to be smaller than the dimension of the phase space itself. Furthermore, trajectories starting from

infinitesimally close points will diverge, because the system exhibits chaos, and after a sufficiently long time will be found in two macroscopically distant points on the attractor. This means that if the trajectory approaches the chaotic attractor in a slightly different way it will later go along it in quite a different fashion. Finally, the trajectory must not intersect itself nor with any other trajectory starting from different initial conditions, which is a fundamental property of a phase space.

It is obvious that it is impossible to satisfy all the above mentioned conditions if the chaotic attractor is some 2-dimensional surface. However, its dimension has to be smaller than 3, hence we may conclude that chaotic attractor has to have fractional dimension, i.e. it is fractal.

A very useful tool for exploring chaotic attractors are Poincaré sections. Poincaré sections provide us with images of the attractor in a $(d-1)$-dimensional hyperplane of d-dimensional phase space. The hyperplane should be chosen so that it is approximately perpendicular to the trajectories in phase space. Sections parallel to the trajectories or those which are crossed by the same trajectory more than once will not give us useful information about the attractor and are not Poincaré sections. Poincaré sections of 3-dimensional phase spaces are of particular use, because they are easily readable 2-dimensional graphs. A correct choice for Poincaré section of a driven pendulum is a section in $\phi = C$ plane, $C \in [0, 2\pi)$. While the motion is periodic with a period of the drive force, a trajectory crosses this plane always at the same point, so the Poincaré section is just one dot (Fig. 3.6a). After period doubling the trajectory crosses the plane at two different points, and the Poincaré section is pair of dots (Fig. 3.6b). The next period doubling will be represented by a four-dot Poincaré section like in Figure (3.6c), and so on. Since the attractor of the pendulum that exhibits chaos is a fractal with a dimension between 2 and 3 its Poincaré section will be a fractal with a dimension between 1 and 2. With a Poincaré section we actually chose to observe the geometric form of a smaller dimension that contains the same amount of information about the motion. Unlike Figures (3.4d)

and (3.5d), the fractal structure and repeating patterns can be revealed by scanning a Poincaré section of the chaotic attractor. Figure 3.7 shows an enlarged top sheet of the chaotic attractor in Figure (3.6d). One can see that chaotic attractor of a driven pendulum is formed by an infinite sequence of stretching and folding of a surface in the pendulum's 3-dimensional phase space. This stretching and folding pattern is sometimes called Baker's transformation because of its similarity with kneading a dough. This is common for chaotic attractors, and it is the way to reconcile at first glance contradictory conditions imposed – trajectories have to be confined to a bounded region and to diverge exponentially at the same time.

3.3 Basins of Attraction

In Section 3.1 we found that a simple damped pendulum has an infinite number of attractors at points $(2k\pi, 0)$, where $k = 0, \pm 1, \pm 2, \ldots$ (Fig. 3.2). Phase space of a damped pendulum is two-dimensional, and basin boundaries are smooth, one-dimensional stable manifolds of saddle points $((2k+1)\pi, 0)$. Infinite number of co-existing attractors is a consequence of a pendulum's periodic potential energy, and occasional jumps from one to another basin correspond to the pendulum making full turns around its suspension point. However the actual position of the pendulum does not change when it moves from one basin to another, and we can define slightly different, but equally valid phase space, by changing pendulum position coordinate like $\theta \to \theta \mod 2\pi$. With such a representation we remove multiple basins and are able to describe the pendulum's behavior within a single basin of attraction. Therefore coexistence of attractors in the case of a damped pendulum depends on how we choose phase space coordinates and does not depend on system's parameters λ and ω_0. Nevertheless, creation and destruction of coexisting attractors with the change of system's parameters does indeed occur for nonlinear systems under certain circumstances. We shall describe these phenomena in the example of a driven pendulum.

Since phase space of a driven pendulum is 3-dimensional, basins of attraction are also 3-dimensional regions in the phase space. Same for attractors, it is convenient to study basins of attractions in a Poincare section $\phi = \text{const}$. The shape of a Poincare section of the basin of attraction for a driven pendulum resembles the shape of the basin of a simple damped pendulum as long as the driving force amplitude is small. The attractor for the system is a period-one limit cycle, which is represented by a single dot, and basin boundaries are smooth sheets, which appear as a smooth lines in the Poincare section.

As the drive force amplitude increases the pendulum performs full rotations during its motion. For certain parameter symmetry breaking occurs [13, 34, 43, 61] in the sense that the average angular velocity $\langle\dot{\theta}\rangle$ becomes different than zero, i.e. the pendulum starts "winding" in one direction. Symmetry breaking usually precedes a period doubling cascade that leads to pitchfork chaos [13]. Since the pendulum is symmetric with respect to the winding direction, and so is the driving force (see Equation 3.8), along with symmetry breaking the limit cycle splits into two – one winding in positive and other in negative direction. The two new attractors are created with their respective basins (Fig. 3.8a). Separatrix between the basins is fractal in nature, showing a characteristic stretch and fold pattern. The fractal nature of basin boundaries, i.e. stable manifolds, indicate the presence of an infinite number of saddle orbits, which could not be detected using simple simulations like in Figures 3.4a-3.6a. Therefore, although the motion of the driven pendulum described in Figure 3.8a is relatively simple, the underlaying dynamics is fairly complex.

With the increase of parameter Q, the driven pendulum goes through a sequence of period doublings (Figs. 3.4-3.6) and becomes eventually chaotic. At the same time the number of new unstable orbits increases, and basins become more interwoven, i.e. fractal dimension of basin boundaries increases (Fig.3.8b).

For $q = 1.559\ldots$ a crisis occurs, as attractors expand in their size and collide with basin boundaries. The two chaotic attractors cease to exist separately, and conjoin

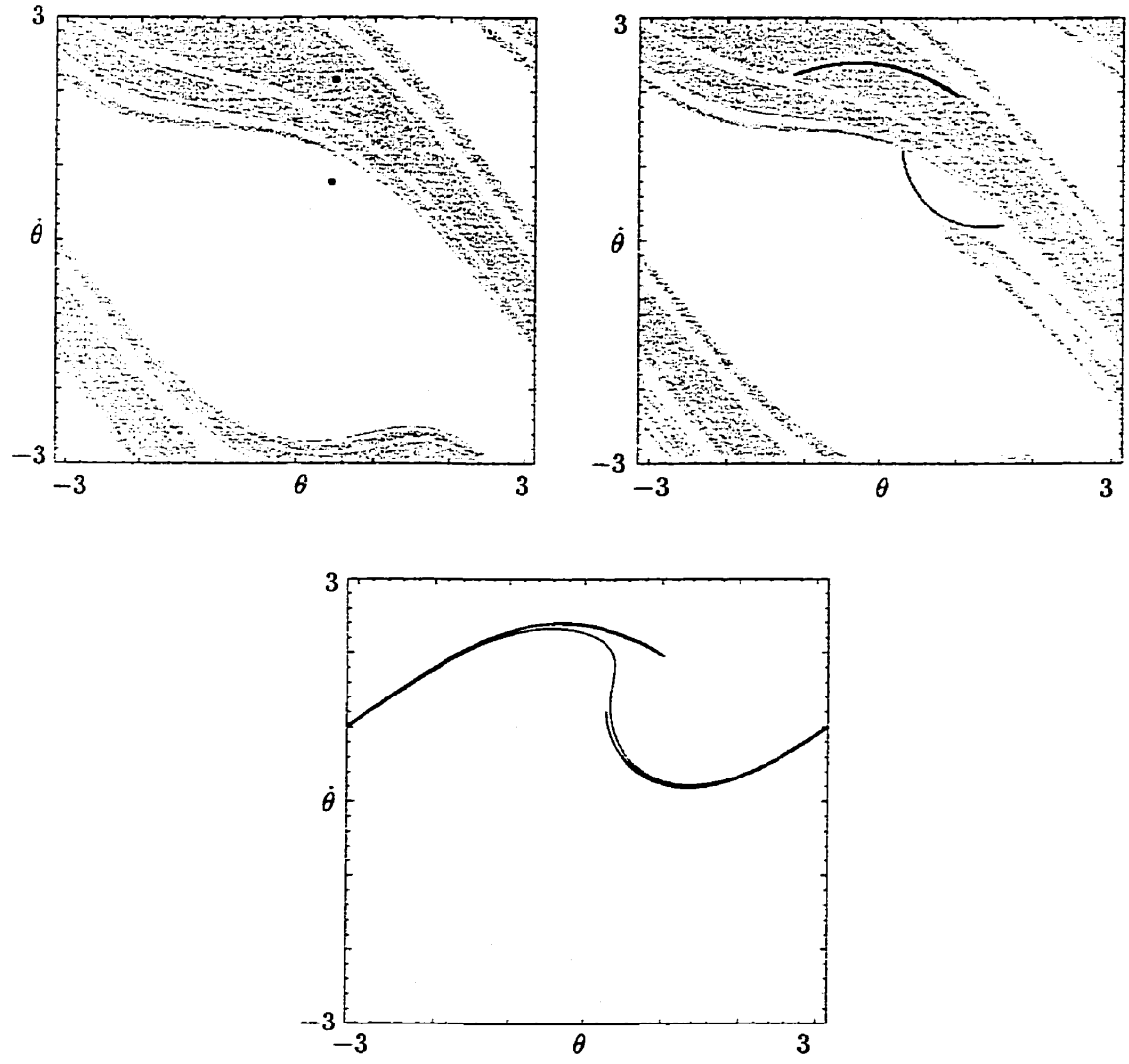

Figure 3.8: Evolution of basins of attraction with change of system's parameter. Two coexisting limit cycles at Q=1.48 (top left). Points representing limit cycles are enlarged for clarity. Two chaotic attractors at the verge of crisis at q=1.555 (top right). Two chaotic attractors conjoin after crisis at Q=1.56 (bottom).

into a single attractor. The newly created attractor expands suddenly in size, as it includes now all of unstable orbits which were previously lying at basin boundaries.

Note on Numerical Methods. It is possible to determine basins of attraction for the driven pendulum by exploring its phase locked modes [34]. After symmetry breaking occurs the angular velocity of the pendulum becomes locked to one of two locking values. Each of these values correspond to the motion over one of two attractors, hence by distinguishing initial conditions that lead to one or another average angular speed we can determine the basin of attraction. We used this algorithm in our research, however figures showing basins of attraction are plotted using package *Dynamics 2* [68]. This package uses more general, but a bit slower "BA" method. We used it because the quality of figures was better than with any other software tool available to us at the time.

3.4 Bifurcation Graphs

A bifurcation graph of the logistic map shows evolution of the logistic map's attractor with the change of parameter μ (fig. 2.6). We are able to give such a comprehensive description of the system's behavior by a 2-dimensional diagram since this simple system is characterized by only one parameter, and its state is determined by only one variable x. It is much more difficult to describe evolution of an attractor for the system with more than one parameter or with multi-dimensional state-space. For the driven pendulum we have a 3-dimensional state space as well as 3-dimensional parameter space. It seems hardly possible to construct a diagram that would describe relations among all of these six values. Usually bifurcation graphs for multi-dimensional dynamical systems are done as a plot of one variable against one parameter, while other parameters are kept constant. Combining bifurcation graphs for different variable-parameter pairs help us determine chaotic regions in parameter space for a particular system. Bifurcation graphs also show us routes to chaos, periodic windows and crisis

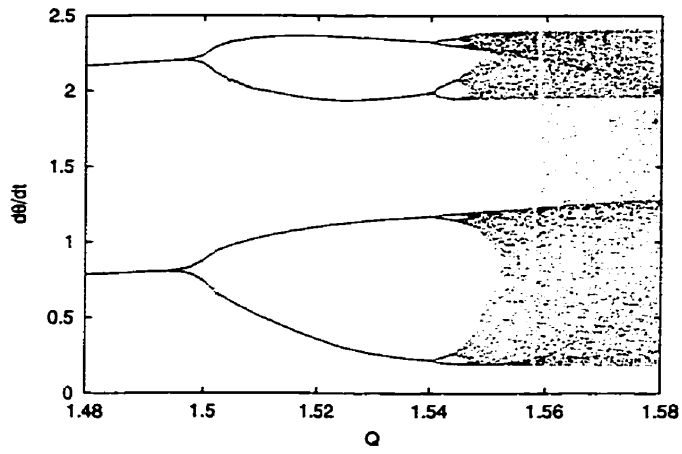

Figure 3.9: Period doubling cascade of the driven pendulum.

that occurs with change of parameters of a dynamical system.

For the bifurcation diagram of a driven pendulum it is usually angular velocity $\dot{\theta}$ that is plotted against a parameter. Here we actually plot the projection of a Poincaré section to the $\dot{\theta}$-axis for each parameter value. In that way the diagram still gives us basic qualitative information about evolution of the pendulum's attractor with the change of a parameter.

A period-doubling cascade of the driven damped pendulum is always preceded by symmetry breaking [34] that results in creation of a pair of attractors from a single attractor. Correspondingly, the basin of attraction of the single attractor gets divided in two. Since the two basins are interwoven, with the change of parameter Q over wider range of values, we occasionally switch from one basin to another, which is manifested in sudden changes in the bifurcation diagram. The generally accepted way to avoid this inconvenience is to superpose bifurcation diagrams for two or if necessary more sets of initial conditions and therefore obtain a diagram that describes evolution of both attractors simultaneously. A caution in interpretation of these diagrams is then needed. For example, at $Q = 1.48$ we do not have a period-2 limit cycle, but two coexisting period-1 cycles.

The route to chaos described in Section 3.2 can be presented by the bifurcation diagram in figure 3.9. Each period doubling corresponds to a pitchfork bifurcation in the graph. In the case of a driven pendulum such a route is the exception than a rule. Period doubling routes are usually intercepted by intermittent chaos [13], and cascades are incomplete. Bifurcation diagrams equally well describe intermittent chaos and sudden changes in attractors due to crises. An interior crisis in the driven pendulum for $Q = 1.56$ is clearly seen in bifurcation diagram 3.9.

3.5 Power Spectra

Spectral analysis is used in nonlinear dynamics to distinguish between chaotic and very complex forms of periodic motion. Sometimes periodic motion with a long period seems quite irregular, and it is virtually impossible to figure out a qualitative difference with chaotic motion from their respective time evolutions. Power spectra of these two motions are on the other hand significantly different. While periodic motion usually consists of just a few harmonics, the power spectrum of chaotic motion is a broad band of frequencies.

We can use power spectra to observe a period doubling route to chaos. Simple periodic motion will show only one peak in the power spectrum at frequency $\nu = 1/T$, and perhaps peaks at integer multiples of ν. In figure 3.10 we show the power spectra for a driven pendulum. Frequency is expressed in units of drive frequency ω_d. When the pendulum exhibits periodic behavior (fig. 3.10a) the power spectrum has peaks at integer multiples of drive frequency only. The peak at $\nu = 0$ indicates that symmetry is broken, and that a period doubling cascade follows. With the change of system parameters, period doubling occurs and integer multiples of $\omega_d/2$ are present in the power spectrum (fig. 3.10b). The next period doubling will bring peaks at frequencies that are multiples of $\omega_d/4$ (fig. 3.10c) in the power spectrum and so on. Finally, at the onset of chaos we obtain a band of frequencies (fig. 3.10d). Although the chaotic

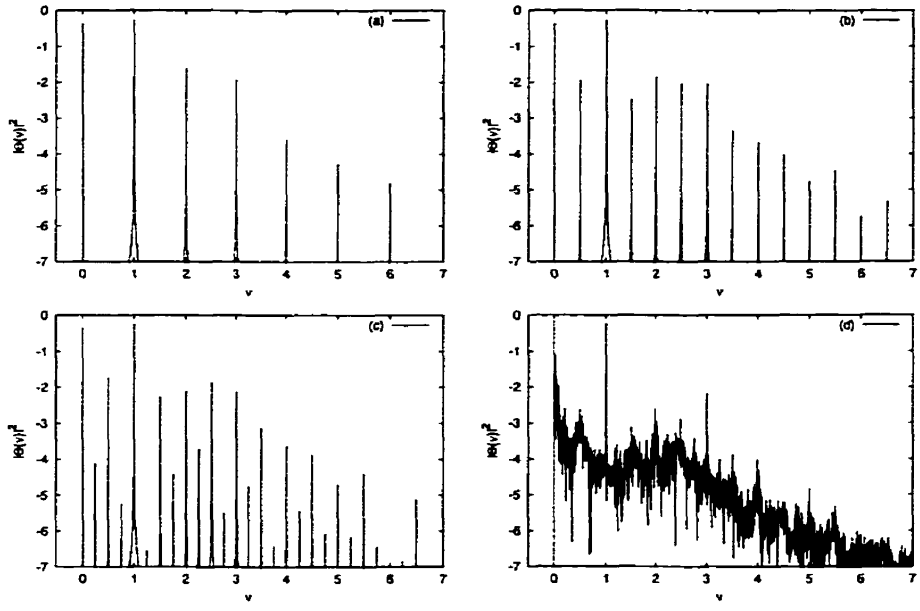

Figure 3.10: Period doubling cascade seen through power spectra. (a) $Q = 1.48$, (b) $Q = 1.52$, (c) $Q = 1.544$, (d) $Q = 1.56$.

spectrum looks like some kind of "pink" noise it is not continuous, like it is the case for a random system. The way it is created – through a sequence of period doublings – indicates it has Cantor-like structure. It should be noted that the peak corresponding to the drive frequency can be distinguished even in a chaotic spectrum.

Spectral analysis is of particular use when we deal with systems that exhibit quasiperiodic motion. Quasiperiodic behavior occurs, for example, when the motion is a superposition of two or more periodic motions whose frequency ratio is an irrational number, i.e. whose frequencies are incommensurate. The trajectory for the system then never retracts itself, and the motion is not periodic. In figures 3.11a and 3.11c two time series of apparently aperiodic functions are presented. However, the former represents relatively simple motion consisted of two incommensurate harmonics (fig. 3.11b), while the latter is a very complex, chaotic solution of a driven pendulum (figs. 3.11d and 3.10d).

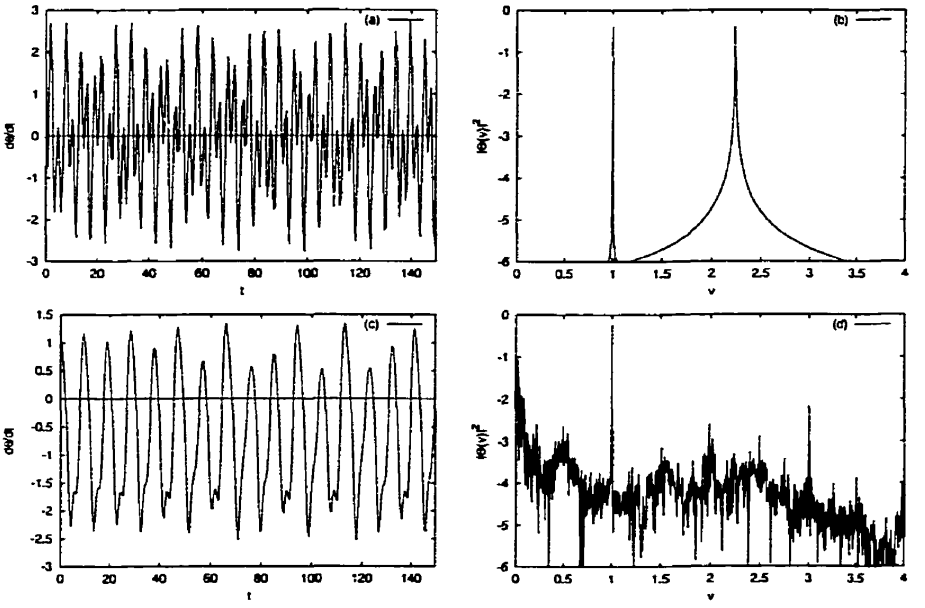

Figure 3.11: Power spectra of chaotic and quasiperiodic motion.

Although a broad power spectrum is not proof of chaos it is usually a reliable indicator of whether or not the motion is chaotic. Spectral analysis is widely used in the theory of chaos because it is equally well applicable to both experimental and numerical data.

3.6 Lyapunov Exponents

We introduced concept of Lyapunov exponents in Section 2.3 at the example of a logistic map. We demonstrated that Lyapunov exponents measure the average rate at which initially close trajectories in phase space diverge from each other. They are used to characterize stability of a dynamical system with respect to a small perturbation of its phase space trajectory. In the same way like for a discrete map Lyapunov exponents for a dynamical flow are defined as an exponential growth rate

of an infinitesimal perturbation of the initial condition:

$$\lambda = \lim_{t\to\infty} \frac{1}{t} \ln \frac{\delta x_i(t)}{\delta x_i(0)} \tag{3.9}$$

Here $\delta x_i(t)$ denotes the separation of two trajectories, and the index i stands for the direction of growth in phase space or Lyapunov direction [84]. The number of Lyapunov directions correspond to the dimensionality of phase space. A set of Lyapunov exponents for a multidimensional dynamical system is also called a Lyapunov spectrum.

Let us elaborate on Lyapunov exponents for one-dimensional dynamical flow first. We write the equation of motion for a one-dimensional dynamical flow as:

$$\dot{x}(t) = f(x(t)) \tag{3.10}$$

and denote its solution with $x^*(t, x_0)$, where $x_0 = x^*(0)$ is the initial condition. Since this is one-dimensional problem there is only one Lyapunov exponent. From expression (3.9) we may conclude that a negative Lyapunov exponent indicates an exponentially stable steady state solution. A positive exponent indicates an exponential instability. Any other type of solution $x^*(t, x_0)$ would be attributed to a zero Lyapunov exponent. Unlike 1-dimensional maps, 1-dimensional flow cannot exhibit chaos. Numerical values of the exponent specifies the exponential rate at which trajectory converges to or diverges from equilibrium point.

Estimation of Lyapunov exponents for a one-dimensional case is straightforward. If we vary equation (3.10) around its solution x^* by some $\delta x(t)$ we get

$$\delta\dot{x}(t) = \frac{\partial f}{\partial x}\Big|_{x=x^*} \delta x(t) \tag{3.11}$$

From the equation above we obtain:

$$\int_0^t \frac{df(x)}{dx}\Big|_{x=x^*} d\tau = \int_0^t \frac{\delta\dot{x}(\tau)}{\delta x(\tau)} d\tau = \ln \frac{\delta x(t)}{\delta x(0)}, \tag{3.12}$$

After substituting this result in definition of Lyapunov exponent (3.9) we get:

$$\lambda(x_0) = \lim_{t\to\infty} \frac{1}{t} \int_0^t \frac{df(x)}{dx}\Big|_{x=x^*} dt \tag{3.13}$$

Here we allow the Lyapunov exponent to be dependent on the initial condition for the solution $x^*(t)$. As we discussed in Section 2.3 Lyapunov exponents are a property of the phase space rather than the particular trajectory. Therefore, when we use them we may drop the initial condition dependence entirely, provided we stay within the same basin of attraction.

For the multidimensional case, estimation of Lyapunov exponents is a bit more complicated, since in our calculations we cannot use expression (3.9) directly any more. We write system of first-order ODEs in a vector form

$$\dot{\mathbf{x}}(t) = \mathbf{f}(\mathbf{x}(t)) \tag{3.14}$$

and we denote its solution with $\mathbf{x}^*(t, \mathbf{x_0})$. By varying this equation we get:

$$\delta\dot{\mathbf{x}}(t) = \mathbf{A}[\mathbf{x}(t)]_{\mathbf{x}=\mathbf{x}^*}\delta\mathbf{x}(t) \tag{3.15}$$

where $\mathbf{A}$ is defined as $A_{ij} = \partial f_i(\mathbf{x})/\partial x_j$. Formally we can integrate (3.15) for $\delta\mathbf{x}(\mathbf{t})$, so we obtain [10, 77]:

$$\delta\mathbf{x}(t) = \mathbf{J}(t)\delta\mathbf{x}(0) \tag{3.16}$$

where

$$\mathbf{J}(t) = Te^{\int_0^t d\tau \mathbf{A}(\tau)} \tag{3.17}$$

Here T stands for time ordering operator as matrices $\mathbf{A}(t)$ do not commute at different times. Matrix $\mathbf{J}$ is called Jacobi matrix of the flow, and is a solution of the equation

$$\dot{\mathbf{J}}(t) = \mathbf{A}[\mathbf{x}(t)]_{\mathbf{x}=\mathbf{x}^*}\mathbf{J}(t) \tag{3.18}$$

for the initial condition $\mathbf{J}(0) = \mathbf{1}$. From (3.9) and (3.16) we find that eigenvectors of $\mathbf{J}$ point to Lyapunov directions and Lyapunov exponents are estimated from magnitudes of eigenvalues of $\mathbf{J}$ as:

$$\lambda_i = \lim_{t\to\infty} \frac{1}{t} \ln |\hat{J}_{ii}(t, \mathbf{x_0})| \tag{3.19}$$

where $\hat{\mathbf{J}}$ stands for the diagonalized Jacobi matrix of the flow. Therefore, in order to estimate Lyapunov spectrum for a n-dimensional system we have to integrate $n \times n$

equations (3.18) along with n equations (3.10), and then solve the eigenvalue problem for $\mathbf{J}$.

This is not a trivial task, though. From expression (3.16) we can see that Lyapunov directions in a general case are not constant in time. Furthermore, all Lyapunov directions tend to collapse along the direction of the largest exponent, since that component of vector $\delta\mathbf{x}(t)$ is dominant. Also, exponential divergence (convergence) of neighboring trajectories in phase space may relatively soon exhaust our computing power, so we can not obtain estimates for sufficiently long time intervals. These problems were studied in works of Benettin at al. [5], and Shimada and Nagashima [80], where an algorithm for calculation of Lyapunov spectrum is presented. It was shown that it is possible to perform suitable re-orthonormalization of eigenvectors of J after each integration step so that the limit 3.9 remains unchanged. In this project we use implementation of that algorithm as given in Ref. [84].

In the case when all Lyapunov exponents are negative trajectories converge from all directions of phase space, and hence terminate eventually at a stable equilibrium point. We say that the attractor of the system is a fixed point. If one exponent is zero and other negative then from (3.19) it follows that trajectories always converge from all but one direction in phase space. The attractor for the system in this case is one-dimensional curve. If the system is further bounded, the attractor is a closed loop, meaning that the system performs periodic motion. Two zero Lyapunov exponents would mean that system's attractor is a two-dimensional surface in phase space, indicating quasiperiodic motion. If at least one Lyapunov exponent is positive, then trajectories of the system separate at exponential rate and we say that the system is unstable. If an unstable system is furthermore bounded we call such a system chaotic.

There is a couple of constraints on Lyapunov exponents values. Haken's theorem [35], states that unless there is an equilibrium point in the phase space, at least one Lyapunov exponent must equal zero. This means that Lyapunov exponents are either

all negative [1] or one or more of them are equal to zero. Another constraint tells us that the sum of all exponents of system (3.14) must equal the expectation value for the dissipation.

If we take determinant of **J** in the expression (3.17) we obtain:

$$\det\mathbf{J} = e^{\mathrm{tr}\int_0^t d\tau \mathbf{A}(\tau)} = e^{\int_0^t d\tau (\nabla\cdot\mathbf{f})(\tau)} \tag{3.20}$$

Since $\det\mathbf{J} = \hat{J}_{11}\hat{J}_{22}\cdots\hat{J}_{ii}$, by taking the logarithm of both sides of the equation above and letting $t \to \infty$ we get:

$$\sum_{i=1}^{n} \lambda_i = \lim_{t\to\infty} \frac{1}{t} \int_0^t (\nabla \cdot \mathbf{f})(\tau)\, d\tau \tag{3.21}$$

Therefore, for a dissipative system the sum of all Lyapunov exponents must have a negative value, while for a conservative system all exponents have to add up to zero. From the equation of motion (3.8) we find that for a driven pendulum sum of all three Lyapunov exponents must equal $\sum_i \lambda_i = -1/Q$.

A Lyapunov spectrum helps us interpret phase space diagrams as it tells us what kind of attractor exists in phase space. It is especially useful for systems with dimension larger than 3, because we can only observe 2-dimensional projections or sections in phase space, so we need some initial guidance how to choose them. It is important to understand that the Lyapunov exponent methods does not provide rigorous mathematical proofs, because we can calculate exponents only for a finite amount of time [2]. We are usually able, though, to interpolate information about a system's stability from finite-time Lyapunov exponent estimation.

3.7 Parametric Resonance

Parametric resonance is a phenomenon that occurs in various cosmological and high energy physics models. It manifests itself as a rapid growth of a physical field at an

[1] According to Haken's theorem it is also allowed to have all exponents positive. However this situation seldom occurs in a physical system, if at all

exponential rate. Recently this phenomenon has been used to explain some physical processes such as reheating in the early universe [50, 46] and in phase transitions in disordered chiral condensates [47]. At the same time a lot of attention has been given to the study of chaotic systems, i.e. systems whose trajectories in phase space diverge exponentially, but at the same time remain within a bounded region. As both types of systems are described by an exponential type of instability one might expect a relationship between the two, and here we investigate quantitatively just such a relationship. We show that for a system exhibiting parametric resonance it is possible to construct an equivalent chaotic system, although the converse is not guaranteed.

3.7.1 Floquet Index

From the general theory of differential equations we know that any second-order linear differential equation

$$\frac{d^2y}{dt^2} + f(t)\frac{dy}{dt} + g(t)y = 0, \tag{3.22}$$

will have two linearly independent solutions. According to Floquet's theorem [67] if $f(t)$ and $g(t)$ are functions periodic in t with a period T, then those solutions will have the form:

$$y(t) = e^{\mu t}P(t), \tag{3.23}$$

where $P(t)$ is periodic function with period T, as well. Therefore, stability of the solution (3.23) is entirely determined by the exponent μ, which is also called the Floquet exponent or Floquet index. There is no general procedure for estimating the Floquet exponent; however, there are a lot of particular cases such as the Mathieu equation where an extensive analysis of the Floquet indices has been done.

3.8 Mathieu Equation

Perhaps the simplest model that exhibits parametric resonance is the Mathieu equation (3.24), which was originally used to describe small oscillations of a pendulum with a vertically driven base.

$$y'' + (A - 2q\cos 2t)y = 0 \tag{3.24}$$

This is a Floquet type equation with two parameters A and q, and it has a solution of the form of Eq. (3.23). The value of the Floquet index μ depends on the equation's parameters. For certain values of A and q (e.g. $A = 2.5$ and $q = 1$) Floquet exponents would be purely imaginary, meaning that the solutions of Eq. (3.23) will both be periodic. Therefore, the solution will be stable, and its trajectory in phase space will remain within a bounded region (see Fig. 3.12a). Otherwise, both Floquet exponents will be purely real, and one of them hence positive. A solution with a positive Floquet exponent is unstable and grows exponentially (see Fig. 3.12b). In some physical models such growth of the field y can be interpreted as a massive production of certain particles. This is also referred to as parametric resonance.

The rate of exponential growth of the solution (i.e. a positive Floquet exponent) can be determined from the graph for $\log|y|^2$ plotted against time t. Since the term in the solution containing a positive exponent is dominant, the slope of envelope of the graph will yield numerical value of 2μ. From Figure 3.13 it is found that $\mu = 0.453 \pm 0.003$, where the parameters are chosen to be $A = 1$ and $q = 1$. Regions of stability in parameter space of the Mathieu equation have been very well studied (see, for example, Ref. [1]). There are bands of stability and instability in the parameter space, and their boundaries are continuous curves.

In analogy with interpreting y as an angle, we impose suitable "winding" conditions on the solution of Eq. (3.24) so that it always stays within segment $[-1, 1]$. We assume that at $|y| = 1$ the magnitude of the field starts to decrease and the velocity y' changes direction: $y' \to -y'$. This condition is rather artificial within

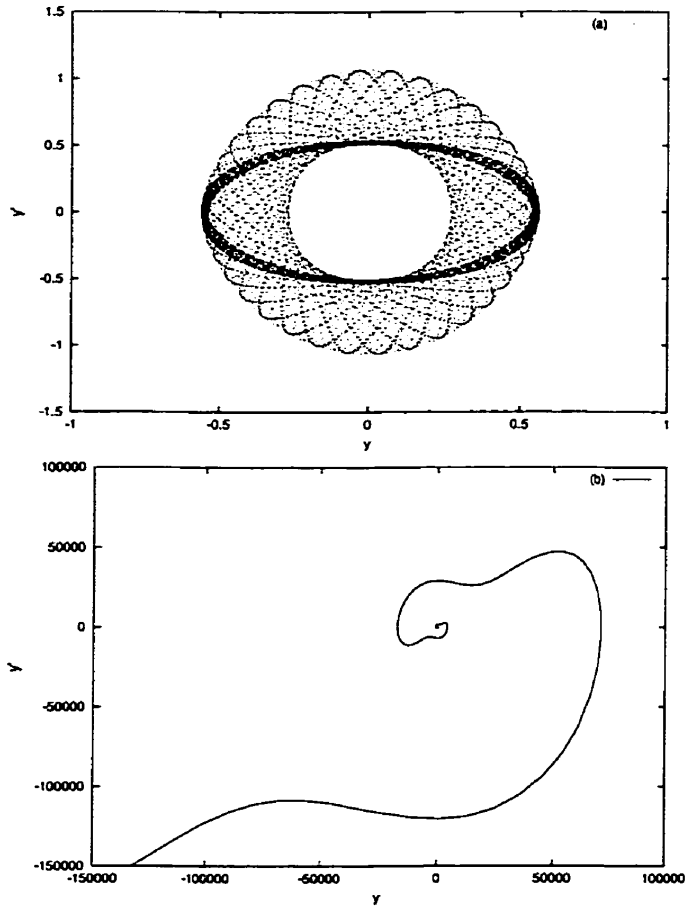

Figure 3.12: Phase space trajectory for the Mathieu equation. (a) $A = 2.5$ and $q = 1$, (b) $A = 1$ and $q = 1$.

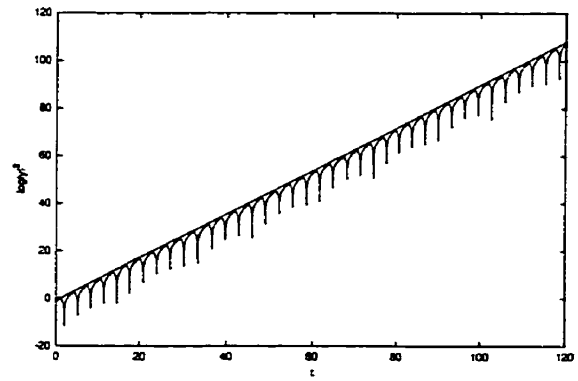

Figure 3.13: Exponential growth of the solution for the Mathieu equation. The Floquet exponent is estimated from the slope to be $\mu = 0.453 \pm 0.003$

the context of parametric resonance as described in Ref. [50, 46]. However, we can think of interpreting this winding condition in terms of a one–dimensional billiard ball whose motion in between bounces is governed by the Mathieu equation (3.24). There is no physical motivation to interpret y as an angle though, since the small angle approximation is not valid for the resonant case.

With this additional nonlinear condition imposed, both stable and unstable solutions are bounded, so parametric resonance does not occur. The stable solution remains periodic and exhibits the same behavior as before (see Fig. 3.14a). The unstable solution, on the other hand, instead of parametric resonance, exhibits chaotic-like behavior (see Fig. 3.14b) which manifests in high sensitivity in change of initial conditions. For this solution we estimated the Lyapunov spectrum, and found the positive Lyapunov exponent to be $\lambda_1 = 0.453 \pm 0.001$, which is the same as the Floquet exponent. This result could be anticipated because the first Lyapunov direction always point to the direction of the fastest growth in phase space. For the Mathieu equation this growth is entirely described by the solution with a positive Floquet exponent. The linearization procedure in the algorithm for the Lyapunov exponents calculation will in a sense "unwind" the trajectory, so that the exponential diver-

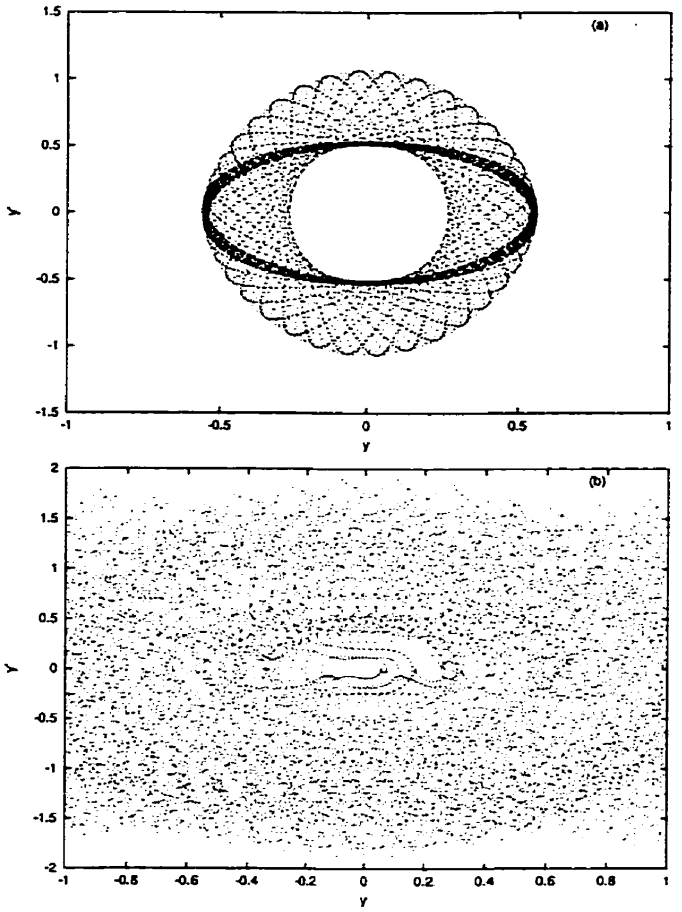

Figure 3.14: Phase space trajectory for the Mathieu equation with appropriate winding condition. The periodic solution (a), $A = 2.5$ and $q = 1$, remains unchanged, while the unstable solution (b), $A = 1$ and $q = 1$, becomes chaotic.

gence measured by the Lyapunov exponent has to be the same as that described by the Floquet index.

3.9 Parametric Resonance Model

If the parameters of the Mathieu equation Eq. (3.24) are not constant, but rather some functions of time, then the solution will eventually switch between regions of stability and instability in parameter space, and therefore phases of quasiperiodicity and exponential growth will interchange during that time. Here is a somewhat simplified system of equations which illustrates such a behavior. Eqs. (3.25, 3.26) may be used to describe the decay of ϕ-particles into χ-particles.

$$\ddot{\chi} + H\dot{\chi} + (m^2 + g\phi^2)\chi = 0 \tag{3.25}$$

$$\ddot{\phi} + (A - 2q\cos 2t)\phi = 0 \tag{3.26}$$

Eq. (3.25) is a Floquet–type of equation, with parameters m and g set near the boundary between the stability and instability regions. Eq. (3.26) is a Mathieu equation which is coupled to Eq. (3.25). If we set the parameters A and q so that Eq. (3.26) has a periodic solution, then the term $g\phi^2$ will periodically drive Eq. (3.25) between its stability and instability regions, and therefore its Floquet exponent will change periodically in time. This is shown in Fig. 3.15, where $\log|\chi|^2$ is plotted versus time. Although the Floquet exponent changes periodically in time, the system spends more time in a region of instability, and parametric resonance occurs. The average value of the Floquet exponent has a positive real part, and its numerical value can be estimated directly from Fig. 3.15.

Now, let us impose the same "winding" conditions like that for the Mathieu equation, so that $\chi \in [-1, 1]$. As before, parametric resonance will not occur, but the field χ will exhibit chaotic–like behavior instead. In order to find the Lyapunov exponent spectrum for this system we need to perform our calculation in 5-dimensional phase

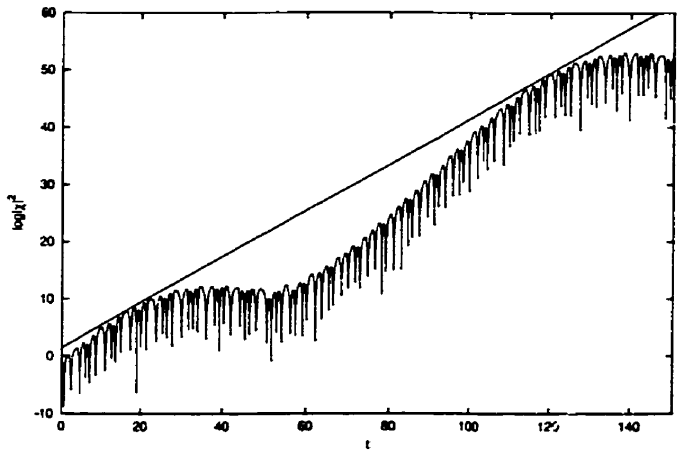

Figure 3.15: Plot of $\log|\chi|^2$ vs. t shows how the Floquet exponent changes during the time. The average Floquet exponent is estimated from the graph to be $\mu_\chi = 0.0973 \pm 0.0007$.

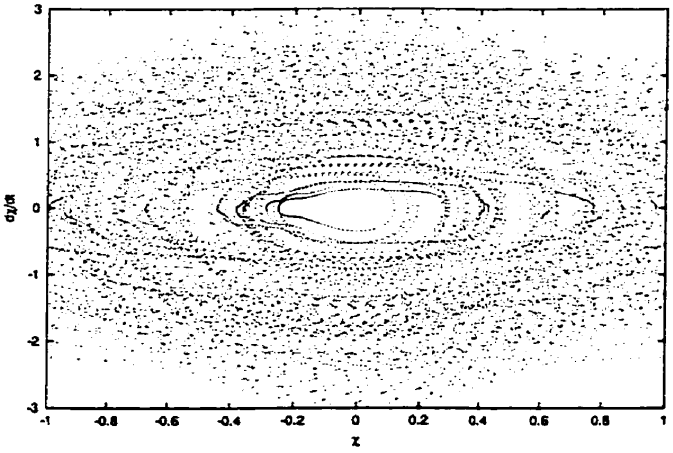

Figure 3.16: Phase space projection of the chaotic pseudo-attractor of Eq. (3.25).

space $(\dot{\chi}, \chi, \dot{\phi}, \phi, t)$. We found two exponents in the spectrum to be positive, and their sum to be $\lambda_1 + \lambda_2 = 0.096 \pm 0.002$, which agrees with the value for average Floquet exponent.

Again, this is an expected result, considering the algorithm for estimation of the Lyapunov exponents. The sum of all positive Lyapunov exponents is an average rate of exponential divergence of the solution of Eq. (3.25). This should be the same as the rate estimated from Fig. 3.15, as the slope there is determined by the average value of Floquet exponent.

If we, however, substitute a chaotic solution of the Mathieu equation into Eq. (3.25), the system will exhibit a very complex behavior. The system will chaotically switch between stability and instability regions so it will be impossible to predict any kind of resonant behavior due to a high sensitivity to change in initial conditions. Furthermore, Eq. (3.25) will not be a Floquet equation any more, and its solution will not have the simple form of Eq. (3.23).

3.10 Conclusion

We demonstrated here that parametric resonance and chaos are two types of exponential instability which are mutually exclusive but related. Starting from a model that satisfies Floquet's theorem and is in a region of parameter space which is exponentially unstable (with a positive Floquet index), we showed that imposing a "winding" type of boundary condition on the field to restrict it to lie within a certain range leads to a model exhibiting chaos, and hence with at least one positive Lyapunov exponent. A quantitative measure of the exponential divergence rate in the two related models of the cases we studied shows that the Floquet exponent is equal to the Lyapunov exponent. Some extensions and applications of this correspondence between these two types of instabilities are currently being studied.

Chapter 4

THE TWO GEARS AND THE ROD

4.1 The Equation of Motion

The system we study consists of two gears and a rod. The first one, the solar gear, has radius R', and is fixed so neither its center of mass can move nor can it rotate around its axis. The second, the planetary gear, is of radius R and is attached to the first gear so when it rotates around its axis at the same time it goes around the fixed gear. We assume that the movable gear is powered by some device which keeps it moving with constant angular velocity ω_d. When the planetary gear rotates for the angle ϕ around its axis it moves around the solar gear for an angle ϕ' (Fig. 4.1). The relation between two angles is

$$R'\phi' = R\phi \tag{4.1}$$

A uniformly dense rod of length L is at one end joined to the fringe of the movable gear. The rod can rotate around the joint, assumed without friction. Both gears and the rod lie in a horizontal plane so the potential energy of the system is constant during the motion. We choose a coordinate system with origin at the center of the fixed gear. The system has two degrees of freedom, and a convenient choice of coordinates are ϕ', the angle that the second gear makes with the x–axis, and ϑ, the angle that the rod makes with the x–axis. Since the potential energy for the system is constant as well as the angular velocity of the planetary gear, the Lagrangian for the system is determined by the kinetic energy of the rod only. A general expression for the kinetic energy for the rigid body that moves in two dimensions is

$$T = \frac{1}{2}\int dm\,(\dot{x}^2 + \dot{y}^2) \tag{4.2}$$

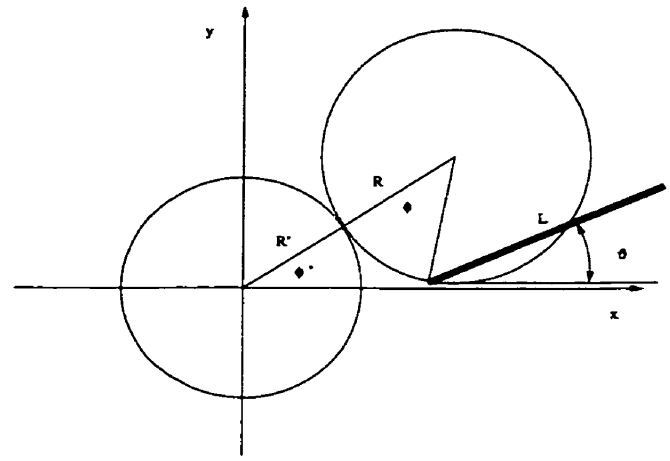

Figure 4.1: Two gears and the rod

We may express the position coordinates for the mass element dm over coordinates ϕ and ϑ as

$$\begin{aligned} x &= (R' + R)\cos\phi' - R\cos(\phi' + \phi) + l\cos\vartheta \\ y &= (R' + R)\sin\phi' - R\sin(\phi' + \phi) + l\sin\vartheta \end{aligned} \tag{4.3}$$

where l is position of the mass element dm at the rod. Deriving x and y over time and eliminating ϕ' rather than ϕ, using (4.1), we get:

$$\begin{aligned} \dot{x} &= -(1+r)R\dot{\phi}\sin r\phi + R(1+r)\dot{\phi}\sin\left[(1+r)\,\phi\right] - l\dot{\vartheta}\sin\vartheta \\ \dot{y} &= (1+r)R\dot{\phi}\cos r\phi - R\dot{\phi}\,(1+r)\cos\left[(1+r)\,\phi\right] + l\dot{\vartheta}\cos\vartheta \end{aligned} \tag{4.4}$$

where $r = R/R'$. Our initial assumption was that angular velocity of the planetary gear was constant $\dot{\phi} = \omega_d$. For simplicity, we will assume that the initial condition is chosen so that $\phi = \omega_d t$. Substituting derivatives (4.4) into (4.2) and integrating over the whole rod, assuming its linear mass is constant, we get the kinetic energy, and therefore the Lagrangian, to be:

$$L = T = \frac{1}{2}I\dot{\vartheta}^2 + \frac{1}{2}(1+r)mLR\omega_d\dot{\vartheta}\left\{\cos(\vartheta - r\phi) - \cos\left[\vartheta - (1+r)\,\phi\right]\right\} \tag{4.5}$$

Here I is the moment of inertia of the rod, and we dropped terms that can be written as a total time derivative of some function and therefore do not contribute to the

Lagrangian. Substituting this Lagrangian into the general expression for the Euler-Lagrange equations of motion of dissipative systems

$$\frac{d}{dt}\frac{\partial L}{\partial \dot{q}_\alpha} - \frac{\partial L}{\partial q_\alpha} = Q_\alpha, \quad \alpha = 1, ..., s \tag{4.6}$$

and choosing ϑ and ϕ for coordinates we obtain the equation of motion to be

$$I\ddot{\vartheta} + \frac{1+r}{2}mLR\omega_d^2 \{r\sin(\vartheta - r\phi) - (1+r)\sin[\vartheta - (1+r)\phi]\} = Q_\vartheta \tag{4.7}$$

where Q_ϑ is some friction force that acts upon the rod, and I is its moment of inertia. If we assume that the friction, as is commonly done for a pendulum, has the simple form $Q_\vartheta = -\eta\dot{\vartheta}$ $(\eta > 0)$, we may write the equations of motion as

$$\ddot{\vartheta} + \frac{\eta}{I}\dot{\vartheta} + \omega_0^2 \left\{\sin(\vartheta - r\phi) - \frac{1+r}{r}\sin[\vartheta - (1+r)\phi]\right\} = 0, \tag{4.8}$$

where

$$\omega_0^2 = r(1+r)\frac{mLR}{2I}\omega_d^2. \tag{4.9}$$

If we introduce now a new variable $\theta = \vartheta - r\phi$ we can bring the equations of motion to the arguably simpler form:

$$\ddot{\theta} + \frac{\eta}{I}\dot{\theta} + \omega_0^2\sin\theta = -\frac{\eta}{I}\omega_d + \frac{1+r}{r}\omega_0^2\sin(\theta - \phi). \tag{4.10}$$

This equation is nonlinear with a coupled term, and must be solved numerically. Therefore, for convenience we will write it in a dimensionless form by introducing the dimensionless time variable $\tau = \omega_0 t$. Equation (4.10) then becomes

$$\ddot{\theta} + \frac{1}{Q}\dot{\theta} + \sin\theta = -\frac{ar}{Q} + \frac{1+r}{r}\sin(\theta - \phi), \tag{4.11}$$

where

$$a = \frac{\omega_d}{\omega_0} = \sqrt{\frac{2L}{3r(1+r)R}}$$
$$Q = \frac{\omega_d}{\eta}\sqrt{r\frac{1+r}{2}mlRI}, \tag{4.12}$$

and

$$\phi = \omega_d t = a\tau. \tag{4.13}$$

Equation (4.11) has a similar form to that of the equation of motion for the driven pendulum, as well as to the Mathieu equation; however, there are some essential differences. The virtual drive frequency a in the normalized equation (4.11) does not depend upon the drive frequency ω_d – the angular velocity of the moving gear – as it is constant which depends only on the dimensions of the rod and gears. On the other hand, the "quality" factor Q is proportional to ω_d, so a change of drive frequency will eventually appear as a change of dissipation in the system.

4.2 Bifurcation Diagrams

Our system has two degrees of freedom, and generally such a system can be described in a four dimensional phase space. For example, we may choose to observe the system in phase space $(\theta, \dot{\theta}, \phi, \dot{\phi})$, where θ and ϕ are the angular position coordinates of the rod and planetary gear respectively. However, since we assume that the planetary gear moves with constant angular velocity ω_d, the attractor for the system lies in the phase subspace $\dot{\phi} = \omega_d$. Therefore, the three dimensional phase space $(\theta, \dot{\theta}, \phi)$, where we take $\theta \in (-\pi, \pi)$ and $\phi \in (0, 2\pi)$, is sufficient to describe the behavior of our system. From the fact that ϕ depends linearly on time we may infer that the attractor will be "smooth" in the ϕ direction, and that all chaotic features, if any, can be observed in the Poincaré section $\phi = \text{const}$. In this way the problem of analyzing this three dimensional dynamical system is reduced to the analysis of a two dimensional map.

In order to explore properties of our system it is necessary to locate regions of chaotic and regular behavior within the parameter space. Bifurcation diagrams show the evolution of the attractor for a dissipative system with a change of the system's parameters. Such diagrams are a convenient tool for a qualitative examination of a

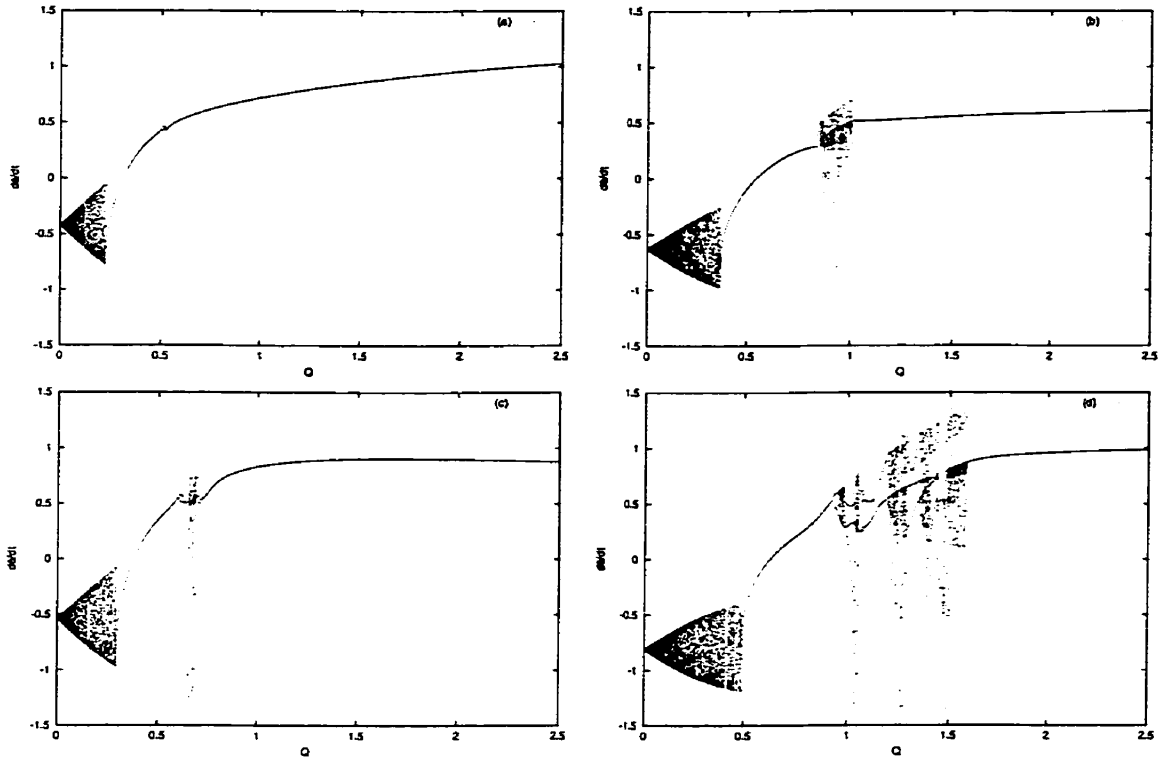

Figure 4.2: Bifurcation diagrams show that periodic motion is dominant over a range of Q for the choice of parameters (a) $a = 0.7$, $r = 0.6$, (b) $a = 0.7$, $r = 0.9$, (c) $a = 0.9$, $r = 0.6$, (d) $a = 0.9$, $r = 0.9$.

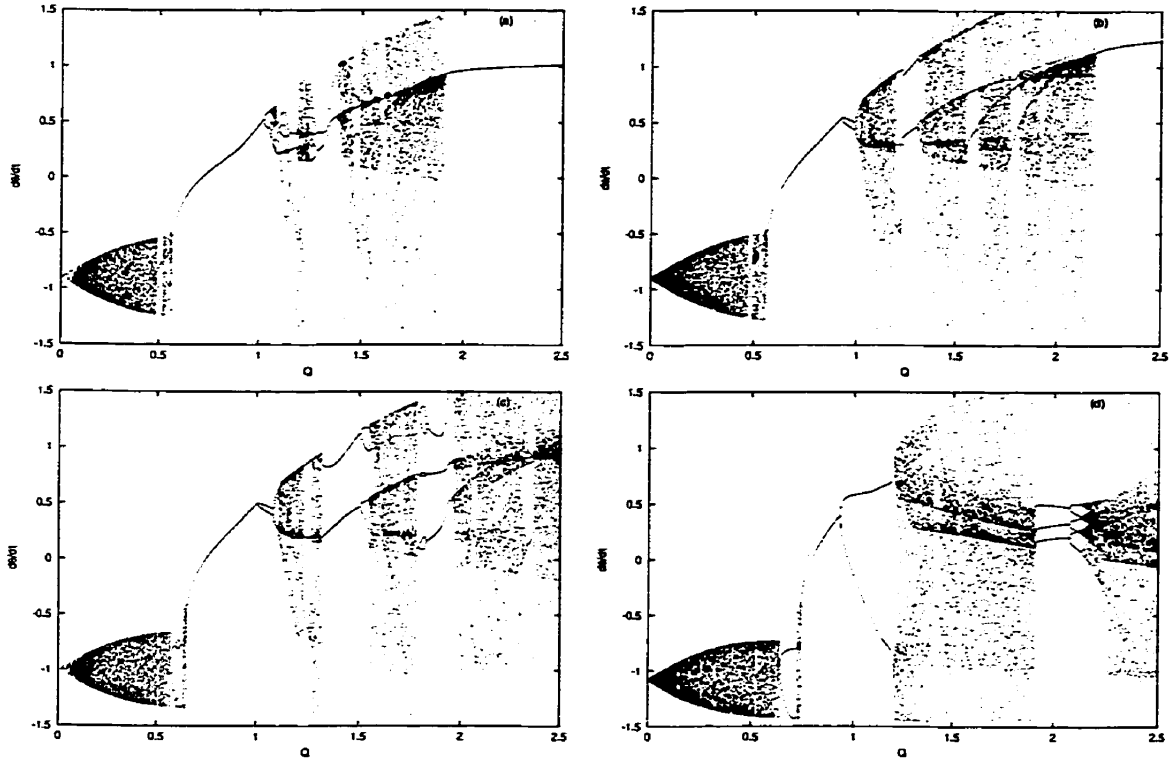

Figure 4.3: Bifurcation diagrams. Broad chaotic regions are found for (a) $a = 0.9$, $r = 1$,(b) $a = 1$, $r = 0.9$, (c) $a = 1$, $r = 1$, (d) $a = 1.2$, $r = 0.9$.

system's behavior, and help us determine regions within the parameter space where the system has a chaotic attractor, i.e. where it exhibits chaos.

The simplest way to generate a bifurcation diagram is to observe a change of a system's attractor with respect to a change in one parameter while others are kept constant. We choose to observe a change of angular velocity of the rod $\dot{\theta}$ with a change of the quality factor Q, while parameters a and r are kept constant. We could vary any of the other two parameters, but this does not give us any significantly different qualitative results.

For every value of Q we plot 30 values of $\dot{\theta}$. The angular velocity of the rod is calculated after every full rotation of the planetary gear. The first 70 rotations are omitted in order to allow the trajectory of the system in phase space to reach the

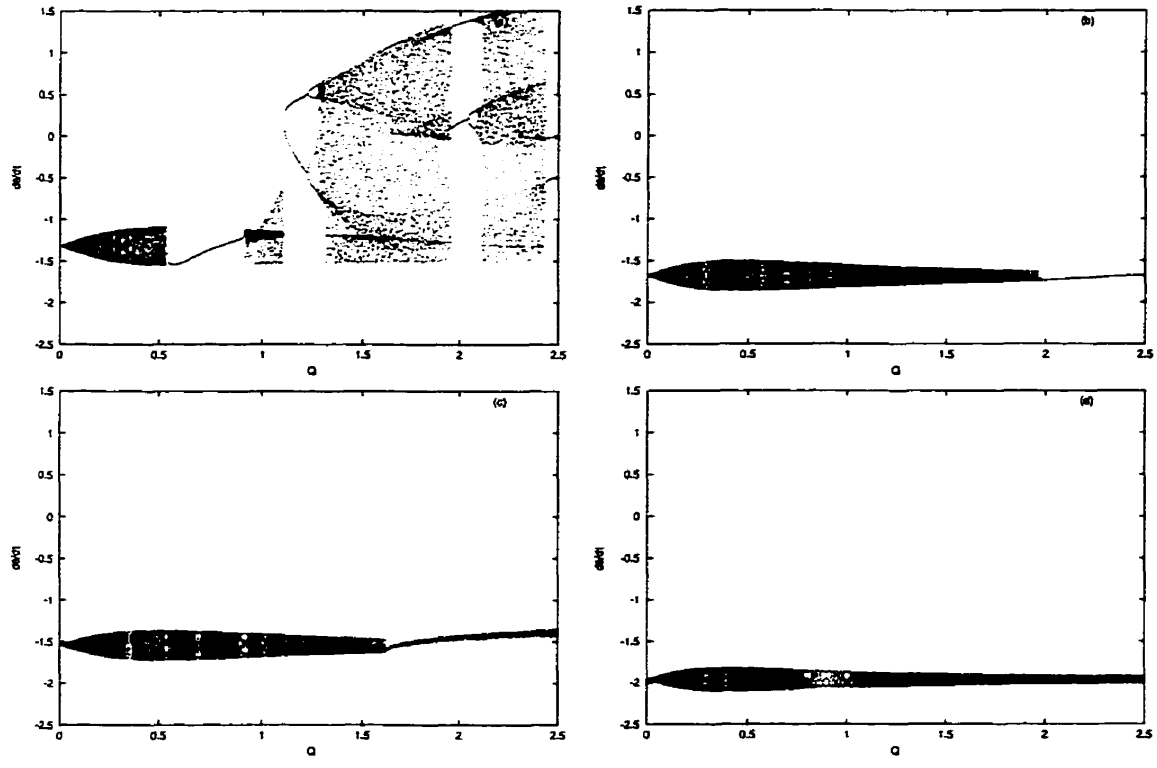

Figure 4.4: Bifurcation diagrams for the choice of parameters (a) $a = 1.1$, $r = 1.2$, (b) $a = 1.4$, $r = 1.2$, (c) $a = 1.1$, $r = 1.4$, (d) $a = 1.4$, $r = 1.4$. quasiperiodic behavior is dominant over the range of Q.

attractor. In this way, for every control parameter value we create a corresponding projection of the Poincaré section of the attractor to the $\dot{\theta}$-axis in the phase space.

For our system, we observe three characteristic regions in the bifurcation diagrams – quasiperiodic, periodic and chaotic. With the increase of Q from zero onwards, the motion of the system is quasiperiodic, which is observed as a smeared region in the bifurcation graph. For certain values of Q the motion suddenly becomes periodic, and with further increase of the quality factor the system reaches chaos through a sequence of period doublings. For the parameters $a, r < 0.5$, the quasiperiodic region is relatively short, and chaos is found only in a narrow region of Q values.

The richest chaotic structure is found for the choice of parameters $a, r \sim 1$. Broad

chaotic regions intercepted by various windows of periodic behavior with complex structure are then found. At the same time, the quasiperiodic region becomes wider with an increase of r and a, so chaos is found only for relatively large values of Q. As a rule of thumb we find that the sum $a + r$ has to be equal or slightly larger than about 2 in order to have a broad chaotic region. Figures 4.2–4.4 show how bifurcation diagrams plotted against Q change with a change of other two parameters.

Finally, for both $a, r > 1$ quasiperiodic motion becomes dominant over the range of Q, and periodic and possible chaotic behavior are found only in narrow isolated regions.

Let us consider the bifurcation diagram for $a = 0.9$ and $r = 1.1$ (Fig. 4.3a). The smeared region in the bifurcation diagram that is observed for the values $0 < Q < 0.6$ corresponds to a quasiperiodic behavior of the system. Although it is generally possible to notice differences between chaotic and quasiperiodic regions in a bifurcation graph, it is necessary to employ other methods in order to have solid evidence of a system's behavior. Analyzing the power spectra is one of the methods that is particularly suitable for examining quasiperiodic motion. Power spectra for $Q = 0.2$ and $Q = 0.4$ (Fig. 4.5a and 4.5b) shows that the motion of the system is a superposition of a finite number of harmonic modes, and therefore is not chaotic. The motion is not periodic though, since frequencies of harmonics are incommensurate, and the trajectory in phase space never retracts itself. The motion is rather performed over a smooth surface in phase space [70], and that is why it is difficult to distinguish it from chaotic motion in the bifurcation diagram.

For values of $0.6 < Q < 1.02$ it is clear from the bifurcation graph that the system's behavior is periodic with period that is equal to the virtual drive period $2\pi/a$. We can confirm this by making a spectral analysis of the solution of the equation of motion (Fig. 4.5c). The trajectory in the phase space retracts itself with every full rotation of the planetary gear, so the attractor of the system is a simple limit cycle. With an increase of Q over 1.02 we observe a pitchfork bifurcation sequence

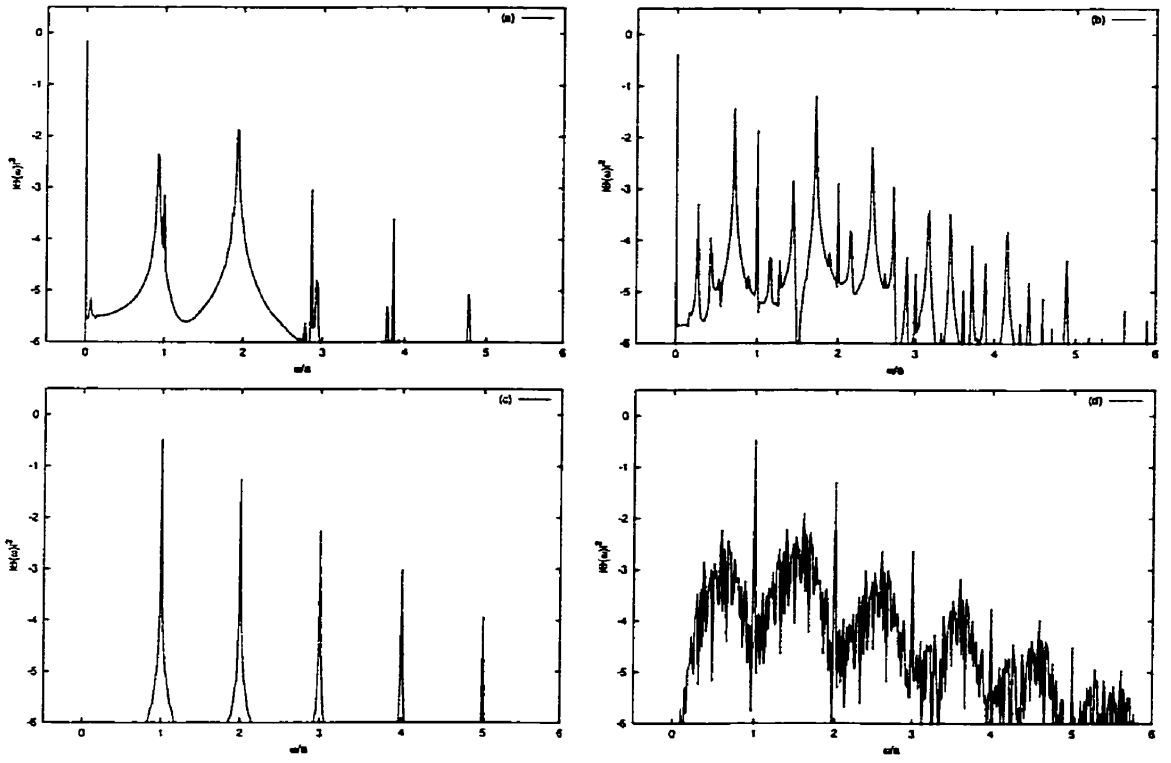

Figure 4.5: Power spectra for different values of quality factor Q: (a) $Q = 0.2$ and (b) $Q = 0.4$, motion is quasiperiodic, (c) $Q = 0.8$, motion is periodic with period one, and (d) $Q = 1.08$, motion is chaotic. $\Theta(\omega)$ is the Fourier transform of $\dot{\theta}(t)$. The frequency on the x–axis is expressed in terms of the virtual drive frequency a.

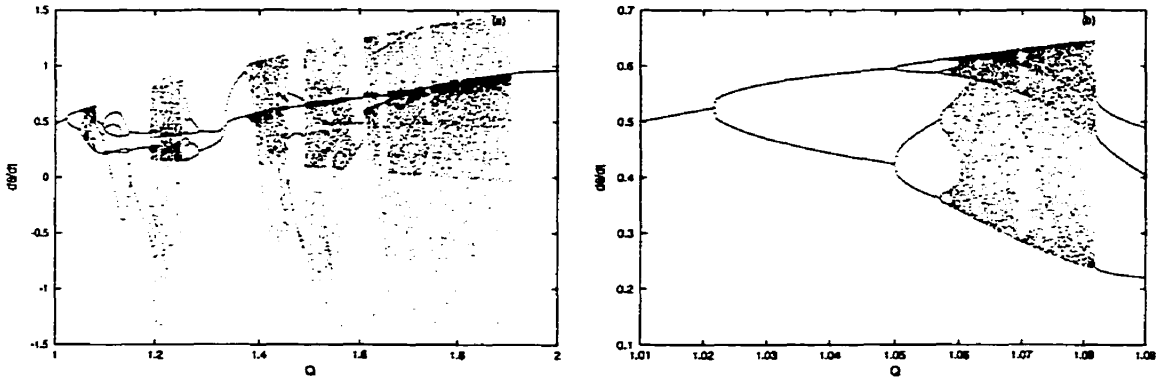

Figure 4.6: (a) Enlarged chaotic region of bifurcation diagram 4.3a. (b)Period doubling route to chaos, enlarged from figure a. $a = 0.9$, $r = 1.0$

(Fig. 4.6b) similar to that of the logistic map. Each pitchfork bifurcation corresponds to a period doubling of the limit cycle.

At $Q = 1.08$ the system is chaotic. The power spectrum does not consist of a finite number of harmonics and their integer multiples any more, but it is rather a broad band over the frequency axis. Yet, the virtual drive frequency is still visible as a distinct peak within the continuous spectrum (Fig. 4.5d). The smeared region in the bifurcation diagram indicates that the attractor for the system has a complex structure in that region of the parameter space. The power spectrum also shows complexity of the system's behavior and indicates chaos in that region of parameter space. In order to obtain a solid evidence of chaos one has to show that at least one Lyapunov exponent for the system is positive in that region [2]. Indeed, at $Q = 1.08$ the largest Lyapunov exponent is found to be $\lambda_1 = 0.049 \pm 0.001$.

After the system becomes chaotic a number of windows of periodic behavior occur (Fig. 4.6a). Periodic behavior is restored by tangent bifurcations [62] or through a sequence of period halving. Period halving is actually an identical process to period doubling, and whether we observe one or the other depends only on how we define parameters. For $Q = 1.9047\ldots$ chaotic behavior ends by a single tangent bifurcation

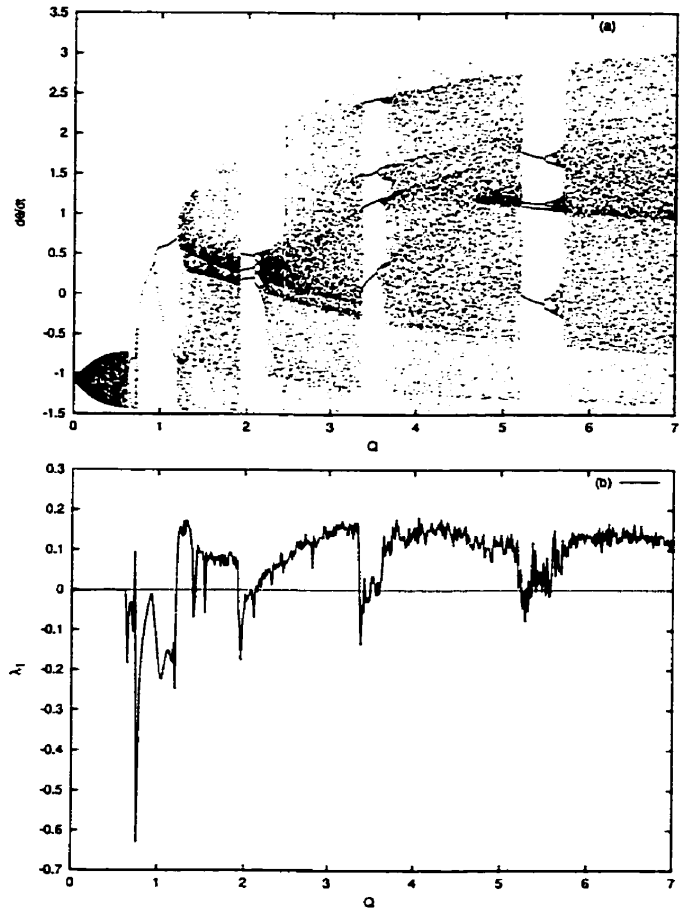

Figure 4.7: (a) Bifurcation graph showing broad chaotic region over segment of Q. $a = 1.2$, $r = 0.9$. (b) Corresponding change of the largest Lyapunov exponent.

(Fig. 4.6), and the system's behavior becomes periodic again. The system remains periodic with a further increase of Q. On the other hand, for slightly different choices of parameters $a = 1.2$ and $r = 0.9$, once the system becomes chaotic it remains so, apart for the windows of periodic behavior (Fig. 4.7).

4.3 Lyapunov Exponents, Dimensions and Conjectures

Solid proof of chaos is the existence of at least one positive Lyapunov exponent. The spectrum of Lyapunov exponents gives us, besides qualitative information about a

system's behavior, also a quantitative measure of the system's stability.

Evolution of the Lyapunov exponent spectrum with a change of parameters gives us additional information about the system's behavior to that from bifurcation graphs. Bifurcation diagrams are easier to construct though, because determining the Lyapunov spectrum for a single value of parameter requires plotting virtually the whole attractor [84], while a bifurcation diagram is, in our case, a plot of the projection of the Poincaré section to the $\dot{\theta}$–axis against the parameter. Combined, these two methods are reliable tools for examining a system's behavior and routes to chaos. Figure 4.7 gives a comparison of the bifurcation diagram and Lyapunov spectrum evolution for a range of Q. Since the system is represented in 3 dimensional space it is sufficient to determine only the largest Lyapunov exponent. The other two can be inferred from Haken's theorem [35], and the fact that the system is dissipative with dissipation coefficient $1/Q$, so the sum of Lyapunov exponents must be (Sec. 3.6):

$$\sum_i \lambda_i = \frac{1}{Q} \tag{4.14}$$

The chaotic attractors, for certain values of parameters, have a non-integer dimension, i.e. they have a fractal form. This is observed as an infinite kneading sequence which results in the attractor showing an interwoven structure at an arbitrary small scale. In the quasiperiodic region the attractor has dimension 2, as motion is performed over a smooth surface, while the limit cycles have dimension 1. Since motion takes place in 3-dimensional phase space it is reasonable to expect that strange attractors have dimension between 2 and 3. We can use the fact that the attractor is always smooth in the ϕ direction, so in order to estimate its dimension we can estimate the dimension of its Poincaré section and obtain the attractor's dimension simply by adding one to it. We shall calculate the dimensions of the attractor at some characteristic points in the parameter space and establish certain conjectures with Lyapunov exponents.

In order to estimate the dimension of an attractor lying in n–dimensional phase

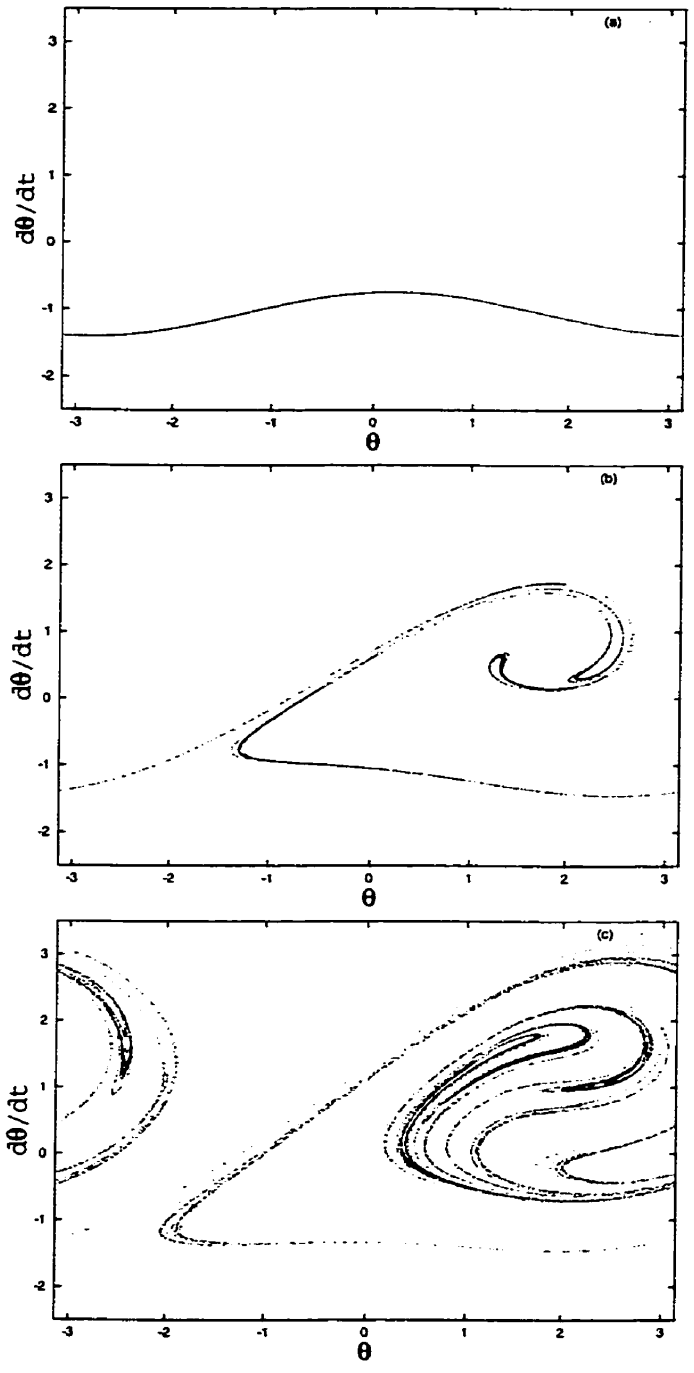

Figure 4.8: (a) Poincaré section of the quasiperiodic attractor is a smooth line. $a = 1.2$, $r = 0.9$, $Q = 0.5$. (b) Poincaré section of the chaotic attractor reveals a kneading sequence. $Q = 1.8$. (c) Higher dimensional chaotic attractor. $Q = 6.5$.

space, the attractor, first, has to be covered by a grid of n-dimensional hypercubes of size ϵ, and then the probability of finding a point of the attractor in each hypercube P_i has to be determined. The index i here refers to a particular cube. In our case we consider a 2-dimensional Poincaré section, so the hypercubes are actually squares. A general expression for the dimensions of the q^{th}-order attractor is then given by:

$$D_q = \lim_{\epsilon \to 0} \frac{1}{q-1} \frac{\ln \sum_i P_i^q}{\ln \epsilon}, \tag{4.15}$$

where the summation is over all hypercubes where $P_i > 0$ [26]. The parameter q ranges from $-\infty < q < \infty$, and for $q_1 > q_2$ we have $D_{q_1} \leq D_{q_2}$. The most commonly used dimensions are D_0, D_1, and D_2, or the capacity, information, and correlation dimension, respectively. We will limit ourselves to estimating these three dimensions only.

In the Kaplan-Yorke conjecture the Lyapunov dimension of the attractor is defined as:

$$D_L = j + \frac{\lambda_1 + \lambda_2 + ... + \lambda_j}{|\lambda_{j+1}|} \tag{4.16}$$

where j is the largest integer for which $\lambda_1 + \lambda_2 + \ldots + \lambda_j \geq 0$ [48]. The Lyapunov dimension represents an upper limit to the information dimension, i.e. $D_L \geq D_1$ [54]. However, it is to be expected that numerical values of these four dimensions fall pretty close to each other [17].

In the bifurcation diagram 4.7 we observe a region of quasiperiodic behavior at $Q = 0.5$. The attractor is a smooth surface, and its Poincaré section is a smooth curve (Fig. 4.8a). As a check we may estimate the dimensions of this attractor. As expected, we obtain the capacity, information and correlation dimension to be equal to 2 within numerical limits of uncertainty. The Lyapunov spectrum is calculated to be $\lambda_1 = 0.000 \pm 0.000$, $\lambda_2 = 0.000 \pm 0.000$, and $\lambda_3 = -2.000 \pm 0.001$. Since the largest exponent is zero within the limits of uncertainty, the Lyapunov dimension is also two. In this case the Kaplan-Yorke conjecture becomes an equality (table 4.1). At $Q = 1.8$ the system exhibits chaos. Characteristic chaotic patterns of stretching and folding

Q	D_L	D_0	D_1	D_2
0.5	2.000 ± 0.001	2.002 ± 0.003	2.007 ± 0.006	1.999 ± 0.002
1.8	2.12 ± 0.01	2.11 ± 0.01	2.044 ± 0.007	2.012 ± 0.003
6.5	2.48 ± 0.01	2.39 ± 0.01	2.389 ± 0.004	2.299 ± 0.001

Table 4.1: Various dimensions of the attractors.

are clearly visible in the Poincaré section (Fig. 4.8b). At larger values of the quality factor the dimension of the chaotic attractors is generally larger. A highly interwoven structure can be found in the chaotic attractors that occur for large values of Q, like the one in Fig. 4.8c, where $Q = 6.5$. The Kaplan-Yorke conjecture in both cases is an inequality with various dimensions having fairly close numerical values. An overview of estimates of the various dimensions is given in Table 4.1.

4.4 Coexisting Attractors and Crisis

For a certain range of parameters the model shows coexisting attractors. Bifurcation diagram 4.9a indicates that at $Q = 1.0105\ldots$ a tangent bifurcation occurs which creates a pair of stable and unstable limit cycles in the phase space. The basin of attraction splits accordingly into a basin of the stable limit cycle and a basin of the chaotic attractor. Basin boundary is the stable manifold of the saddle limit cycle, which is shown as a black dot in the Poincaré section in Figure 4.10. The basin boundary is, therefore, a smooth surface with no fractal features present. Creation of a new, phase-locked limit cycle may also be observed if we plot the average angular

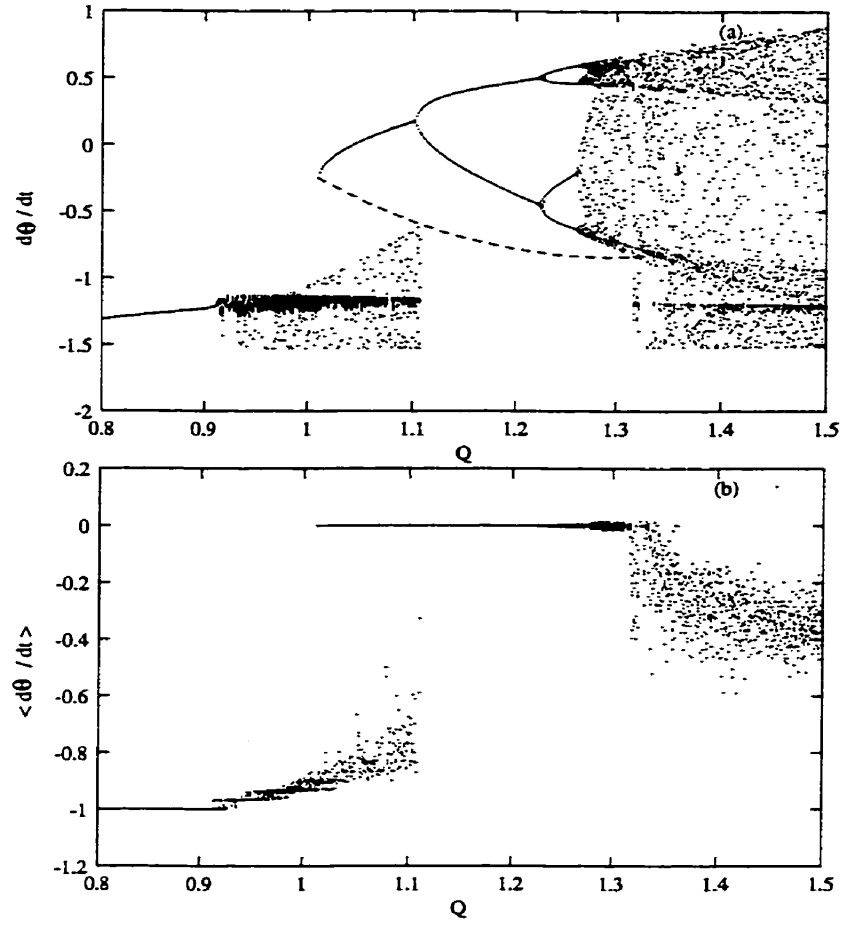

Figure 4.9: (a) Bifurcation diagram indicating coexisting attractors. Dashed line shows unstable limit cycle. (b) Corresponding plot of average angular velocity.

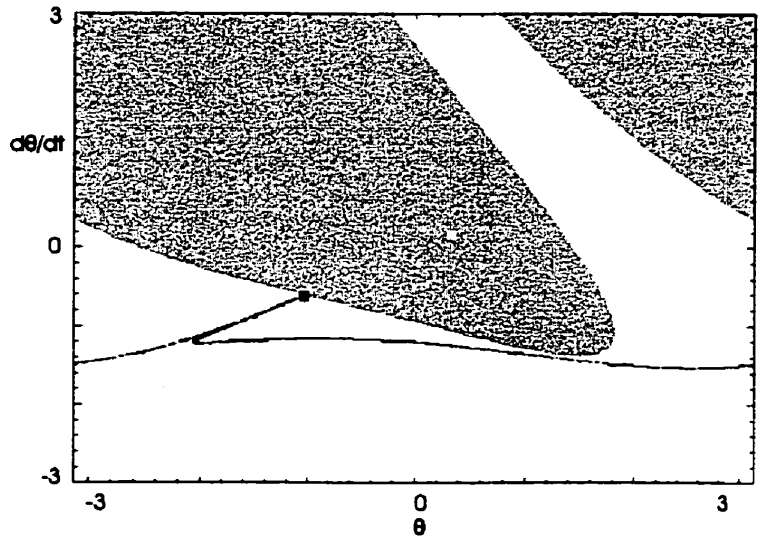

Figure 4.10: Poincaré section of the chaotic attractor at the verge of crisis, shown within its basin of attraction. White dots represent a stable, and black dots an unstable, limit cycle. $Q = 1.1$.

velocity of the rod $\langle\dot{\theta}\rangle$ against Q (fig.4.9b).

It is interesting to note that the behavior of the system in this parameter range will be determined by the initial conditions. Thus, merely by changing the initial position of the rod we might move the system from one basin of attraction in phase space to another. The system will then exhibit periodic or chaotic behavior depending on whether it is found in a basin of attraction of a limit cycle or a chaotic attractor, respectively.

With an increase of the control parameter Q the basin of attraction for the limit cycle expands until the unstable limit cycle, which lies on its boundary, collides with the chaotic attractor (Fig. 4.10). The chaotic attractor experiences a boundary crisis [29] and disappears along with its own basin. The basin of the limit cycle then suddenly expands, occupying the whole phase space.

This phenomenon is also known as the escape from the potential well [82]. When

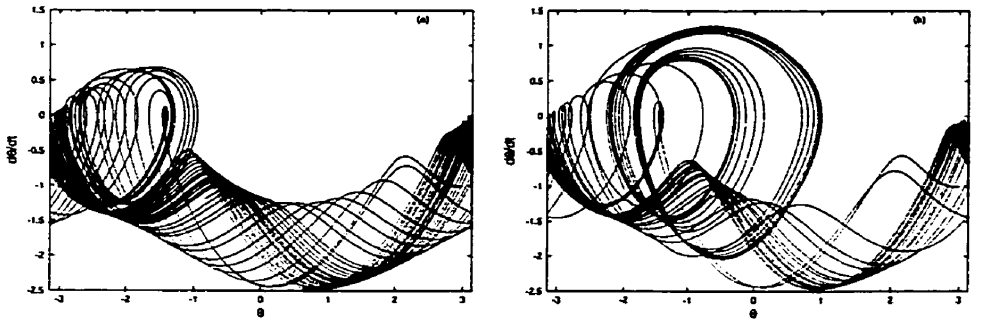

Figure 4.11: (a) Two-dimensional projection of a chaotic attractor at $Q = 1.1$. (b) Two-dimensional projection of the limit cycle at $Q = 1.2$ along with its transient. Both simulations were done for 200 time units.

chaotic attractor crosses the stable manifold of the saddle orbit it will eventually eject every trajectory from its own potential well into the potential well of the stable limit cycle. Of course, when it happens, the chaotic attractor ceases to be an attractor. A more accurate statement would be that system's trajectory can move from white into gray basin (Fig. 4.10) only if the unstable manifold (and the attractor is a part of the unstable manifold) in the white basin crosses the stable manifold of the saddle orbit. Once found in the vicinity of the stable limit cycle, the system's trajectory will reach it asymptotically and stay there for the rest of the motion. Therefore, the only attracting set in the phase space is the limit cycle, but all of the unstable orbits that were embedded in the chaotic attractor are still present, as well. This results in very long transient behavior of the system when initialized in the region of phase space where unstable orbits lie (Fig. 4.11).

With a further increase of the control parameter the limit cycle evolves into a chaotic attractor through a sequence of period doublings. The newly created chaotic attractor expands in size as the parameter Q increases, and eventually collides with the unstable limit cycle. The system comes to a crisis again, but since the unstable orbit is not at the basin boundary any more the crisis is internal, and the attractor

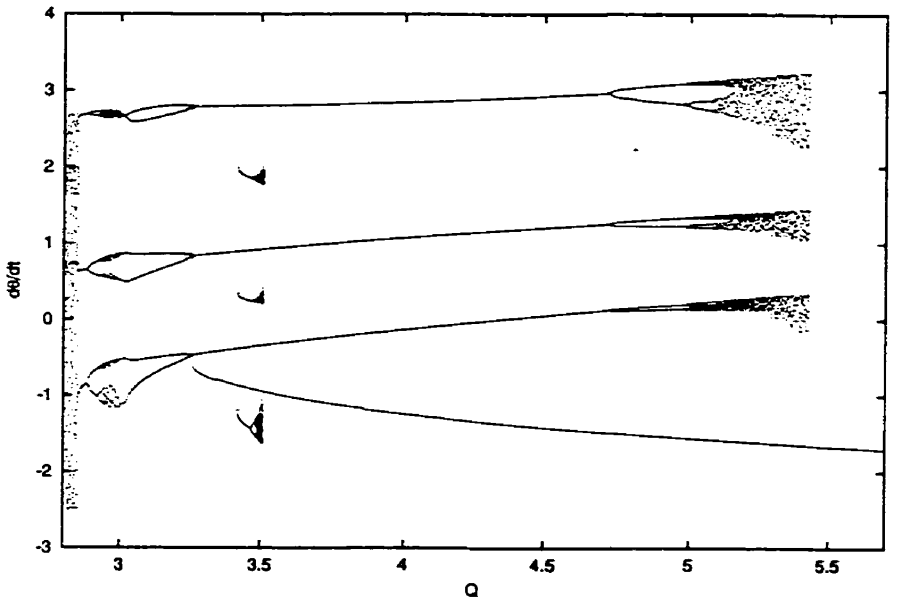

Figure 4.12: Bifurcation diagram shows creation of coexisting attractors.

suddenly expands its size [29]. This expanded attractor contains features of the chaotic attractor destroyed in the boundary crisis, indicating that information about the system's behavior at lower values of Q has "survived" the crisis. In fact, the unstable manifold, which was previously contained within the gray area of Figure 4.10, now intersects the stable manifold of the saddle orbit. Hence, trajectories can move in both ways – from one potential well to another. As a result, unstable orbits of the chaotic attractor, which previously disappeared in boundary crisis, are now embedded into a new attractor.

As we increase the control parameter Q further, we observe another occurrence of coexisting attractors (Fig. 4.12). There is another tangent bifurcation at $Q = 3.2398\ldots$ that creates a stable–unstable pair of period one orbits. Period three and period one limit cycles coexist there, but there is also an infinite number of unstable orbits in the phase space. This means that the stable manifold must have very complex geometry, and as a consequence basin boundary is a locally disconnected

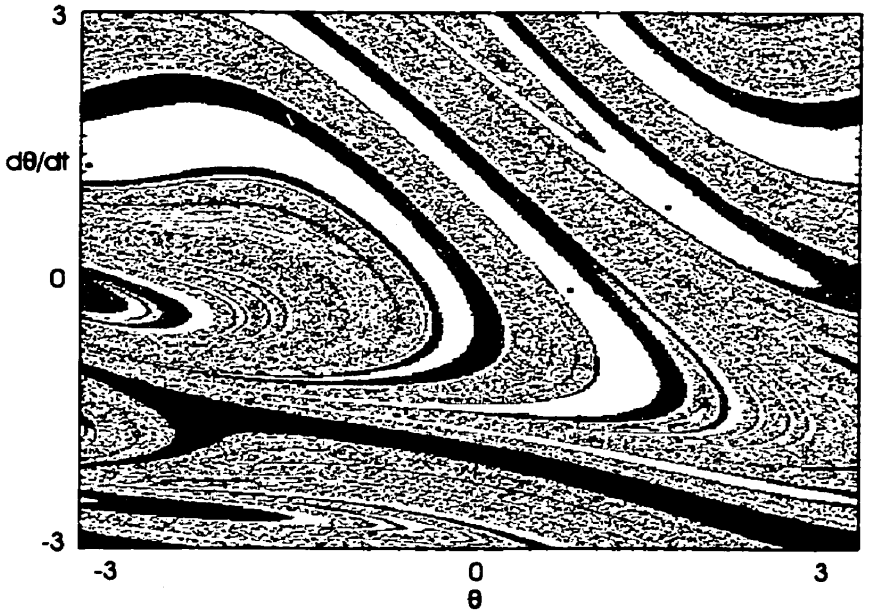

Figure 4.13: Three coexisting attractors. Period-three limit cycle (black points) and period-one limit cycle (white point) are enlarged for clarity. $Q = 3.515$.

fractal curve [65]. At $Q = 3.4177\ldots$ another tangent bifurcation creates a period 3 orbit, so there are three coexisting attractors in that region. Basins of attraction are highly interwoven in this region, and it is difficult to determine initial conditions that would lead to a particular attractor. The newly created period 3 orbit quickly evolves to chaotic attractor with an increase of the control parameter (Fig. 4.13), and disappears in a boundary crisis. The former period 3 attractor becomes chaotic also through a period doubling cascade, and gets to a boundary crisis itself at $Q = 5.4200\ldots$ (Fig. 4.14). For $Q > 5.43$ the system's attractor is a period-one limit cycle, the only one that "survives" the crisis.

Similar occurrences of coexisting attractors are found at many other places within the parameter space of our system.

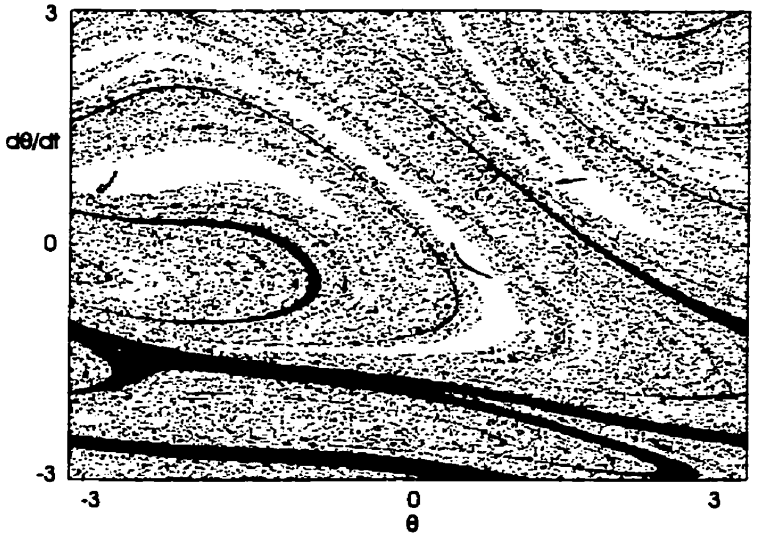

Figure 4.14: Basin of attraction for $Q = 5.3$.

4.5 Symbolic Dynamics

In Section 2.5 we demonstrated basic concepts of symbolic dynamics analysis using the example of a unimodal map. Symbolic dynamics of one dimensional maps is well understood, and so far these techniques have been extended to that of two-dimensional maps. Two much-studied 2D models are the Hénon map [40] and its piecewise linear version, the Lozi map [59, 91]. However, there is still no extension of symbolic dynamics to higher dimensional maps. This is indeed a serious limitation, but still there are a lot of physical models which can be reduced to a two-dimensional map by suitable choice of Poincaré section or by exploiting their symmetry properties. There are no guarantees, though, that symbolic dynamics can be constructed for an arbitrary map. There are even some one-dimensional models for which full symbolic dynamic has not been developed [37]. This opens up a wide research area.

It has been convincingly demonstrated that a properly constructed two-dimensional symbolic dynamics provides a powerful tool to capture global, topological aspects of low-dimensional dissipative systems of ordinary differential equations (ODEs) [55, 56,

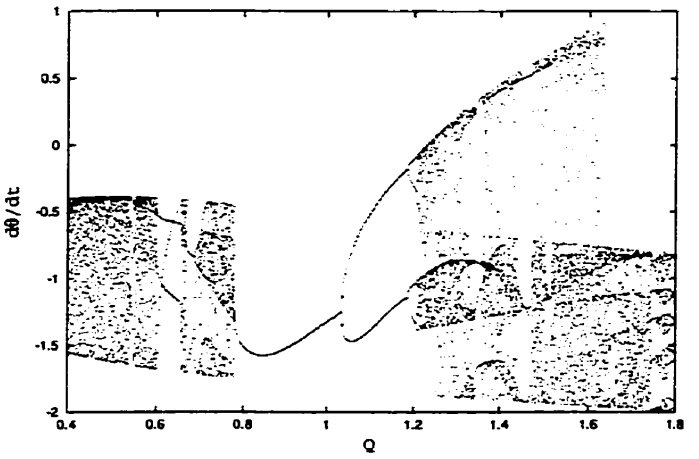

Figure 4.15: Bifurcation graph taken against parameter Q with parameter a varying as $a = 0.8 + 0.3Q$.

89, 92, 57, 38, 39, 90]. However, at this time only a few dynamical flows have been analyzed this way. To the best of our knowledge, the symbolic dynamics has been applied to the analysis of the NMR–laser chaos model [92, 57], the two–well Duffing equation [89], the Lorenz system [38] and the forced Brusselator [55, 56].

We develop symbolic dynamics for our system, consisting of two gears and a rod. We observe evolution of system dynamics with the change of system parameters described by $a = 0.8 + 0.3Q$, where Q varies from 0.5 to 2. Parameter r is kept at fixed value $r = 1.088$. Bifurcation diagram (4.15) reveals complex dynamics in that region of parameter space. The pattern shown in the bifurcation diagram, when chaos occurs as a perturbation on a quasiperiodic attractor, is common for our system, and was described before in this thesis.

For convenience we shall choose a slightly different phase space by substituting $x = \theta/2\pi$, $y = \dot{x}$ in the equation of motion (4.11), and write the equation of motion in its nonautonomus form:

$$\begin{aligned} \dot{x} &= y, \\ \dot{y} &= -y/Q + [-ar/Q - \sin(2\pi x) + (1+r)/r \sin(2\pi x - at)]/(2\pi). \end{aligned} \tag{4.17}$$

We study the evolution of the system's attractor in detail at five characteristic points of the bifurcation diagram (4.15). We plot Poincaré sections of the attractors, first return map $x_n \rightarrow x_{n+1}$, and Poincaré section in polar coordinates μ-ν, where $\mu = 1 - (0.4 + y)\cos(2\pi x)$ and $\nu = 1 - (0.4 + y)\sin(2\pi x)$. The former gives us a section of a torus which is natural description of a quasiperiodic attractor. One can clearly see chaotic kneading pattern occurring as a perturbation on a quasiperiodic torus. While the motion of the system is quasiperiodic, its dynamics can be described by a one-dimensional map. On the other hand, the first return map does not describe chaotic dynamics of the system uniquely, as there is an infinite number of kneading branches – a feature of a chaotic two-dimensional map.

As for the logistic map, we first create an appropriate partition of the phase space, and assign a letter to each partition. That way we can encode any orbit in phase space with a sequence of letters, or itinerary, which describes the sequence at which that orbit visits specific partitions. Next we investigate whether any sequence of letters is allowed, or there are some sequences which are inadmissible.

4.6 Partitioning of the Poincaré section

For a unimodal map partition of "phase space" is done at the critical point of the mapping function. When iteration moves the system across that point, say from the left to the right, stretching of the orbit changes its direction, i.e. the fold occurs. There is no such an obvious choice in a 2-D map. In partitioning phase space we used ideas proposed by Grassberger and Kantz [27], later more elaborated by Zheng (See for example Ref. [56]).

Eigenvectors of a Jacobi matrix of a 2-D map each create fields. We plot field lines of stable and unstable eigenvectors, so we obtain forward and backward foliations, respectively. These are actually generalizations of a stable and unstable manifold of the system. Stable manifolds are a subset of forward foliations, and unstable

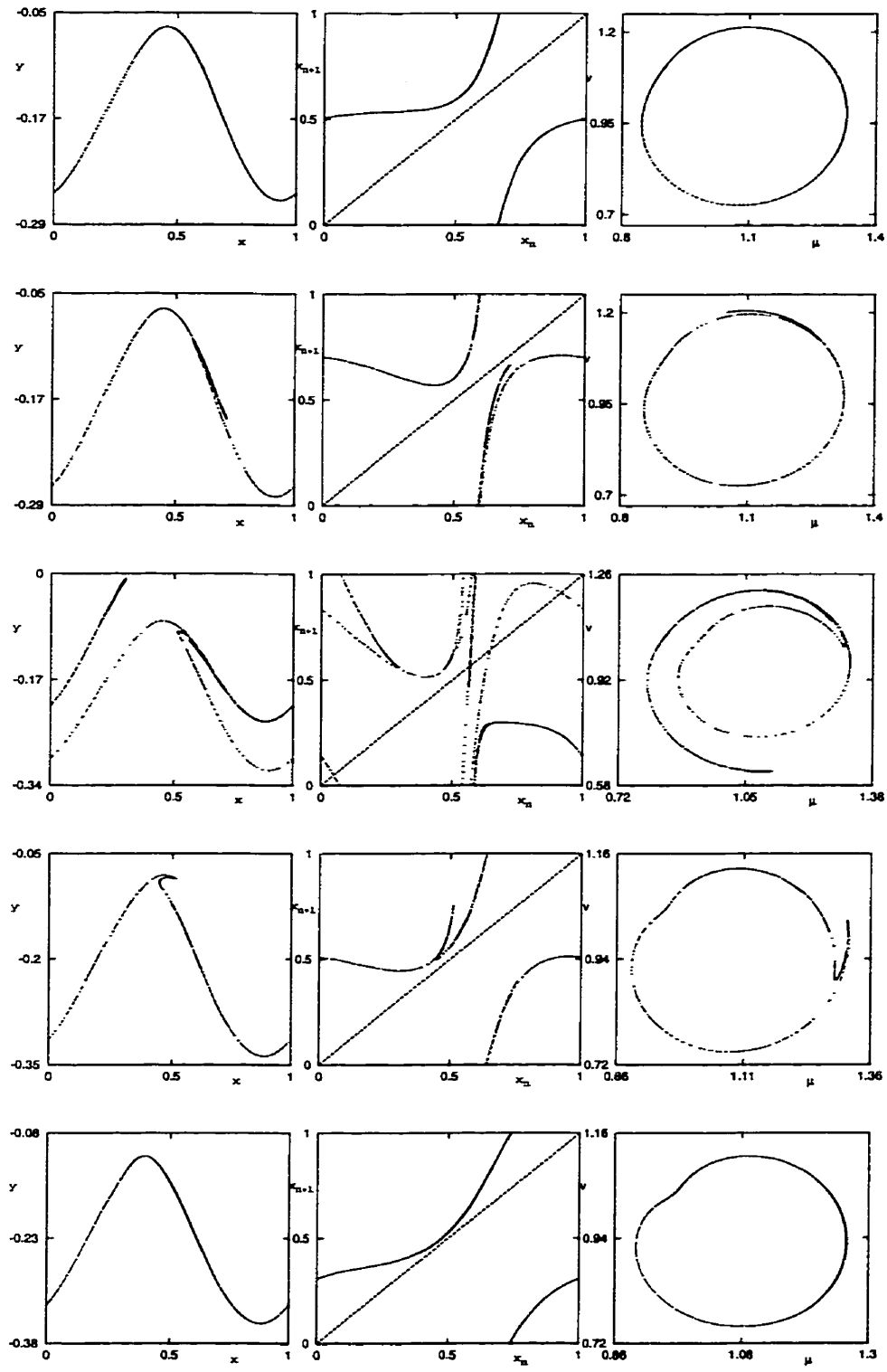

Figure 4.16: Attractors shown in the $x - y$, $x_n - x_{n+1}$, and $\mu - \nu$ planes at $Q = 0.57, 0.76, 1.2577, 1.68$, and 2.0 from top to bottom for $r = 1.088$, and $a = 0.8 + 0.3Q$.

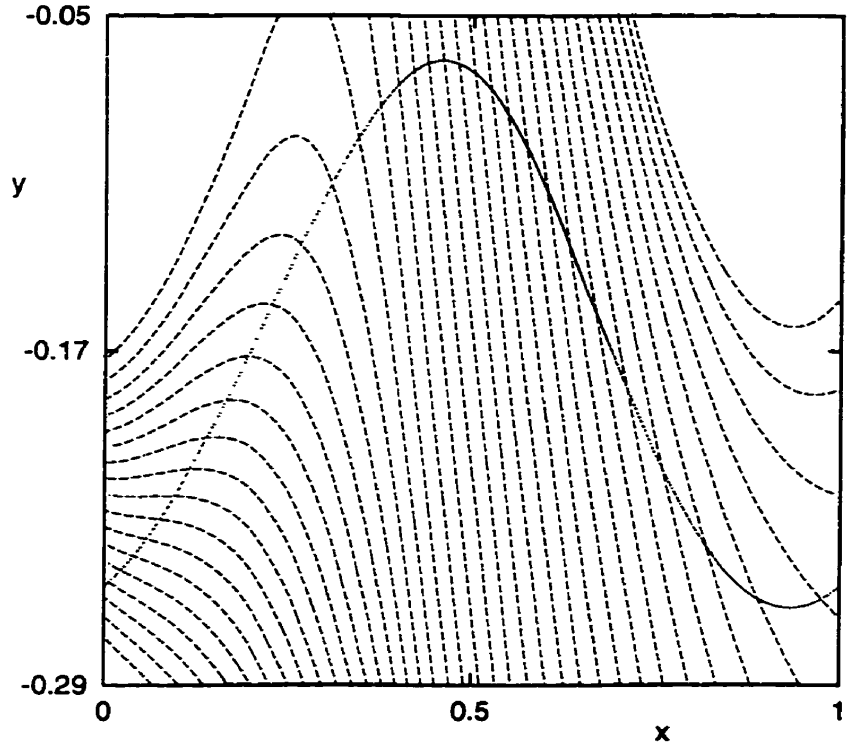

Figure 4.17: Attractor (dots) and forward foliations (dash curves) for $Q = 0.57$.

manifolds, including attractor, are a subset of backward foliations. Tangent points of those field lines correspond to points in phase space where both fields are equal. Since it is a dissipative map we study, this means that at these points both eigenvalues must be smaller than one, so there is no stretch accross these points. Since the system is chaotic we conclude that a fold must occur whenever an orbit passes beyond tangencies. By connecting tangency points between forward and backward foliations we obtain phase space partition lines that divide 2-dimensional space into monotonic regions analog to those for 1-dimensional maps.

We draw forward and backward foliations in phase space x-y, and by connecting tangency points between them we find partition lines at parameter values $Q = 0.76$ and $Q = 1.2577$. As a check we also draw foliations at $Q = 0.57$, where the system exhibits quasiperiodic motion. The quasiperiodic attractor and forward foliations at $Q = 0.57$ are shown in Figure 4.17, from which one can see clearly that there is no tangency between the attractor, which is part of backward foliations, and the forward foliations. When Q increases over that value the tangencies begin to appear, and correspondingly the first return map $x_{n+1} - x_n$ assumes the form of a critical circle or annular map [37]. As Q keeps increasing, the map becomes supercritical. With further increase of Q motion becomes quasiperiodic again. There are no tangencies and the map becomes subcritical again (see Fig. 4.16). This shows the close connection between the geometric properties of an attractor, such as tangencies, and the dynamical behavior of a system like quasiperiodicity and chaos.

Let us now observe phase space partitions at $Q = 0.76$. In Figure 4.18 we show the chaotic attractor and a family of forward foliations. For better clarity we do not show any backward foliations other than the attractor itself. By connecting tangency points we find two primary partition lines, marked with •B and •C, and partition line •A, which is the pre-image of •B. We divide the phase space, and accordingly the attractor, into three regions, which we denote by letters L, R and N. We also plot a return map, and sketch partition lines on it (Fig. 4.19). We notice that

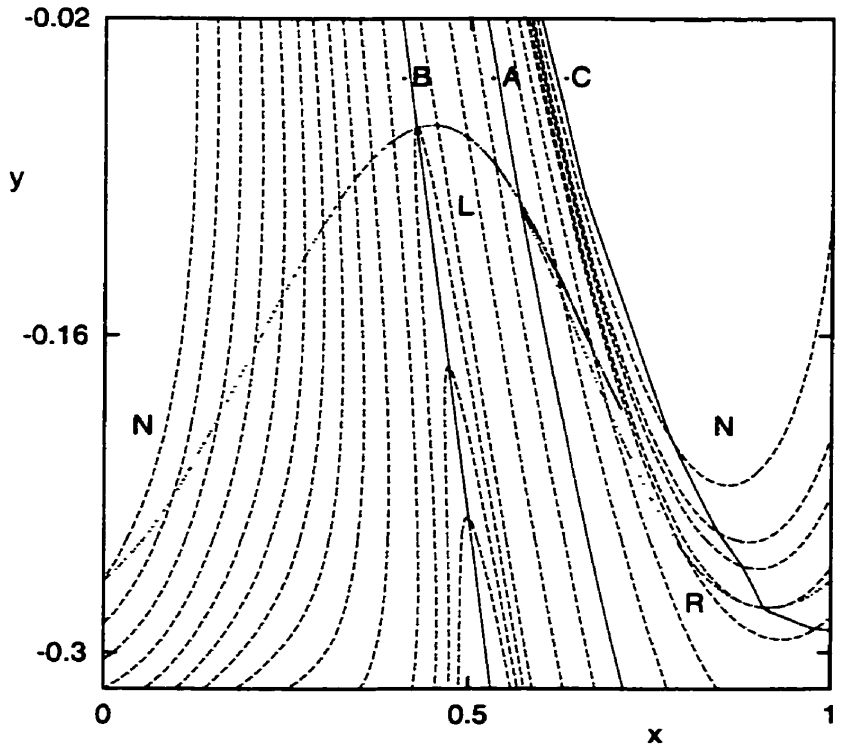

Figure 4.18: The Poincaré map (dots) and forward foliations (dash curves) at $Q = 0.76$. The primary partition lines •B, •C, and the pre-image •A of •B divide the attractor into three parts labeled by the letters L, R and N.

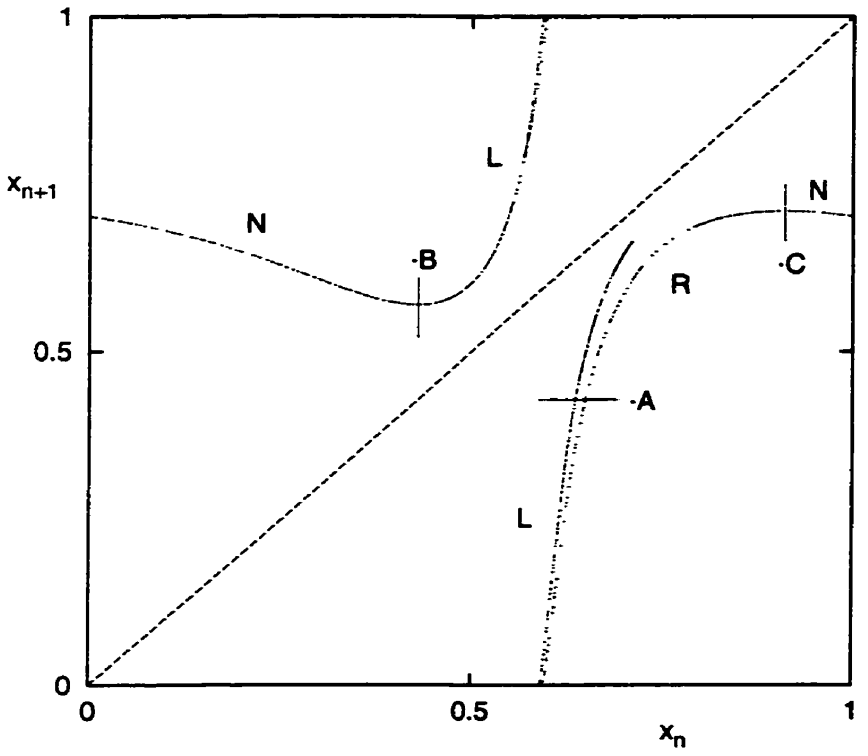

Figure 4.19: The $x_{n+1} - x_n$ first return map at $Q = 0.76$.

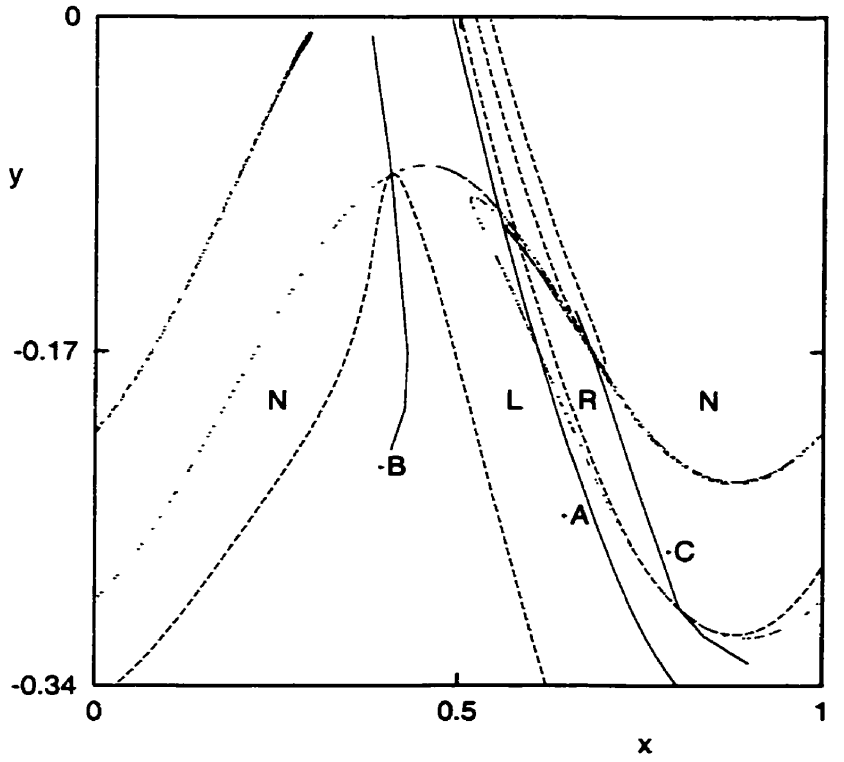

Figure 4.20: The chaotic attractor (dots), forward foliations (dashed lines), and partition lines •A, •B, and •C at $Q = 1.2577$.

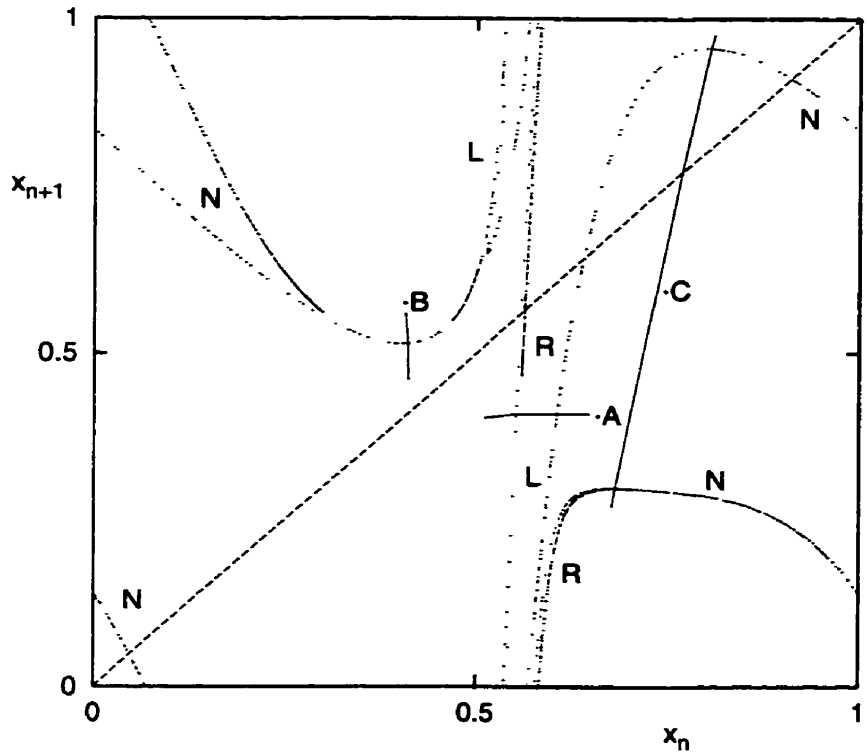

Figure 4.21: The $x_{n+1} - x_n$ first return map constructed from Fig. 4.20.

partition lines divide return map into three monotonic parts. This is confirmation that the partitioning is done properly. The three monotone segments in Figure 4.19 are assigned the letters L, R, and N, in accordance with the two-dimensional partitions in Figure 4.18.

A more interesting case is encountered at $Q = 1.2577$, where two dimensional features of the attractor are more emphasized. In Figure 4.20 we plot the attractor, three forward foliations passing tangencies and partition lines. As in the previous case we have three partition lines, and therefore we establish similar three-letter symbolic dynamics. We also separately plot in Figure 4.21 the $x_{n+1} - x_n$ first return map constructed from Figure 4.20 by using the x coordinates in order to confirm validity of the partition we made.

4.7 Ordering rules and admissibility conditions

After we determine phase space partitions we may encode any point at the attractor with a sequence of three letters R, L and N. Unlike for the 1-dimensional map (Section 2.5) we need a doubly infinite sequence of characters in order to uniquely encode the point at 2-dimensional chaotic attractor [9, 10]:

$$\cdots s_{\overline{m}} \cdots s_{\overline{2}} s_{\overline{1}} \bullet s_1 s_2 \cdots s_n \cdots \tag{4.18}$$

Letter s_n is the code for the n-th point of the forward orbit, and $s_{\overline{m}}$ the code for the m-th point of the backward orbit. The "present" position is indicated by a solid dot, which divides the doubly infinite sequence into two semi-infinite sequences, i.e., the backward sequence $\cdots s_{\overline{m}} \cdots s_{\overline{2}} s_{\overline{1}} \bullet$ and the forward sequence $\bullet s_1 s_2 \cdots s_n \cdots$. A forward sequence determines the position at the x-axis of the return map (Figs. 4.19 and 4.21), while the backward sequence determines the sheet on the chaotic attractor at which the point lies [9].

A metric representation for symbolic sequences can be introduced by assigning numbers in $[0, 1]$ to forward and backward sequences in a similar fashion which we

used for the logistic map in Section 2.5. Since we have one monotonically decreasing region in phase space, N, we first assign an integer $\epsilon_i = -1$ or 1 to the symbol s_i when it is the letter N or otherwise. Then we assign to the forward sequence $\bullet s_1 s_2 \cdots s_n \cdots$ the number

$$\alpha = \sum_{i=1}^{\infty} \mu_i 3^{-i}, \tag{4.19}$$

where

$$\mu_i = \begin{cases} 0 \\ 1 \\ 2 \end{cases} \quad \text{for} \quad s_i = \begin{cases} L \\ R \\ N \end{cases} \quad \text{if} \quad \prod_{j=1}^{i-1} \epsilon_j = 1, \tag{4.20}$$

or,

$$\mu_i = \begin{cases} 2 \\ 1 \\ 0 \end{cases} \quad \text{for} \quad s_i = \begin{cases} L \\ R \\ N \end{cases} \quad \text{if} \quad \prod_{j=1}^{i-1} \epsilon_j = -1. \tag{4.21}$$

Similarly, the β assigned to the backward sequence $\cdots s_{\overline{m}} \cdots s_{\overline{2}} s_{\overline{1}} \bullet$ is defined by

$$\beta = \sum_{i=1}^{\infty} \nu_{\overline{i}} 3^{-i}, \tag{4.22}$$

where

$$\nu_{\overline{i}} = \begin{cases} 0 \\ 1 \\ 2 \end{cases} \quad \text{for} \quad s_i = \begin{cases} R \\ N \\ L \end{cases} \quad \text{and} \quad \prod_{j=1}^{i-1} \epsilon_{\overline{j}} = 1, \tag{4.23}$$

or

$$\nu_{\overline{i}} = \begin{cases} 2 \\ 1 \\ 0 \end{cases} \quad \text{for} \quad s_i = \begin{cases} R \\ N \\ L \end{cases} \quad \text{and} \quad \prod_{j=1}^{i-1} \epsilon_{\overline{j}} = -1. \tag{4.24}$$

According to the definition we have

$$\begin{aligned} &\alpha(\bullet NL^{\infty}) = \beta(L^{\infty}\bullet) = 1, && \alpha(\bullet L^{\infty}) = \beta(R^{\infty}\bullet) = 0, \\ &\alpha(\bullet NNL^{\infty}) = \alpha(\bullet RNL^{\infty}) = 2/3, && \beta(R^{\infty}L\bullet) = \beta(R^{\infty}N\bullet) = 2/3, \\ &\alpha(\bullet RL^{\infty}) = \alpha(\bullet LNL^{\infty}) = 1/3, && \beta(L^{\infty}N\bullet) = \beta(L^{\infty}R\bullet) = 1/3. \end{aligned} \tag{4.25}$$

In this representation a bi-infinite symbolic sequence with the present dot specified corresponds to a point in the unit square of the $\alpha - \beta$ plane, the so-called symbolic

plane. In the plane, forward and backward foliations become vertical and horizontal lines, respectively. We may define the ordering rules of forward (or backward) sequences according to their α (or β) values. From Eqs. (4.19-4.24) we then have

$$\bullet EL\cdots < \bullet ER\cdots < \bullet EN\cdots, \qquad \bullet OL\cdots > \bullet OR\cdots > \bullet ON\cdots, \tag{4.26}$$

and

$$\cdots RE\bullet < \cdots NE\bullet < \cdots LE\bullet, \qquad \cdots RO\bullet > \cdots NO\bullet > \cdots LO\bullet, \tag{4.27}$$

where the finite strings E and O consist of letters L, R and N and contain an even and odd number of letters N, respectively. This ordering rule is similar to that for sequences of the dissipative standard map at some values of the parameters [56].

4.7.1 Pruning Rules

The following task is to find pruning rules, which would tell us if there are any inadmissible sequences among all possible combinations of letters L, R and N. For the logistic map we derived a simple pruning rule from its kneading sequence (2.42). In a similar fashion, a doubly infinite sequence originating from the tangency point between chaotic attractor and a forward foliation imposes restriction on allowed symbolic sequences. A point on the partition line $C\bullet$ (image of $\bullet C$) may symbolically be represented as $QC \bullet P$. The rectangle enclosed by the lines $QN\bullet$, $QR\bullet$, $\bullet P$, and $\bullet NL^{\infty}$ forms a forbidden zone (FZ) in the symbolic plane. Therefore, a symbolic sequence IJ with $I\bullet$ between $QN\bullet$ and $QR\bullet$, and at the same time $\bullet J > \bullet P$ must be forbidden by the tangency $QC \bullet P$. In the symbolic plane the sequence IJ corresponds to a point inside the forbidden zone of $QC \bullet P$. Similarly, $UB \bullet V$ stands for a tangency on the partition line $B\bullet$ (image of $\bullet B$). The lines $UL\bullet$, $UN\bullet$, $\bullet V$ and $\bullet L^{\infty}$ enclose a rectangle FZ in the symbolic plane. Any sequence KT with $K\bullet$ between $UL\bullet$ and $UN\bullet$ while $\bullet T < \bullet V$ is forbidden by the $UB \bullet V$.

Each tangency point on a partition line rules out a rectangle in the symbolic plane. But, for a 2-dimensional map there are infinitely many such points. Altogether they create a pruning front [9, 10, 36] in the symbolic plane. The pruning front is a curve which is nonsmooth at every point, and it encloses fundamental forbidden zone (FFZ), a set of all points in the symbolic plane representing forbiden sequences. Consider a finite set of tangencies $\{Q_iC \bullet P_i\}$ (or $\{U_jB \bullet V_j\}$). If the shift of a sequence $\cdots s_{k-2}s_{k-1} \bullet s_ks_{k+1}\cdots$ satisfies the condition that the backward sequence $\cdots s_{k-2}s_{k-1}\bullet$ is not between $Q_iN\bullet$ and $Q_iR\bullet$ (or $U_jN\bullet$ and $U_jL\bullet$), and at the same time $\bullet P_i > \bullet s_ks_{k+1}\cdots$ (or $\bullet V_j < \bullet s_ks_{k+1}\cdots$) for some i (j), then this shift is not forbidden by any tangencies of $C\bullet$ or $B\bullet$, owing to the property of well-ordering of foliations. Thus, we may say that the shift is allowed according to that tangency. A necessary and sufficient condition for a sequence to be allowed is that all of its shifts are allowed according to the two sets of tangencies. To check the admissibility condition, we consider again the two cases $Q = 0.76$ and $Q = 1.2577$, and draw 10000 points representing real sequences generated from the Poincaré map together with the FFZ in the symbolic plane, as seen in Figs. 4.22 and 4.23. One can see that the FFZ indeed contains no point of allowed sequences. A blow-up of the right-hand side pruning front in Fig. 4.23 is displayed in Fig. 4.24. The structure means a two-dimensional feature, related to the two tangent points in the upper part of attractor on the partition line $\bullet C$ (see Fig. 4.20). We shall use the two tangencies to make 2D analysis of periodic sequences later on (see T_3 and T_4 in the next section).

4.8 Unstable periodic orbit sequences

Pruning rules tell us which orbits are frobidden rather than which are allowed at certain point in system's parameter space. Therefore, in order to to find unstable periodic orbits embedded in a chaotic attractor, we have to start looking at all possible combinations of letters, and then eliminate those words which violate pruning rules

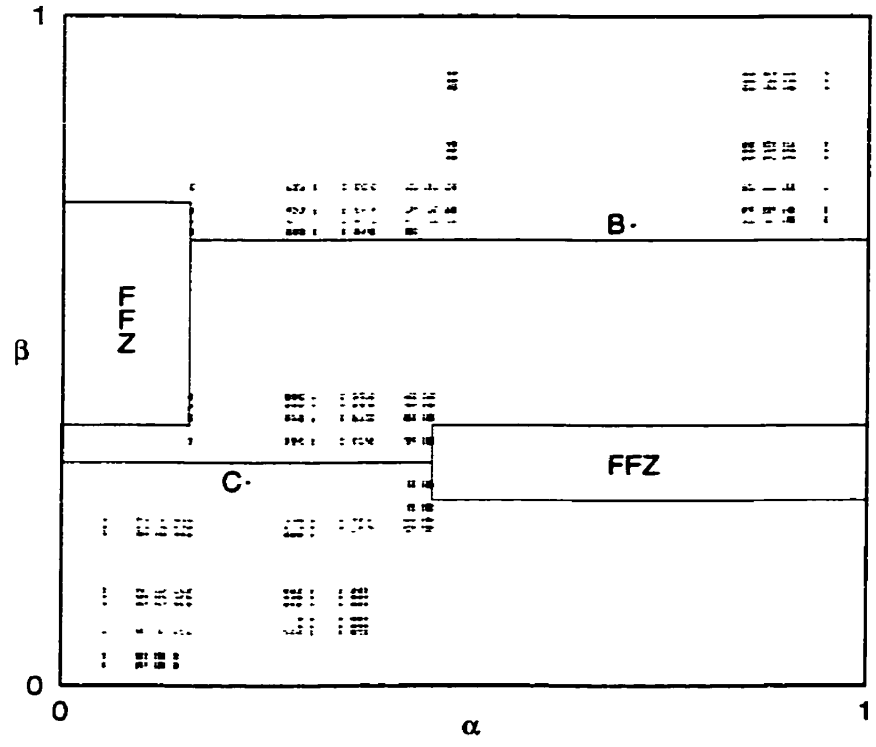

Figure 4.22: The symbolic plane at $Q = 0.76$. 10000 points of real orbits generated from the Poincaré map are also shown together with the FFZ in which no point falls.

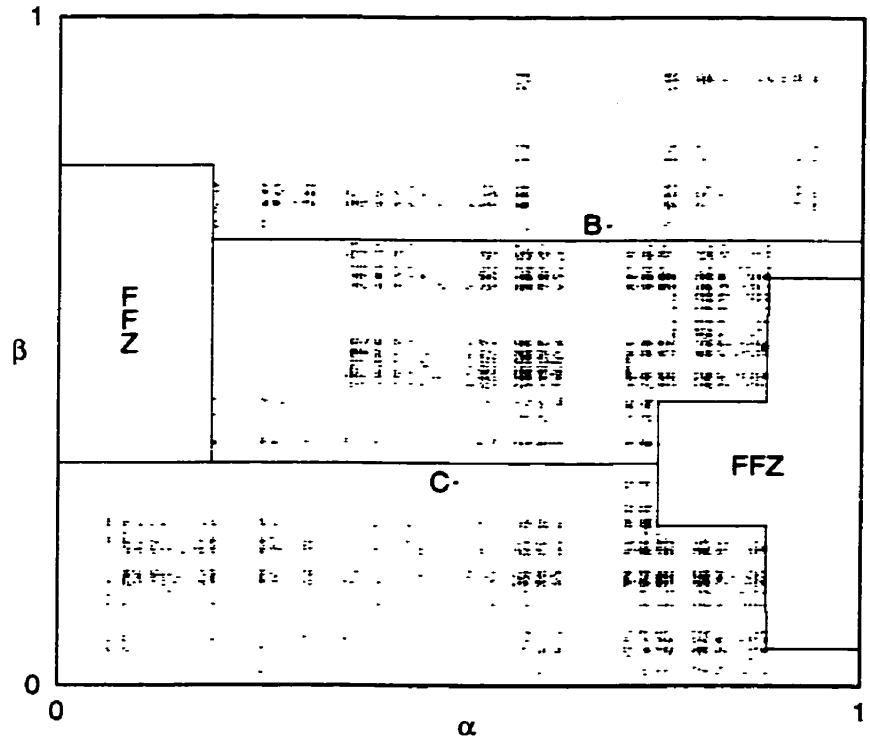

Figure 4.23: The symbolic plane at $Q = 1.2577$. Together with the FFZ, 10000 points representing real orbits are drawn. None of them falls inside the FFZ.

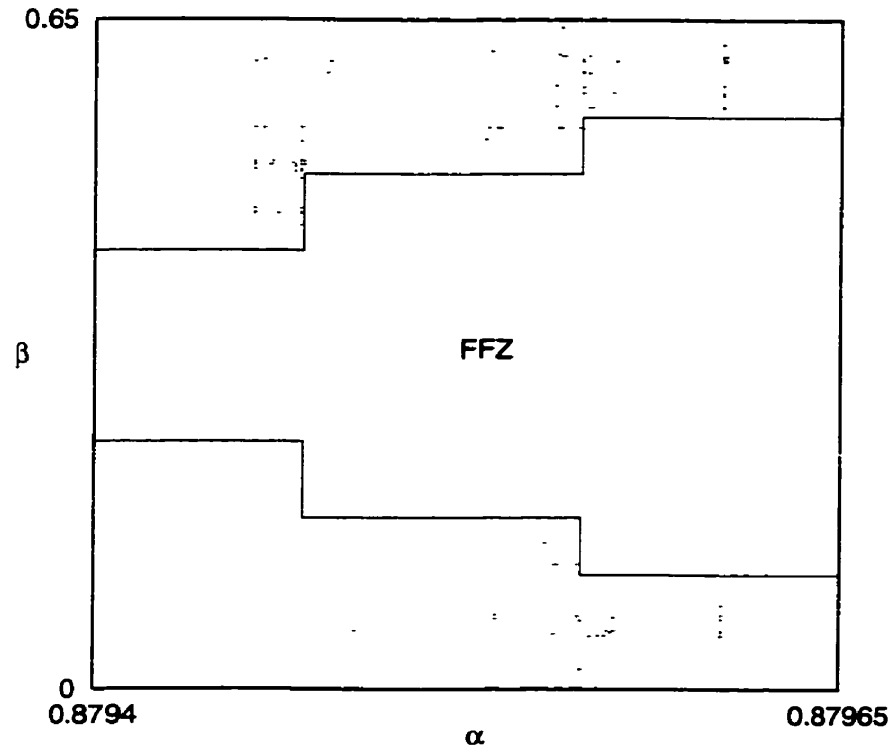

Figure 4.24: A blow-up of the symbolic plane Fig. 4.23 in the intervals $\alpha = [0.8794, 0.87965]$ and $\beta = [0, 0.65]$.

and those which are just shifts of some other admissible words. Considering that there is, for example, a total of $3^8 = 6561$ possible eight-letter words that can be made of three letters, this looks like very time consuming task. In order to develop more efficient way to find and count all admissible orbits, we use the fact that our system can be to a certain extent approximated by a 1-dimensional supercritical circle map. In that way we can use some of methods for constructing admissible words developed for one-dimensional maps. The one-dimensional map puts less restrictions to admissible orbits than a two-dimensional, so the only thing left after we develop symbolic dynamics for a 1-D model is to "prune out" those orbits forbidden by its 2-D counterpart.

The attractor at $Q = 0.76$ does not show much two-dimensional nature, so the reduction to symbolic dynamics of one-dimensional circle map may capture much of the essentials. We start from this simple case. The attractor resembles that of a one-dimensional circle map except for a segment with two sheets, one of which is without an N part (see Figures 4.18 and 4.19). From the two primary partition lines $\bullet C$ and $\bullet B$ in Figure 4.18, we get the following sequences for attractor points:

$$\begin{aligned} \mathrm{T}_1 &: \cdots NN\cdots NNAB \bullet LRRLNLNLNLRRRLLRRR\cdots, \\ \mathrm{T}_2 &: \cdots NN\cdots NNLC \bullet RRLRLNLRRRLRLNRLNL\cdots. \end{aligned}$$

In order to reduce the two-dimensional attractor to a one-dimensional return map, we need to determine two kneading sequences K_B and K_C. They are the forward sequences of T_1 and T_2, respectively.

$$\begin{aligned} \mathrm{K_B} &= LRRLNLNLNLRRRLLRRR\cdots, \\ \mathrm{K_C} &= RRLRLNLRRRLRLNRLNL\cdots. \end{aligned} \tag{4.28}$$

Compared with the original 2D map, the 1D circle map given by these $\mathrm{K_B}$ and $\mathrm{K_C}$ puts less constraints on allowed orbits. Since the attractor has only one sheet crossing each primary partition line nearly no difference between the 1D and 2D maps can be recognized if the sequences of short periodic orbits are concerned.

The knowledge of the two kneading sequences (4.28) determines everything in the symbolic dynamics of the circle map [90]. For example, one may define a *rotation number* W, also called a *winding number*, for a symbolic sequence by counting the weight of letters R and N in the total number n of all letters:

$$W = \lim_{n\to\infty} \frac{1}{n}(\text{Number of R and N}). \tag{4.29}$$

A chaotic regime is associated with the existence of a rotation interval, a closed interval in the parameter plane [44]. Within a rotation interval there must be well-ordered orbits. We can construct some of these well-ordered sequences explicitly, knowing the kneading sequences K_B and K_C.

In our case it can be verified that the ordered periodic orbits $(RL)^\infty$ and $(RRL)^\infty$ are admissible. These two sequences have rotation numbers 1/2 and 2/3, so the rotation interval of the circle map contains [1/2, 2/3], inside which there are rational rotation numbers 3/5, 4/7 and 5/8 with denominators up to 8. Their corresponding ordered orbits are $(R^2LRL)^\infty$, $[R^2L(RL)^2]^\infty$ and $[(R^2L)^2RL]^\infty$. A very easy way to construct a longer well-ordered periodic sequence with a given rational rotation number from two shorter well-ordered periodic sequences can be found in Ref.[37]. Take, for example $W = 3/5$,

$$\frac{3}{5} = \frac{2}{3} \oplus \frac{1}{2} = \frac{2+1}{3+2},$$

$$RRLRL = RRL + RL.$$

We can further construct not-well-ordered sequences from well-ordered ones by the following transformation. One notes that in Figure 4.19 the lower limit of $\bullet A$ is the greatest point on the subinterval L, while the upper limit of $\bullet A$ is the smallest R. When $\bullet A$ is crossed by a continuous change of initial points the corresponding symbolic sequences must change as follows:

$$\text{greatest } LN \cdots\cdots \rightleftharpoons \text{smallest } RL \cdots\cdots.$$

Similarly, on crossing $\bullet C$ another change of symbols takes place:

$$\text{greatest } R \rightleftharpoons \text{smallest } N.$$

Neither change has any effect on rotation numbers. As an example, starting with the ordered period 7 orbit $[R^2(LR)^2L]^\infty$ we obtain

$$RRLRLRL \to NRLRLRL \to NRLRLNL \to NRLNLNL \to NRLNRLL$$

$$\to NRRLRLL \to RRRLRLL \to RRRLLNL \to NRRLLNL \to NNRLLNL$$

and

$$NRLRLNL \to NRLRRLL \to RRLRRLL$$

as candidates for the fundamental strings in not-well-ordered sequences of period 7. Among these sequences, $(NNRLLNL)^\infty$ and $(RRLRRLL)^\infty$ are forbidden by K_C and K_B, respectively.

In this way we have determined all periodic sequences up to period 8, allowed by the two kneading sequences (4.28). The result is summarized in Table 4.2. We have examined the admissibility of all these sequences by checking if all their shifts fall into the FFZ in the symbolic plane of Fig. 4.22. They all turn out to be allowed. In fact, by determining the symbolic sequence of every point in the attractor, we have numerically found all these orbits easily and listed the coordinate of the first letter in a sequence in Table 4.2.

For the more interesting case $Q = 1.2577$, based on Figure 4.20 we list the following five tangencies along the $B\bullet$ and $C\bullet$ lines:

$$\begin{aligned}
&T_1 : \cdots L \cdots LLAB \bullet\bullet LRNNRLLNNNNNRLRLLN \cdots,\\
&T_2 : \cdots N \cdots NNRC \bullet NRLLRNNNNRLRLRNNRN \cdots,\\
&T_3 : \cdots L \cdots LLNC \bullet\bullet NRLLNNNRNRNNRNRNNR \cdots,\\
&T_4 : \cdots N \cdots NNNC \bullet NRLLNNNRLRNNNNRLLN \cdots,\\
&T_5 : \cdots N \cdots NRLC \bullet NNNNRLRLNRNRLNNNRN \cdots.
\end{aligned}$$

Table 4.2: Allowed unstable periods up to 8 for $Q = 0.76$. Only non–repeating strings of the sequences are given. P denotes the period and W the rotation number.

P	W	Sequence
2	1/2	*RL NL*
3	2/3	*RLR RLN*
4	2/4	*NRLL*
5	3/5	*RRLRL NRLRL NRLNL*
5	3/5	*NRRLL RRRLL RRLNL*
6	3/6	*NRLRLL NRLLNL*
6	4/6	*RRRLRL NRRLRL RRLNRL*
7	4/7	*RRLRLRL NRLRLRL RRLLNRL*
7	4/7	*NRLRLNL NRLLNRL NLNLNRL*
7	4/7	*RRRLLNL NRRLLNL RRRLRLL*
7	4/7	*NRRLRLL*
8	4/8	*NRLRLRLL NRLRLLNL NRLLNLNL*
8	5/8	*RRLRRLRL NRLRRLRL NRLNRLRL*
8	5/8	*NRRLRLRL RRRLRLRL NRLNLNRL*
8	5/8	*NRLNRRLL NRLRRRLL RRLNLNRL*
8	5/8	*RRLNRLRL NLNRRLRL NLRRRLRL*

From T_1 and T_2 whose forward sequence is the greatest among the tangencies along $C\bullet$, we get

$$K_B = LRNNRLLNNNNNRLRLLN\cdots,$$
$$K_C = NRLLRNNNNNRLRLRNNRN\cdots.$$

For the 1D circle map, we have determined all allowed periodic sequences up to period 7, which are listed in Table 4.3. We have examined their admissibility by using the tangencies of the 2D Poincaré map and found that ten of these cycles are now forbidden by the tangency T_5. An asterisk denotes those forbidden sequences in Table 4.3. The allowed periodic orbits have been located numerically.

4.9 Conclusions

We successfully developed symbolic dynamics for this model, consisting of two gears and a rod. We find that by constructing the proper Poincaré section in the phase space for a system of ODEs, the symbolic dynamics can be constructed based on the appropriate partitioning of the phase portrait, and it turns out to be an efficient and powerful way to explore the global properties of the system both in the phase and parameter spaces. Along a certain direction in the parameter space this model exhibits various properties, such as, periodicity, quasiperiodicity, chaos, 1D and 2D features, and so forth. In some other directions or regions of the parameter space the model would also display more or less similar behavior. We have established the 3-letter symbolic dynamics for the model and found that the ordering rules of sequences, the forced Brusselator in the regime of annular dynamics and the dissipative standard map at some parameters are the same. As a matter of fact, the NMR-laser chaos model, the forced Brusselator in the regime of interval dynamics and the Hénon map with a positive Jacobian also have similar 2-letter symbolic dynamics and share the same ordering rules of sequences. It therefore is meaningful in a sense to classify the systems of ODEs according to their ordering rules of sequences. The

Table 4.3: Allowed unstable periods up to 7 for $Q = 1.2577$ in the 1D case; those with an asterisk are forbidden by 2D tangency T_5.

P	W	Sequences
1	1/1	*R N*
2	2/2	*RN*
2	1/2	*RL NL*
3	3/3	*NRR RNN*
3	2/3	*RLR RLN*
4	4/4	*RRRN RRNN RNNN*
4	2/4	*NRLL*
4	3/4	*RRRL NRRL NNRL**
5	5/5	*RRRRN RRRNN RRNNN RNNNN RNNRN RRNRN*
5	3/5	*RRLRL NRLRL NRLNL NRRLL NNRLL**
5	4/5	*RRRRL NRRRL NNRRL NNNRL RNRRL RNRLN RNRLR*
6	6/6	*RRRRRN RRRRNN RRRNNN RRNNNN RNNNNN*
6	6/6	*RRRNRN RRNNRN RNNNRN NNRRNR*
6	3/6	*RLRLLN RLLNLN*
6	4/6	*RRRLRL RLNRRL RLNNRL* NLNNRL* RLRRLN RRLNLN*
6	5/6	*RRRRRL NRRRRL NNRRRL NNNRRL NNNNRL**
6	5/6	*RNRRRL NRNRRL RRNRRL NNRNRL* RNRNRL**
6	5/6	*RRRNRL RRNNRL RNNNRL**
7	7/7	*RRRRRRN RRRRRNN RRRRNNN RRRNNNN RRNNNNN*
7	7/7	*RNNNNNN RRRRNRN RRRNNRN RRNNNRN RRNRNRN*
7	7/7	*RNNNNRN RNNRNRN RRNRNNN RNNRRRN*

Table 4.4: Table 4.3 cont'd.

P	W	Sequences
7	4/7	*RRLRLRL NRLRLRL RRLLNRL NRLRLNL NRLLNRL*
7	4/7	*NLNLNRL RRLLNLN RRLRLLN NRLLNLN**
7	5/7	*RRLRRLR RRLRRLN RRLNRLN NRLNRLN*
7	5/7	*RRLNLNN* NRLNLNN*
7	6/7	*RRRRRRL NRRRRRL NNRRRRL NNNRRRL*
7	6/7	*NNNNRRL NNNNNRL RNRRRRL NRNRRRL*
7	6/7	*RRNRRRL NNRNRRL RNRNRRL RRRNRRL*
7	6/7	*NNNRNRL NRNRNRL NRRRNRL RRRRNRL*
7	6/7	*NRRNRRL RNNNNRL RNNRNRL RRNRNRL*

ODEs investigated under the guidance of symbolic dynamics to date are quite limited though.

Chapter 5

CONTROL THEORY

5.1 Lyapunov's Direct Method

Lyapunov's Direct method has been for a long time the main tool in control engineering and robotics. The method does not require solving equations of the motion for observed system, but it does provide a rigorous mathematical proof of stability. Before we describe the method let us first state some useful mathematical definitions [93].

Definition. A scalar function $V(\mathbf{x})$, whose argument is a vector $\mathbf{x} \equiv (x_1, x_2, \ldots, x_n)$, is positive definite if $V(\mathbf{x}) = 0$ for $|\mathbf{x}| = 0$, and $V(\mathbf{x}) > 0$ for $|\mathbf{x}| \neq 0$. The function $V(\mathbf{x})$ is negative definite if $-V(\mathbf{x})$ is a positive definite function.

Definition. A scalar function $V(\mathbf{x})$ is positive semidefinite if $V(\mathbf{x}) = 0$ for $|\mathbf{x}| = 0$, and $V(\mathbf{x}) \geq 0$ for $|\mathbf{x}| \neq 0$.

Definition. Assume a system of ODEs

$$\dot{\mathbf{x}} = \mathbf{f}(\mathbf{x}) \tag{5.1}$$

has a solution in $\mathbf{x} = \mathbf{0}$. We say that the solution is stable in the sense of Lyapunov, or marginally stable, if for any $\varepsilon > 0$ and $t_0 \geq 0$ there exists $\delta > 0$ such that for $|\mathbf{x}(0)| < \delta$ it is $|\mathbf{x}(t)| < \varepsilon$ when $t \geq t_0$.

Definition. The solution $\mathbf{x} = \mathbf{0}$ of system (5.1) is asymptotically stable if it is stable in the sense of Lyapunov and $|\mathbf{x}(t)| \to 0$ as $t \to \infty$.

Lyapunov's direct method is based upon the Second Theorem of Lyapunov, which we state here.

Theorem. The solution $\mathbf{x} = \mathbf{0}$ of system (5.1) is marginally stable if there exists a positive definite scalar function $V(\mathbf{x})$, such that its time derivative

$$\dot{V}(\mathbf{x}) = \nabla V(\mathbf{x}) \cdot \dot{\mathbf{x}} = \nabla V(\mathbf{x}) \cdot \mathbf{f}(\mathbf{x}) \leq 0$$

is negative semidefinite. If $\dot{V}(\mathbf{x})$ is negative definite the solution is asymptotically stable. Any function which satisfies the marginal or asymptotic stability criteria is called a Lyapunov function.

Note that this theorem provides a sufficient condition only, and the Lyapunov function is not unique. If one cannot find a function that satisfies the above conditions, one cannot draw any conclusions about stability of the system either.

Lyapunov's Direct Method is constructive, and it can be used not only as a check to ensure that system is stable, but also as a tool to build a controller for the system. If it is obvious that the system (5.1) does not have a stable solution in $\mathbf{x} = \mathbf{0}$, some external force $\mathbf{g}(\mathbf{x})$ has to be applied to the system in order to obtain the desired stability. This procedure consists of finding a good Lyapunov function candidate first, and get as close as possible to meeting criteria of the Second Theorem of Lyapunov. Then, we add a function $\mathbf{g}(\mathbf{x})$ to the right hand side of (5.1), which would cancel all remaining nonegative terms in (5.1). This is a nontrivial task, and finding the right Lyapunov function candidate and right controller sometimes entails a lot of trial and error effort. Also, such a strategy leaves a lot of room for optimization, because the Lyapunov function is not unique, and there is a possibility that a better candidate may be found which would require a simpler controller $\mathbf{g}(\mathbf{x})$.

5.1.1 Discontinuous problems

The proof of the Second Theorem of Lyapunov assumes that the right hand side of system (5.1) is a continuous function. Paden and Sastry [71], and later Shevitz and Paden [79], extended Lyapunov's theory to systems of ODEs with a discontinuous right hand side, using Fillipov's theory of differential inclusion [20, 21]. It is

beyond the scope of this thesis to discuss the stability theory of discontinuous systems. Instead, we shall point out a very important consequence of it. If we are able to prove stability for a system of discontinuous equations, we are then also able to use a discontinuous controller $g(x)$. In a number of instances [86, 88, 87] it appears that it is much easier to find a discontinuous controller which satisfies this rigorous mathematical proof of stability.

5.2 Application to the Double Pendulum

The inverted double pendulum is a model often used in robotics to study the human walk. The lower link of the pendulum approximates legs and the upper link the torus of a person. Although it is a very crude approximation it still addresses some of the main stability concerns in robotics. The goal is to keep the pendulum in its upright position when gravity acts downward. Also, when a person walks with each step she or he adds some acceleration to her or his body. In a double pendulum model this manifests itself as a mild perturbation of the base point. Let us observe a two dimensional double pendulum model as shown in Figure 5.1. For simplicity, we assume that motion of the system is in a 2-dimensional plane.

Moments of inertia for lower and upper link are $I_{01} = 2.256$ kg m^2 and $I_{02} = 2.71$ kg m^2, respectively; their masses are $m_1 = 30$ kg and $m_2 = 45$ kg; distances from suspension point to their centers of mass are $a_1 = 0.5$ m and $a_2 = 0.45$ m, and the length of the lower link is $l_1 = 0.95$ m. The base point is perturbed so it acquires vertical acceleration $g(t)$ and horizontal acceleration $f(t)$. We allow functions $f(t)$ and $g(t)$ to be arbitrary, but bounded functions in time such that $|f(t)| < \overline{f}$, $|g(t)| < \overline{g}$, where $\overline{f}$, $\overline{g}$ =const.

Let us first derive the equation of motion for the system. We denote vertical inclination of the lower link as θ_1, and the angle between two links as θ_2 (Fig. 5.1).

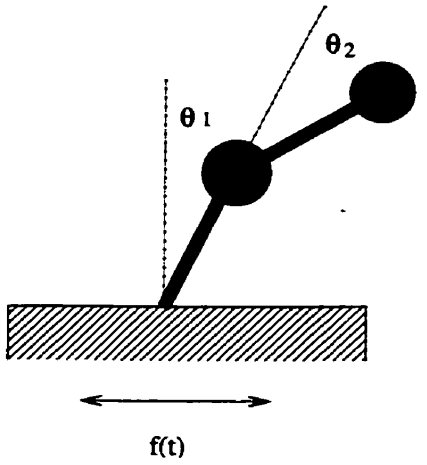

Figure 5.1: An inverted double pendulum. Base point moves with acceleration $f(t)$ horizontally and $g(t)$ vertically.

The kinetic energy of this system is then given as:

$$T = \frac{1}{2}I_{01}\dot{\theta}_1^2 + \frac{1}{2}I_{02}(\dot{\theta}_1 + \dot{\theta}_2)^2 + \frac{1}{2}m_1 v_{C1}^2 + \frac{1}{2}m_2 v_{C2}^2 \tag{5.2}$$

where v_{C1} and v_{C2} are velocities of the centers of mass for the lower and upper link, respectively. In polar coordinates the positions of respective centers of mass are given

$$\begin{aligned} x_{C1} &= a_1 \sin(\theta_1) \\ y_{C1} &= a_1 \cos(\theta_1) \end{aligned} \tag{5.3}$$

and

$$\begin{aligned} x_{C2} &= l_1 \sin(\theta_1) + a_2 \sin(\theta_1 + \theta_2) \\ y_{C2} &= l_1 \cos(\theta_1) + a_2 \cos(\theta_1 + \theta_2) \end{aligned} \tag{5.4}$$

By taking first derivatives and squaring expressions above we get

$$v_{C1}^2 = a_1^2\dot{\theta}_1^2 \tag{5.5}$$

$$v_{C2}^2 = l_1^2\dot{\theta}_1^2 + a_2^2(\dot{\theta}_1 + \dot{\theta}_2)^2 + 2l_1a_2\cos\theta_2\dot{\theta}_1(\dot{\theta}_1 + \dot{\theta}_2) \tag{5.6}$$

and subsequently the kinetic energy is found to be:

$$T = \frac{1}{2}I_1\dot{\theta}_1^2 + \frac{1}{2}I_2(\dot{\theta}_1 + \dot{\theta}_2)^2 + \frac{1}{2}m_2 l_1 a_2 \cos\theta_2 \dot{\theta}_1(\dot{\theta}_1 + \dot{\theta}_2) \tag{5.7}$$

where $I_1 = I_{01} + m_1 a_1^2 + m_2 l_1^2$, and $I_2 = I_{02} + m_2 a_2$. The effective potential energy for the system is found as a sum:

$$V = f(t)(m_1 x_{C1} + m_2 x_{C2}) + [g_0 + g(t)](m_1 y_{C1} + m_2 y_{C2}) \tag{5.8}$$

Substituting (5.3) and (5.4) into (5.8) and writing the Lagrangian as $L = T - V$ we obtain:

$$\begin{aligned} L &= \frac{1}{2}I_1\dot{\theta}_1^2 + \frac{1}{2}I_2(\dot{\theta}_1 + \dot{\theta}_2)^2 + m_2 l_1 a_2 \cos\theta_2\, \dot{\theta}_1(\dot{\theta}_1 + \dot{\theta}_2) \\ &\quad -[g_0 + g(t)]\left\{(m_1 a_1 + m_2 l_1)\cos\theta_1 + m_2 a_2 \cos(\theta_1 + \theta_2)\right\} \\ &\quad -f(t)[(m_1 a_1 + m_2 l_1)\sin\theta_1 + m_2 a_2 \sin(\theta_1 + \theta_2)] \end{aligned}$$

Equations of motion are then derived as

$$\frac{d}{dt}\frac{\partial L}{\partial \dot{\theta}_i} - \frac{\partial L}{\partial \theta_i} = R_i, \quad i = 1, 2 \tag{5.9}$$

where R_i are control torques. Finally we get the equations of motion as:

$$\begin{aligned} \ddot{\theta}_1 &= A(\theta_2)\{\beta \sin\theta_2[I_2(\dot{\theta}_1 + \dot{\theta}_2)^2 + \beta\cos\theta_2\dot{\theta}_1^2 \\ &\quad +[g_0 + g(t)][I_2(m_1 a_1 + m_2 l_1)\sin\theta_1 - \beta\cos\theta_2 m_2 a_2 \sin(\theta_1 + \theta_2)] \\ &\quad +f(t)[I_2(m_1 a_1 + m_2 l_1)\cos\theta_1 - \beta\cos\theta_2 m_2 a_2 \cos(\theta_1 + \theta_2)] \\ &\quad +I_2 R_1 - (I_2 + \beta\cos\theta_2)R_2\} \end{aligned} \tag{5.10}$$

$$\begin{aligned} \ddot{\theta}_2 &= -A(\theta_2)\{\beta\sin\theta_2[(I_2 + \beta\cos\theta_2)(\dot{\theta}_1 + \dot{\theta}_2)^2 + (I_1 + \beta\cos\theta_2)\dot{\theta}_1^2] \\ &\quad +[g_0 + g(t)][(I_2 + \beta\cos\theta_2)(m_1 a_1 + m_2 l_1)\sin\theta_1 - (I_1 + \beta\cos\theta_2)m_2 a_2 \sin(\theta_1 + \theta_2)] \\ &\quad +f(t)[(I_2 + \beta\cos\theta_2)(m_1 a_1 + m_2 l_1)\cos\theta_1 - (I_1 + \beta\cos\theta_2)m_2 a_2 \cos(\theta_1 + \theta_2)] \\ &\quad +(I_2 + \beta\cos\theta_2)R_1 - (I_1 + I_2 + 2\beta\cos\theta_2)R_2\} \end{aligned} \tag{5.11}$$

where $\beta = m_2 l_1 a_2$, and

$$A(\theta_2) = \frac{1}{I_1 I_2 - \beta^2 \cos^2 \theta_2} \tag{5.12}$$

In the series of articles Wu at al. [86, 88] developed a discontinuous Lyapunov controller for this system of equations.

$$\begin{aligned} R_1 &= -k_{p1}\theta_1 - k_{d1}\dot{\theta}_1 \\ &\quad -m_2 a_2 g(\theta_1 + \theta_2) - (m_1 a_1 + m_2 l_1) g \theta_1 \dot{\theta}_1 \\ &\quad -(m_1 a_1 + m_2 l_1 + m_2 a_2)(f + g)\,\mathrm{sgn}(\dot{\theta}_1) \end{aligned} \tag{5.13}$$

$$\begin{aligned} R_2 &= -k_{p2}\theta_1 - k_{d2}\dot{\theta}_2 \\ &\quad -m_2 a_2 g(\theta_1 + \theta_2) - m_2 a_2 (f + g)\,\mathrm{sgn}(\dot{\theta}_2) \end{aligned}$$

Stability proof is conducted for linear control gains k_{pi} and k_{di} set to zero, but they are included in the controller for "fine-tuning" in simulations. The main advantage of such a control technique is that it provide us with a rigorous mathematical proof for any bounded functions $g(t)$ and $f(t)$. On the other hand, it is very difficult to implement discontinuous control torque in a real engineering system. The solution proposed by Wu at al. was to smooth the discontinuous controller by substituting

$$\mathrm{sgn}(\dot{\theta}_i) \to \tanh(\alpha_i \dot{\theta}_i), \quad i = 1, 2 \tag{5.14}$$

The idea is to use the discontinuous controller as a guide towards a reliable smooth controller. However, it is very difficult to obtain a rigorous proof of stability when using a smooth controller. We propose calculating the Lyapunov spectrum in order to study the transition from discontinuous to smooth controller [87]. The Lyapunov spectrum gives us a qualitative description of system's stability. A positive exponent indicates that system is unstable – either chaotic or divergent. Any combination of negative and zero exponents suggests periodic or quasiperiodic motion (Section 3.6). This approach is particularly useful for systems whose phase space has more than

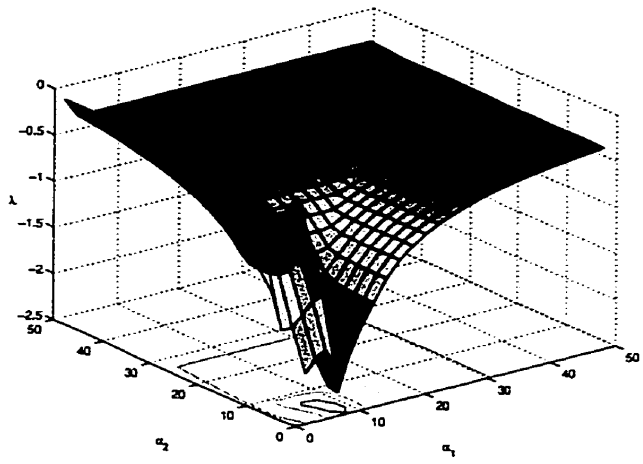

Figure 5.2: Leading Lyapunov exponent plotted against control parameters α_1 and α_2.

three dimensions, and visualization of the dynamics is difficult. However, caution is necessary, since a particular Lyapunov spectrum tells us that there is an attractor in the phase space, but it does not tell us if it is around the desired position.

In order to be able to calculate Lyapunov exponents we have to write system (5.10-5.11) in an autonomous form, adding equation $\dot{t} = 1$ to the system, and hence formally using time as a fifth state space coordinate. However, any perturbation of time coordinate would result in a time shift that would remain unchanged throughout the motion. This means that there is always at least one Lyapunov direction with associated zero exponent, regardless of what continuous controller we use. Therefore we cannot expect to have a stable equilibrium point in our state space. The best we can achieve is a marginal stability when there is an asymptotically stable limit cycle around the desired position. If the limit cycle is small enough we can in this way obtain the desired behavior of our system.

We make the substitution (5.14) into controller (5.13), and plot the leading Lyapunov exponent against parameters α_1 and α_2 (Fig. 5.2). The leading Lyapunov exponent is the largest nonzero exponent, and it should give us a good idea as to what

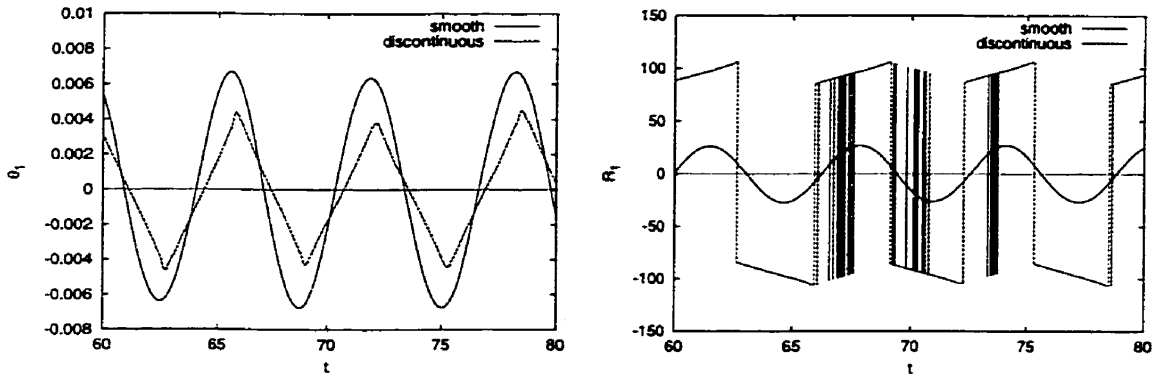

Figure 5.3: Position of lower link (left), and control torque exerted upon it (right) for discontinuous and smooth controller, respectively.

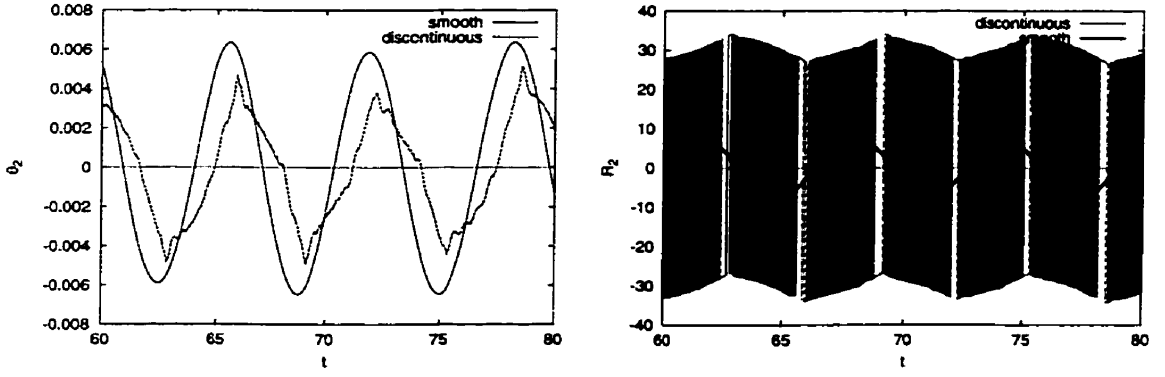

Figure 5.4: Position of upper link (left), and control torque exerted upon it (right) for discontinuous and smooth controller, respectively.

is the Lyapunov spectrum. In Figure 5.2 the leading exponent is strictly negative, so the attractor for the system is a limit cycle. Furthermore, there is no indication of bifurcations meaning that the limit cycle remains stable for a wide range of parameters α_i. Finally, we observe a saturation of the leading Lyapunov exponent for $\alpha_1, \alpha_2 > 30$. This implies that the attractor will not change significantly with the further increase of α_1 and α_2, and therefore stability with the smooth controller is similar to that achieved with the discontinuous one.

Our simulations (Figs. 5.3 and 5.4) show that we do have satisfactory stabilization of the double pendulum around its upright position. Both links oscillate with slightly larger amplitudes, but they are still within 0.01 rad. However, we use a smooth control torque with up to three times a smaller amplitude than that of the discontinuous controller. This numerical result gives us a very strong indication that there indeed exists an asymptotically stable limit cycle in 5-dimensional state space of the system (5.10-5.11) with its associated basin of attraction. This means that the system exhibits an overall stable behavior, and diagrams in Figures 5.3 and 5.4 may be interpreted as 2-dimensional projections of its limit cycle.

The Lyapunov exponents calculation gives us an indication about the system's local stability. It can be shown though [70] that Lyapunov exponents are the same almost everywhere within a basin of attraction, i.e. they can be viewed as a property of the phase space rather than an individual trajectory. Therefore we have to examine the basin of attraction of the limit cycle in order to find its region of stability. For our numerical study of the basin of attraction we utilized a simple algorithm, motivated by the technique presented in Ref. [68]. We divide the region of interest in phase space into boxes of size 0.1, starting from the box whose center is in the origin of our state space. Since a stable limit cycle lies in this box we assume that if the state space trajectory stays within it for 20 seconds, the trajectory will eventually end up on the limit cycle. We started state space trajectories systematically from neighboring boxes, and checked if they would get into the central box within 15 seconds and then

if they would stay there for next 20 seconds. If this criterion is met, the whole box is tagged as a part of basin of attraction for the limit cycle. Applying this algorithm we have not found any box within the range $\theta_1 \in (-\pi/2, \pi/2)$, $\theta_2 \in (-1, 1)$, and $\dot{\theta}_1, \dot{\theta}_2 \in (-1/2, 1/2)$ which does not belong to the basin of attraction. This indicates that this whole region lies within the region of stability of interest.

This is a very crude technique and it is far from being a rigorous mathematical proof. However, we can increase the test time for which the trajectory has to stay in the central box, use a finer grid of boxes, or further improve our algorithm for tracking attractors (Ref. [68]). In this way we can at the expense of computation time achieve accuracy which is sufficient for practical purposes. With the higher resolution algorithm, even if we miss a few points which do not belong to the basin of our desired attractor, these are most likely to be wiped off as soon as we add some random noise signal to our solution for the system (5.10-5.11).

5.3 Conclusion

In this project we demonstrated some prospects for the use of Lyapunov exponents analysis in control design. Lyapunov's direct method, though very powerful, requires us to reduce a nonlinear problem to a steady state problem first, i.e. we need to define a phase space which contains an equilibrium point in it. On the other hand, the Lyapunov exponents calculation is more suited for dynamical systems where existence of equilibrium points is not necessary. However, Lyapunov exponent analysis does not enable us to construct a controller from scratch, it only help us test and fine tune an already given controller. In that regard, we may view it as a complement rather than an alternative for Lyapunov's direct method. In this project we proposed a way to combine the two approaches in order to design an optimal controller. We suggested designing a discontinuous controller first, because it is relatively easy to do it using Lyapunov's direct method. The next step is to "smooth-out" a discontinuous

controller utilizing the Lyapunov exponent analysis, and obtain a suitable continuous controller. We believe that our method may prove very efficient especially for systems with a large number of degrees of freedom.

Chapter 6

CONCLUSION

In chapter 5 we demonstrated a detailed analysis of the dynamics of periodically driven nonlinear system. We showed that chaotic behavior, being a purely deterministic phenomenon, may be analyzed and decomposed into its "building blocks" – unstable periodic orbits. With such a comprehensive knowledge about a system's dynamics it is reasonable to ask if we can take advantage of a chaotic behavior, instead of treating it like random noise and trying to avoid it.

There are two control techniques proposed which exploit chaotic properties of a dynamical system. The first one is so called "OGY" (Ott-Grebogi-Yorke) algorithm [69]. It is shown that by a small periodic variation of a control parameter it is possible to lock onto a single periodic orbit embedded in a chaotic attractor. Since there are infinitely many periodic orbits embedded, the assumption is that the desired motion can be extracted from the chaotic attractor. This means that chaotic systems require less control force, and therefore are easier to control. Furthermore, locking onto different orbits requires only a small change in the way the control parameter is varied, so stabilizing a chaotic system also enables us to switch between different periodic modes easily. This technique has been extensively studied, and experimentally verified [8, 12] over the past ten years. The remaining issue to address is that systems stabilized in this manner may exhibit very long transient motion.

The other technique is the targeting algorithm [51, 52, 7]. Instead of locking the system onto a single trajectory we try to keep it on desired path by slightly pushing it from one unstable orbit to another, by a sequence of time dependent parameter variations. The idea of hopping from one trajectory to another is not completely

new. In celestial mechanics scientists have been using gravitational assistance to get spacecraft to the destination point for a long time.

Detailed knowledge about specific chaotic behavior, such as that provided by symbolic dynamics analysis, is absolutely essential for designing efficient control mechanisms, using both of these techniques. We need to be able to identify all low period orbits within the attractor, or if necessary to modify chaos by suitable change of system parameters in order to obtain orbits we need. Let us further elaborate these ideas using the example of a double pendulum control from Chapter 5.

6.1 Double Pendulum Control Revisited

Instead of using a Lyapunov controller (5.13) let us apply a simple linear controller to the double pendulum system:

$$\begin{aligned} R_1(\theta_1, \dot{\theta}_1) &= -k_{p1}\theta_1 - k_{d1}\dot{\theta}_1 \\ R_2(\theta_2, \dot{\theta}_2) &= -k_{p2}\theta_1 - k_{d2}\dot{\theta}_2 \end{aligned} \tag{6.1}$$

We set the control gains $k_{d1} = k_{d2} = 20$, and vary the other two, k_{p1} and k_{p2} from zero onwards. We study the evolution of the dynamics for such a system by observing the change of leading Lyapunov exponent with the change of control parameters. We notice (Fig. 6.1) that for low values of control parameters the leading Lyapunov exponent is negative, therefore the attractor for the system is a stable limit cycle. With a relatively small increase of control gains such a limit cycle changes its stability, and at some places in parameter plane k_{p1}-k_{p2} it evolves into a chaotic attractor. As we further increase the control gains, motion along a stable limit cycle is restored.

To have a closer look at these processes we plot phase space diagrams in θ_1-$\dot{\theta}_1$ and θ_2-$\dot{\theta}_2$ planes (Fig. 6.2). For small control gains, the torque created by the controller is smaller than the torque due to gravity, so the limit cycle we obtain lies left or right of the desired position, depending on the initial condition. For control torques that

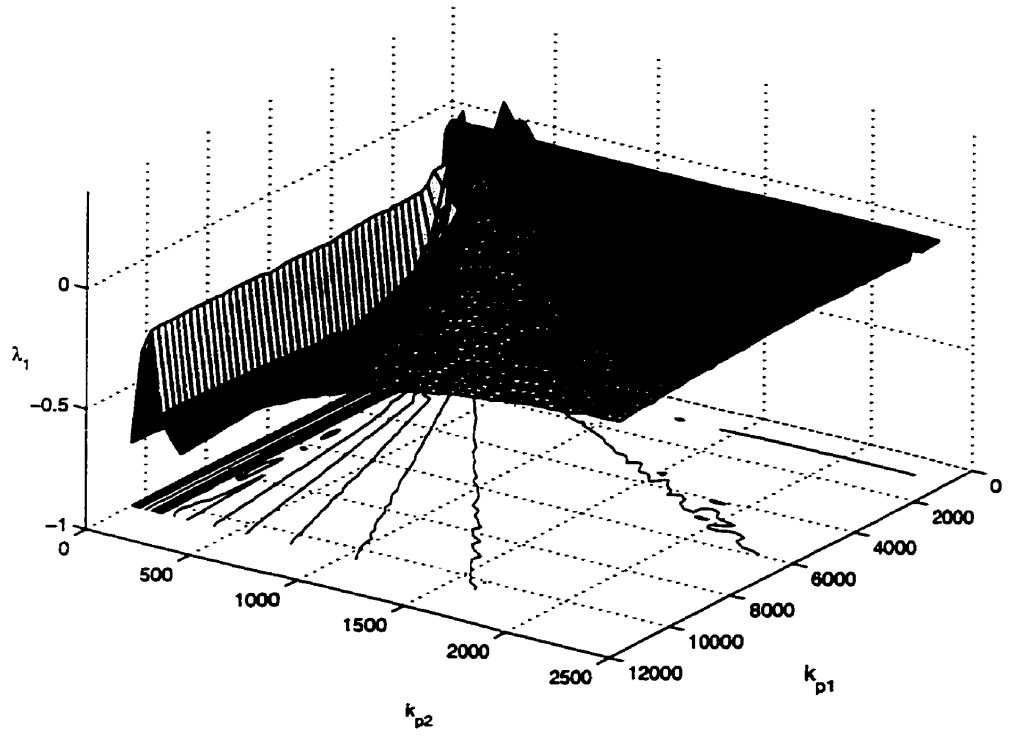

Figure 6.1: Leading Lyapunov exponent plotted against control parameters k_{p1} and α_{p2}.

are relatively close, but still smaller than, the torque of gravity, perturbation of the base point causes the system to occasionally escape from one potential well and get caught by another, so the motion becomes chaotic. By increasing control gains over these values we eventually obtain satisfactory stability around the desired position such as one shown in Figures 6.2e and 6.2f.

It appears from Figure 6.1 that if we are able to control the double pendulum system when it exhibit chaos we would need much smaller control gains than if we use a linear or Lyapunov controller. Since algorithms for controlling chaos require a miniscule control torques we infer that we can stabilize this system with control torques which total less than the gravity torque acting upon it. This means that controlling a chaotic double pendulum with base point perturbation requires less control torque than controlling one with fixed base point. This is in agreement with experiment which every one of us can easily conduct. Try to stay still, without moving your feet at all for, say, ten minutes, and try to walk slowly for the same amount of time. The more exhausting task is undoubtedly to stand still, meaning that our body spends more energy in keeping our balance when we stand than when we walk slowly. Although the double pendulum is a very crude model of human walk we shall go one step further and assume that some sort of chaos control is indeed what helps us keep our balance. The fact that our body is a highly nonlinear system, and that torques produced by our muscles are much closer to those of a chaotic controller than those produced by a Lyapunov controller make our assumption credible. It is, therefore, quite possible that by studying chaos control in this model we may learn more about the dynamics of a human body. Such research may be applied, for example, towards design of prosthetic devices.

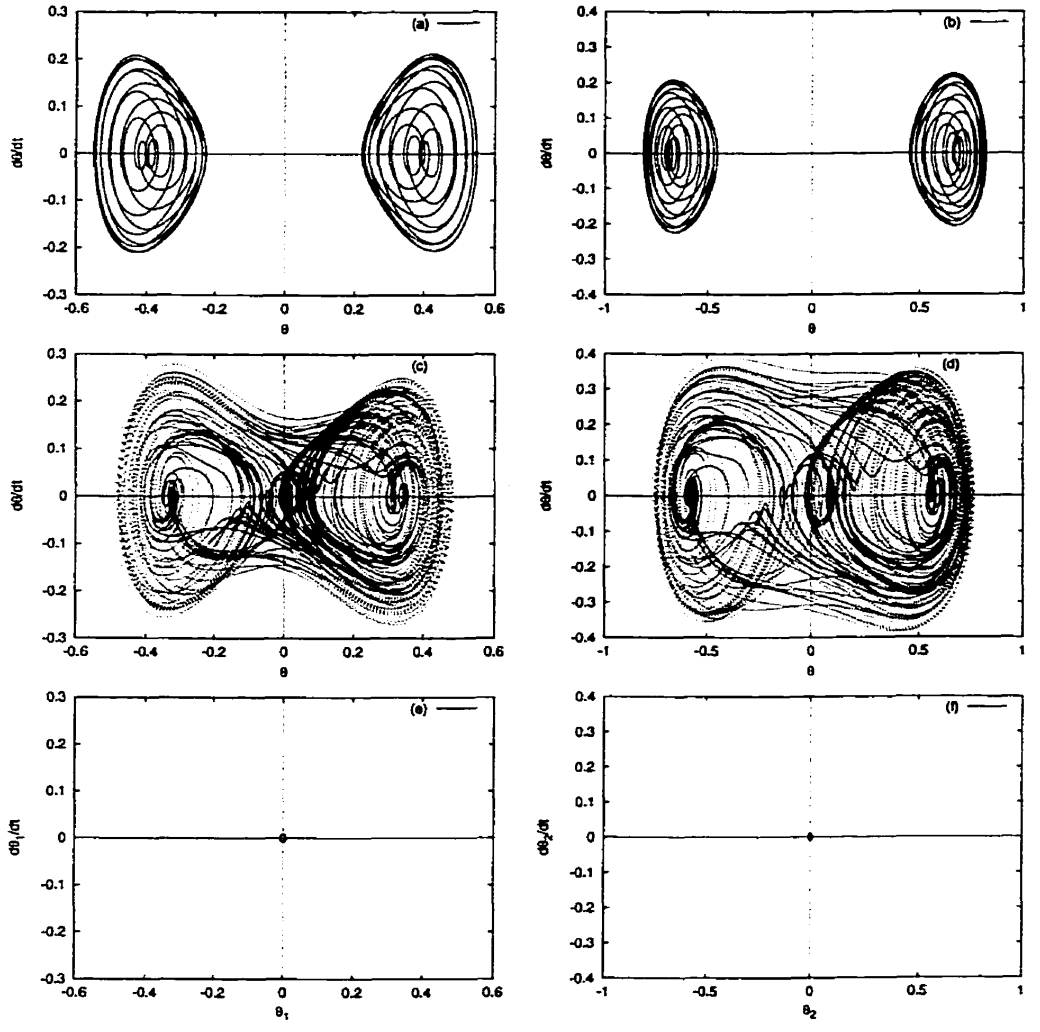

Figure 6.2: Phase plane projections for lower and upper link respectively at $k_{p1} = 900$ $k_{p1} = 260$, (a) and (b); $k_{p1} = 1050$ $k_{p1} = 270$, (c) and (d); $k_{p1} = 3000$ $k_{p1} = 800$, (e) and (f).

6.2 Future Prospects

Chaos control of a double pendulum model of human walk is indeed a very promising research topic. However there are a few obstacles along the way. Both the OGY and targeting algorithm are at their early stages of development, and there are some serious issues to be addressed such as long transient behavior and robustness of controllers. Also, symbolic dynamic theory is developed for 1- and 2-dimensional maps only, and extending it to more than two dimensions is not a simple task at all. All of these problems are currently studied by numerous scientists worldwide, and for some of those there may not be a solution. In this thesis we studied some fundamental problems along this line of research. We demonstrated that symbolic dynamics analysis can be successfully extended to a dynamical flow describing a periodically driven mechanical system, and we improved "conventional" control theory and stability analysis by applying methods of chaotic dynamics.

BIBLIOGRAPHY

[1] M. Abramovitz and I. A. Stegun, *"Handbook of Mathematical Functions"*, p. 727, (New York, Dover, 1965).

[2] Alligood, K. T., Sauer, T. D., Yorke, J. A. (1997). *Chaos, an Introduction to Dynamical Systems.* Springer-Verlag New York, Inc.

[3] Arneodo, A., Coullet, P., Tresser, C., Libchaber, A., Maurer, J. and d'Humieres, D. (1983). "On the observation of an Uncompleted Cascade in a Rayleigh-Bénard Experiment", *Physica*, 6D, 385-92.

[4] Baker, G. L. and Gollub, J. P. (1996). *Chaotic Dynamics.* Cambridge University Press. New York

[5] Benettin, G., Galgani L., Giorgilli A. and Strelcyn J. (1980) "Lyapunov Characteristic Exponents for Smooth Dynamical Systems and for Hamiltonian Systems; A Method for Computing All of Them". *Meccanica*, Vol. 15, No. 1, 9-19

[6] Binruo, W., Zhou-jing, Y., Blackburn, J. A., Vik, S., Smith, H. J. T. and Nerenberg, M. A. H. (1988). "Analog simulation of coupled superconducting weak links: Locking and chaos", *Phys. Rev.* B, Vol. 37, No. 7, 3349-58.

[7] Boccaletti, S., Farini, A., Kostelich, E. J. and Arecchi, F. T.(1997). "Adaptive targeting of chaos", *Phys. Rev.* **E55**, no. 5, part A, R4845–R4848.

[8] Cristini, D. J. and Collins, J. J. (1995). *Phys. Rev. Lett.* **75**, p. 2782.

[9] Cvitanović, P., Gunaratne, G. H. and Procaccia, I. (1988). "Topological and metric properties of Hénon-type strange attractors", *Phys. Rev.* **A38**, p. 1503-20.

[10] Cvitanović, P., Artuso, R., Mainieri, R., Tanner, G. and Vattay, G. (2001). "Classical and Quantum Chaos", **www.nbi.dk/ChaosBook/**, Niels Bohr Institute, Copenhagen.

[11] Delbourgo, R., Hart, W. and Kenny, B. G. (1985). "Dependance of Universal Constants Upon Multiplication Period in Nonlinear Maps" *Phys. Rev.* A, Vol. 31, No.1, 514-6.

[12] Ditto, W. L., Rauseo, S. N. and Spano, M. L. (1990). *Phys. Rev. Lett.* **65**, p. 3211.

[13] D'Humieres, D., Beasley, M. R., Huberman, B. A. and Libchaber, A. (1982). "Chaotic States and Routes to Chaos in the Forced Pendulum", *Phys. Rev.* A, Vol. 26, No. 6, 3483-96.

[14] Ding, M., Grebogi, C., Ott, E., Sauer, T. and Yorke, J. A. (1993). "Estimating correlation dimension from a chaotic time series: when does plateau onset occur?", *Physica*, D 69, 404-24.

[15] Myers, M., Wicklin, R. and Worfolk, P. (1992). "Computer Assisted Exploration of Dynamical Systems", *Notices of the American Mathemtical Society*, **39**, p. 303-9. URL: **http://www.cam.cornell.edu/guckenheimer/dstool.html**

[16] Farmer, J. D. (1982). "Chaotic Attractors of an Infinite-Dimensional Dynamical System", *Physica*, 4D, 366-393

[17] Farmer, J. D., Ott, E. and Yorke, J. A. (1983). "The Dimension of Chaotic Attractors", *Physica*, 7D, 153-180

[18] Feigenbaum, M. J. (1978). "Quantitative Universality for a Class of Nonlinear Transformations", *J. Stat. Phys.*, Vol. 19, No. 1, 25-52

[19] Feigenbaum, M. J. (1978). "The Universal Metric Properties of Nonlinear Transformations", *J. Stat. Phys.*, Vol. 21, No. 6, 669-706

[20] Filippov, A. F. (1960). "Differential equations with discontinuous right-hand side", *Math Sbornik*, Vol. 51, p. 99-128. (English translation: *Amer. Math. Soc. Translations*, 1964, Vol 42, p. 191)

[21] Filippov, A. F. (1979). "Differential equations with second members discontinuous on intersecting surfaces", *Differentialnye Uravneniya*, Vol. 15, p. 1814. (English translation: *Differential Equations*, 1980, Vol 15, p. 1292-99)

[22] Goldstein, H. (1965). *Classical Mechanic.* Addison-Wesley Publishing Company, Inc.

[23] Grassberger, P. (1981). "On the Hausdorf Dimension of Fractal Attractors", *J. Stat. Phys.*, Vol. 26, No. 1, 173-179

[24] Grassberger, P. and Procaccia, I. (1983). "Measuring the Strangeness of Strange Attractors". *Physica*, 9D, 189-208

[25] Grassberger, P. and Procaccia, I. (1983). "Characterization of Strange Attractors", *Phys. Rew. Letters*, Vol. 50, No. 5, 346-9.

[26] Grassberger, P. and Procaccia, I. (1984). "Dimensions and Entropies of Strange Attractors from a Fluctuating Dynamics Approach", *Physica* 13D, 34-54.

[27] Grassberger, P. and Kantz, H. (1985). "Generating Partitions for the Dissipative Hénon Map", *Phys. Lett.* **113A**, p. 235.

[28] Grebogi, C., Ott, E. and Yorke, J. A. (1983). "Chaotic Attractors in Crises", *Phys. Rev. Lett.*, Vol. 48, No. 22, 1507-10

[29] Grebogi, C., Ott, E. and Yorke, J. A. (1983). "Crises, Sudden Changes in Chaotic Attractors and Transient Chaos", *Physica*, 7D, 181-200

[30] Grebogi, C., Ott, E., Pelikan, S. and Yorke, J. A. (1984). "Strange Attractors That Are Not Chaotic", *Physica*, 13D, 261-268

[31] Greene, J. M. and Kim, J. S. (1987). "The Calculation of Lyapunov Exponents", *Physica*, **24D**, 213-25.

[32] Gu, Y. (1987). *Phys. Lett.* **A124**, p. 340.

[33] Gwinn, E. G. and Westervelt, R. M. (1985). "Intermittent Chaos and Low-Frequency Noise in the Driven Damped Pendulum", *Phys. Rew. Letters*, Vol. 54, No. 15, 1613-6

[34] Gwinn, E. G. and Westervelt, R. M. (1986). "Fractal Basin Boundaries and Intermittency in Driven Damped Pendulum", *Phys. Rev.* A, Vol. 33, No. 6

[35] Haken, H. (1983). "At Least One Lyapunov Exponent Vanishes If the Trajectory of an Attractor Does Not Contain a Fixed Point", *Physics Letters*, Vol. 94A, No. 2, 71-72

[36] Hansen, K. (1986). Ph. D. Thesis, University of Copenhagen, Denmark.

[37] Hao Bai-lin, *Elementary Symbolic Dynamics and Chaos in Dissipative Systems*, (World Scientific, Singapore, 1989).

[38] Hao, B.-L., Liu, J.-X. and Zheng, W.-M. (1998). "Symbolic dynamics analysis of the Lorenz equations", *Phys. Rev.* **E57**, p. 5378-96.

[39] Hao, B.-L. (1998). "Applied Symbolic Dynamics", *Chao-dyn/9806025.*

[40] Hénon, M. (1976). *Commun. Math. Phys.* **50**, p. 69.

[41] Hilborn, R. C. (1994). *Chaos and Nonlinear Dynamics.* Oxford University Press, Inc. New York

[42] Hirsch, M. W. and Smale, S. (1974). *Differential Equations, Dynamical Systems, and Linear Algebra*, Academic Press, Inc. New York

[43] Huberman, B. A. and Rudnick, J. (1980). "Scaling Behavior of Chaotic Flows", *Phys. Rew. Letters*, Vol. 45, 154-6

[44] Ito, R. (1981). *Math. Proc. Camb. Phil. Soc.* **89**, p. 107.

[45] Jakobson, M. V. (1981). "Absolutely Continuous Invariant Measures for One-Parameter Families of One-Dimensional Maps", *Comm. Math. Phys.* **81**, p. 39.

[46] Kaiser, D. (1997). *Phys. Rev.* **D56**, p. 706.

[47] Kaiser, D. (1999). *Phys. Rev.* **D59**, p. 117901.

[48] J. L. Kaplan and J. A. Yorke, *Lecture Notes in Mathematics*, Vol. 730, 204-227, Springer-Verlag, Berlin (1979).

[49] Kobes, R., Liu, J-. X. and Peleš, S. (2001). "Analysis of a Parametrically Driven Pendulum", *Phys. Rev.* **E63**, p. 036219.

[50] Kofman, L., Linde, A. and Starobinsky, A. (1994). *Phys. Rev. Lett.* **73**, p. 3195.

[51] Kostelich, E. J., Grebogi, C., Ott, E. and Yorke, J. A.(1993). "Higher-dimensional targeting", *Phys. Rev.* **E47**, no. 1, p. 305–315.

[52] Kostelich, E. J. and Barreto, E. (1997). "Targeting and control of chaos", *Math. Model.* **8**, Control and chaos (Honolulu, HI, 1995), p. 158–169, Birkhuser Boston, Boston, MA, 1997.

[53] Landau, L. D. and Lifshitz, E. M. (1976). *Mechanics, Volume 1 of Course of Theoretical Physics.* Pergamon Press Ltd. New York

[54] F. Ledrappier, *Commun. Math. Phys.* **81**, 229-238 (1981).

[55] Liu, J.-X. and Zheng, W.-M. (1995). *Commun. Theor. Phys.* **23**, p. 315.

[56] Liu, J.-X., Zheng, W.-M. and Hao,B.-L.(1996). "From Annular to Interval Dynamics: Symbolic Analysis of the Periodically Forced Brusselator", *Chaos, Solitons and Fractals* **7**, p. 1427-53.

[57] Liu, J.-X., Wu, Z.-B. and Zheng, W.-M. (1996). *Commun. Theor. Phys.* **25**, p. 149.

[58] Lorenz, E. N. (1984). "The Local Structure of a Chaotic Attractor in Four Dimension", *Physica* 13D, 90-104.

[59] Lozi, R. (1978). *J. de Physique* **39C**, p. 9.

[60] Lundqvist, S. (1988). "Chaos, Order, Patterns, Fractals - An Overview", in *Order and Chaos in Nonlinear Physical Systems*, ed. Lundqvist, S., March, N. H., Tosi, M. P. Plenum Press, New York

[61] MacDonald, A. H. and Plischke, M. (1983). "Study of the Driven Pendulum: Application to Josephson Junction and Charge- Density-Wave Systems", *Phys. Rev.* **B27**, No. 1, 201-11.

[62] Manneville, P. and Pomeau, Y. (1979). "Intermittency and the Lorenz Model", *Physics Letters*, Vol. 75A, No. 1,2, 1-2

[63] McCauley, J. L. (1988). "Shift Maps and Chaos in Conservative Systems", *Physica Scripta*, Vol. 20, 21-33.

[64] McDonald, S. W., Grebogi, C., Ott, E. and Yorke, J. A. (1985). "Structure and Crises of Fractal Basin Boumdaries", *Physics Letters*, Vol. 107A, No. 2, 51-54.

[65] McDonald, S. W., Grebogi, C., Ott, E. and Yorke, J. A. (1985). "Fractal Basin Boumdaries", *Physica* 17D, 125-153.

[66] Metropolis, M., Stein, M. L. and Stein P. R. (1973). *J. Comb. Theo.* **A15**, p. 25.

[67] Morse, P. M. and Feshbach, H. (1953). *Methods of Theoretical Physics, Part I*, McGraw–Hill, New York, p. 557.

[68] Nusse, H. and Yorke, J. A.(1998). *Dynamics: Numerical Exploration*, Springer-Verlag New York, Inc.

[69] Ott, E., Grebogi, C. and Yorke, J. A. (1989). "Controlling Chaos", *Phys. Rev. Letters* **64**, No. 11, p. 1196.

[70] Ott, Edward (1993). *Chaos in Dynamical Systems.* Cambridge University Press, New York

[71] Paden, B. E. and Sastry, S. S. (1987). "A Calculus for computing Filippov's differential inclusion with application to the variable structure control of robot

manipulators", *IEEE Transactions on Circuits and Systems*, Vol. CAS-34, No. 1, p. 73-82.

[72] Peitgen, H., Jurgens, H. and Saupe, D. (1992). *Chaos and Fractals, New frontiers of Science.* Springer-Verlag New York, Inc.

[73] Peleš, S (2000). "Analysis of a Periodically Driven Mechanical System", *Prog. The. Phys. Sup.* **139**, p. 496-506.

[74] Press, W. H., Teukolsky, S. A., Vetterling, W. T. and Flannery, B. P. (1992). *Numerical Recipes in C, The Art of Scientific Computing.* Cambridge University Press, New York

[75] Rowlands, G. (1988). "An introduction to the Properties of One-Dimensional Difference Equations", in *Order and Chaos in Nonlinear Physical Systems*, ed. Lundqvist, S., March, N. H., Tosi, M. P. Plenum Press, New York

[76] Russell, D. A., Hanson, J. D. and Ott, E. (1980). "Dimension of Strange Attractor", *Phys. Rev. Letters*, Vol. 45, No. 14, 1175-8.

[77] Schuster, H. G. (1995) *Deterministic Chaos.* VCH Verlagsgesellschaft mbH. Weinheim, Germany

[78] Sharkovskii, A. N. (1964). "Coexistence of Cycles of a Continuous Map of a Line Into Itself", *Ukr. Mat. Z.* **16**, p. 61.

[79] Shevitz, D. and Paden, B. (1994). "Lyapunov stability theory of nonsmooth systems", *IEEE Transactions on Automatic Control*, Vol. 39, No. 9, p. 1910-14.

[80] Shimada, I. and Nagashima, T. (1979). "A Numerical Approach to Ergodic Problem of DissipativeDynamical Systems", *Prog. The. Physics*, Vol. 61, No. 6, 1605-16.

[81] Smith, H. T. J. and Blackburn, J. A. (1994). "Multiperiodic Orbits in a Pendulum with a Vertically Oscillating Pivot", *Phys. Rev.* E, Vol. 50, No. 1.

[82] Thompson, J. M. T. (1989). "Chaotic phenomena triggering the escape from potential well", *Proc. R. Soc. Lond.* A **421**, p. 195-225.

[83] Vetterling, W. T., Teukolsky, S. A., Press, W. H. and Flannery, B. P. (1992). *Numerical Recipes, Example Book (C)*, Cambridge University Press, New York

[84] Wolf, A., Swift, J. B., Swinney, H. L., and Vastano, J. A. (1984). "Determining Lyapunov Exponents from a Time Series". *Physica*, 16D, 285-317

[85] Wolf, A. (1986). "Quantifying Chaos with Lyapunov Exponents", in *Chaos*, ed. Holden, A. V. Princeton University Press, Princeton, New Jersey

[86] Wu, Q. and Thornton-Trump, A. B. (1997). "Control of base excited inverted pendulum with two degrees of rotational freedom", *J. Franklin Inst.*, Vol. 334B, No. 1, p. 63-92.

[87] Wu, Q., Sekhavat, P., Peles, S., Abo-Shanab, R.F., and Sepehri, N. (2001). "An Improved Design Procedure of Lyapunov Feedback Control", Accepted for *IEEE International Symposium on Computational Intelligence in Robotics and Automation (IEEE CIRA 2001).*

[88] Wu, Q., Thornton-Trump, A. B. and Seperi, N. (1998). "Lyapunov stability control of inverted pendulums with general base point motion", *Int. J. Non-Linear Mechanics*, Vol. 33, No. 5, p. 801-818.

[89] Xie, F.-G., Zheng, W.-M.and Hao, B.-L. (1995). *Commun. Theor. Phys.* **24**, p. 43.

[90] Zheng, W.-M. (1991); *Int. J. Mod. Phys.* **5B**, p. 481.

Zheng, W.-M. (1994). *Chaos, Solitons and Fractals* **4**, p. 1221.

[91] Zheng, W.-M. and Liu, J.-X. (1994). *Phys. Rev.* **E50**, p. 3241.

[92] Zheng, W.-M. and Liu, J.-X. (1995). *Phys. Rev.* **E51**, p. 3735.

[93] Zubov, V. I. (1964). *Methods of A. M. Lyapunov and Their Application.* P. Noordhoff Ltd., Groningen, Netherlands

Appendix A

SOURCE CODE FOR NUMERICAL EXPERIMENTS

A.1 Note on Numerical Methods

Numerical experiments have been essential part of our research. In order to ensure that our results are not a numerical artifact we used different software for the numerical analysis, such as commercial package *Dynamics 2* [68] or a free software package *DsTool* [15], and utilized different algorithms and numerical integrators. We also developed our own software, using Numerical Recipes library [74, 83]. All numerical results presented in this thesis were obtained and confirmed using at least two different methods. Here we present source code of the software we developed for internal use within our research group.

A.2 Program for Creating Bifurcation Graphs

```
#include <stdio.h>
#include <math.h>
#include "nr.h"
#include "nrutil.h"

#define Pi 3.1415927
#define N 3
#define NKOR 500

#define a 1.1
```

```
#define r 1.2

float dxsav=0.0, *xp, **yp, q, q1=3.2, q2=3.8, korak;
int kmax=0, kount;


void derivs(float x, float y[],float dydx[])
{
    dydx[1] = -y[1]/q-sin(y[2])-r*a/q+(1.0+r)/r*sin(y[2]-y[3]);
    dydx[2] = y[1];
    dydx[3] = a;
}

int main(void)
{
    int i,j,nbad,nok;
    float eps=1.0e-4, h1=0.1, hmin=0.0, x1=0.0, x, *ystart, step;
    FILE *tocke, *fopen();

    ystart=vector(1,N);
    xp=vector(1,50);
    yp=matrix(1,10,1,50);
    tocke = fopen("bifur.dat","w");

    korak = (q2-q1)/NKOR;
    q=q1;

    for (i=1;i<=NKOR;i++) {
```

```
        ystart[1]=3.0;  /* 3 or 0 */
        ystart[2]=3.0;
ystart[3]=0.0;
x=x1;

step = 2.0*Pi/a;

for (j=1;j<=200;j++) {
    odeint(ystart,N,x,x+step,eps,h1,hmin,&nok,&nbad,derivs,rkqs);
    if (ystart[3]>2*Pi) ystart[3] -= 2*Pi;
    if (fabs(ystart[2])>Pi)
      ystart[2]=ystart[2]-2.0*Pi*fabs(ystart[2])/ystart[2];
    if (j>170) fprintf(tocke,"%f %f\n",q,ystart[1]);
    x += step;
}
q += korak;
    }

    free_matrix(yp,1,10,1,50);
    free_vector(xp,1,50);
    free_vector(ystart,1,N);
    fclose(tocke);

    return 0;
}
```

A.3 Program for Calculating Power Spectrum

```
#include <stdio.h>
#include <math.h>
#include "nr.h"
#include "nrutil.h"

#define Pi 3.1415926
#define N 3
#define NSTEP 2048

#define omegaD 1.1
#define r 1.2
#define q 0.94


float dxsav, *xp, **yp;
int kmax, kount;

void derivs(float x, float y[], float dydx[])
{
    dydx[1] = -y[1]/q-sin(y[2])-omegaD*r/q+(1.0+r)/r*sin(y[2]-y[3]);
    dydx[2] = y[1];
    dydx[3] = omegaD;
}

void fafut(float *glava, long NN, float Delta)
{
```

```
long i;
int isign;
float t,*data,*dcmp,*dfft;
FILE *fopen(),*tocke,*tacke,*macke;

data=vector(1,NN*2);
dcmp=vector(1,NN*2);
dfft=vector(1,NN*2);

tacke=fopen("sla04.dat","w");
tocke=fopen("sla05.dat","w");
macke=fopen("sla06.dat","w");

data = glava;

for (i=1;i<NN*2;i+=2) {
    dcmp[i] = dfft[i] = data[i];
    dcmp[i+1] = dfft[i+1] = data[i+1];
}

isign = 1;
four1(data,NN,isign);
four1(dfft,NN,isign);
isign = -1;
four1(data,NN,isign);
fprintf(macke,"%f %f\n",0.0,-10.0);

for (i=1;i<NN;i+=2){
```

```
fprintf(tacke,"%f %f\n",(i-1.0)/2.0*Delta, dcmp[i]);
fprintf(tocke,"%f %f\n",(i-1.0)/2.0*Delta, data[i]/NN);
fprintf(macke,"%f %f\n",Pi*(i-1.0)/(NN*Delta)/omegaD,
log(SQR(dfft[i]/NN)+SQR(dfft[i+1]/NN))/log(10.0));
}

fclose(tacke);
fclose(tocke);
fclose(macke);

free_vector(dcmp,1,NN*2);
free_vector(data,1,NN*2);
free_vector(dfft,1,NN*2);

return;
}

int main(void)
{
    int nbad, nok;
    float eps=1.0e-4, h1=0.1, hmin=0.0;
    long i;
    float *data, *ystart, delta, x, x1=0.0, x2=256.0*Pi/omegaD;

    data = vector(1,NSTEP);
    ystart = vector(1,N);
    xp = vector(1,100);
    yp = matrix(1,10,1,100);
```

```
    ystart[1] = 0.0;
    ystart[2] = 0.0;
    ystart[3] = 4.0*Pi/3.0;

    kmax=10;
    delta = (x2-x1)/NSTEP;
    dxsav = delta/4.0;
    x = x1;

    for(i=1;i<NSTEP*2;i+=2){
odeint(ystart,N,x,x+delta,eps,h1,hmin,&nok,&nbad,derivs,bsstep);
if (i>NSTEP){
    /*printf("%4ld %4ld %12.6f\n",i,i-NSTEP,yp[2][kount]);*/
    data[i-NSTEP] = ystart[1];
    data[i+1-NSTEP] = 0.0;
}
x += delta;
    }

    fafut(data,NSTEP/2,delta);
    return 0;
}
```

A.4 Program for Calculating Lyapunov Spectrum

```
#include <stdio.h>
#include <math.h>
#include "nr.h"
#include "nrutil.h"

#define Pi 3.1415926
#define N 3
#define NN 12
#define NSTEP 40000

#define omegaD 1.2
#define r 0.9
#define q 1.8


float dxsav, *xp, **yp;
int kmax, kount;


void derivs(float x, float y[],float dydx[])
{
  int i;
    dydx[1] = -y[1]/q-sin(y[2])-r*omegaD/q+(1+r)/r*sin(y[3]);
    dydx[2] = y[1];
    dydx[3] = y[1]-omegaD;
    for(i=0;i<=2;i++){
```

```
      dydx[4+i] = -y[4+i]/q-y[7+i]*cos(y[2])+(1+r)/r*y[10+i]*cos(y[3]);
      dydx[7+i] = y[4+i];
      dydx[10+i] = y[4+i];
    }
}

int main(void)
{
    int i,j,k,l,nbad,nok;
    float eps=1.0e-5, h1=0.1, hmin=0.0, x1=0.0, x2;
    float step,*ystart,*GSC,*lambda,*lyap,*Norm;
    FILE *tocke, *fopen();

    tocke=fopen("ly00.dat","w");
    ystart=vector(1,NN);
    xp=vector(1,100);
    yp=matrix(1,20,1,100);

    GSC=vector(1,N-1);
    lambda=vector(1,N);
    lyap=vector(1,N);
    Norm=vector(1,N);

    ystart[1]= 2.5;
    ystart[2]= 0.0;
    ystart[3]= 0.0;

    for(i=N+1; i<=NN; i++) ystart[i] = 0.0;
```

```
    for(i=1; i<=N; i++){
ystart[(N+1)*i] = 1.0;
lambda[i] = 0.0;
    }

    kmax=10;
    step=0.01; //2.0*M_PI/(omegaD*50.0);
    dxsav=(step)/4.0;

    for(i=1;i<=NSTEP;i++){
odeint(ystart,NN,x1,x1+step,eps,h1,hmin,&nok,&nbad,derivs,rkqs);
/*if (ystart[3]>2*M_PI) ystart[3] -= 2*M_PI;*/
if (fabs(ystart[2])>M_PI) {
  ystart[2]=ystart[2]-2.0*M_PI*fabs(ystart[2])/ystart[2];
  fprintf(tocke,"\n");
}

fprintf(tocke,"%f %f\n",ystart[2],ystart[1]);
for (j=1;j<=N;j++) {

    if (j>1) {
for (k=1;k<j;k++){
    GSC[k] = 0.0;
    for (l=1;l<=N;l++)
GSC[k] += ystart[N*l+j]*ystart[N*l+k];
}
for (l=1;l<=N;l++)
```

```
    for (k=1;k<j;k++)
ystart[N*l+j] -= GSC[k]*ystart[N*l+k];
    }

    Norm[j]=0.0;
    for (k=1;k<=N;k++)
Norm[j] += SQR(ystart[N*k+j]);
    Norm[j] = sqrt(Norm[j]);
    for (k=1;k<=N;k++)
ystart[N*k+j] /= Norm[j];

  }

  for (j=1;j<=N;j++)
    lambda[j] += log(Norm[j]);

 for (j=1;j<=N;j++) lyap[j]=lambda[j]/(x1+step);
 if (i%1000 == 0) printf("%12.2f %12.6f %12.6f %12.6f %12.6f %12.6f\n",
    x1,lyap[1],lyap[2],lyap[3],lyap[1]+lyap[2]+lyap[3],1/q);
x1 += step;
    }
    printf("Lyapunov dimension is: %f\n",
   2.0+(lyap[1]+lyap[2])/fabs(lyap[3]));
    free_matrix(yp,1,20,1,100);
    free_vector(xp,1,100);
    free_vector(ystart,1,NN);
    free_vector(GSC,1,N-1);
    free_vector(Norm,1,N);
```

```
    free_vector(lambda,1,N);
    free_vector(lyap,1,N);
    fclose(tocke);

    return 0;
}
```

A.5 Program for Finding Basins of Attraction

```
#include <stdio.h>
#include <math.h>
#include "nr.h"
#include "nrutil.h"

#define N 3
#define NKOR 100
#define NSTEP 1000
#define Pi 3.1415927

#define omegaD 1.1
#define r 1.2
#define q 1.1 /* 1.96 */

float dxsav=0.0, *xp, **yp;
int kmax=0, kount;


void derivs(float x, float y[],float dydx[])
{
    dydx[1] = -y[1]/q-sin(y[2])-omegaD*r/q+(1+r)/r*sin(y[2]-y[3]);
    dydx[2] = y[1];
    dydx[3] = omegaD;
}

float dotplot(float u, float v)
```

```
{
    int i,j,nbad,nok;
    float eps=1.0e-4, h1=0.1, hmin=0.0, x1=0.0, x;
    float *ystart, step, w;

    ystart=vector(1,N);
    xp=vector(1,50);
    yp=matrix(1,10,1,50);


ystart[1]=v;
ystart[2]=u;
ystart[3]=0.0;
w=0;

step = 2.0*Pi/omegaD/10.0;
x=x1;

for(j=1;j<=NSTEP;j++) {
    odeint(ystart,N,x,x+step,eps,h1,hmin,&nok,&nbad,derivs,rkqs);
    if (j > 500)  w += ystart[1];
    x += step;
}
    free_matrix(yp,1,10,1,50);
    free_vector(xp,1,50);
    free_vector(ystart,1,N);

    return w/(NSTEP-500.0);
```

```
}

void main(void)
{
  float u,v, v1=-3.0, v2=3.0, stepu, u1=-Pi, u2=Pi, stepv;
  int i,j;
  FILE *tocke, *fopen();

  tocke = fopen("basin.dat","w");

  stepu=(u2-u1)/NKOR;
  stepv=(v2-v1)/NKOR;

  u=u1;
  v=v1;

  for(i=0;i<=NKOR;i++){
    for(j=0;j<=NKOR;j++){
      /*printf("%f\n",dotplot(u,v));*/
      if (dotplot(u,v) > -0.05)  /* 0.545 */
         fprintf(tocke,"%f %f\n",u,v);
      u += stepu;
    }
    v += stepv;
    u = u1;
  }
  fclose(tocke);
}
```

A.6 Program for Finding Phase Locked Modes

```
#include <stdio.h>
#include <math.h>
#include "nr.h"
#include "nrutil.h"

#define N 3
#define NKOR 200
#define NSTEP 100
#define Pi 3.1415927

#define omegaD 1.1
#define r 1.2


float dxsav, *xp, **yp, q, q1=0.8, q2=1.5, korak;
int kmax, kount;


void derivs(float x, float y[],float dydx[])
{
    dydx[1] = -y[1]/q-sin(y[2])-omegaD*r/q+(1+r)/r*sin(y[2]-y[3]);
    dydx[2] = y[1];
    dydx[3] = omegaD;
}

float phaselock(void)
```

```
{
    int i,j,nbad,nok;
    float eps=1.0e-4, h1=0.1, hmin=0.0, x1=0.0, x2=360.0*Pi/omegaD;
    float *ystart, step, w;

    ystart=vector(1,N);
    xp=vector(1,50);
    yp=matrix(1,10,1,50);


ystart[1]=3.0;
ystart[2]=0.0;
ystart[3]=0.0;
w=0;

kmax=10;

step = (x2-x1)/NSTEP;
dxsav=step/4.0;

for(j=1;j<=NSTEP;j++) {
    odeint(ystart,N,x1,x1+step,eps,h1,hmin,&nok,&nbad,derivs,rkqs);
    if (j > 50)  w += ystart[1];
    x1 += step;
}

    free_matrix(yp,1,10,1,50);
    free_vector(xp,1,50);
```

```
    free_vector(ystart,1,N);

    return w/(NSTEP-50.0);
}

void main(void)
{
  int i,j;
  FILE *tocke, *fopen();

  tocke = fopen("lock.dat","w");

  korak=(q2-q1)/NKOR;
  q=q1;

  for(i=1;i<=NKOR;i++){
    fprintf(tocke,"%f %f\n",q, phaselock());
    q += korak;
  }
  fclose(tocke);
}
```

A.7 Program for Calculating Capacity Dimension

```
#include <stdio.h>
#include <math.h>
#include "nr.h"
#include "nrutil.h"

#define Pi 3.1415927

double capacity(char ime[], float maxvalue, float minvalue, float epsilon)
{
  int i,j,k,l,n=0,**grid;
  long nbox,npoints=0;
  float x, y;
  double S=0.0,p;
  FILE *fopen(),*tocke;

  nbox = 1+(int)((maxvalue-minvalue)/epsilon);
  printf("nbox=%ld\n",nbox);

  grid=imatrix(1,nbox,1,nbox);
  tocke=fopen(ime,"r");

  for(i=1;i<=nbox;i++)
    for(j=1;j<=nbox;j++)
      grid[i][j]=0;

  while(fscanf(tocke,"%f %f",&x,&y) != EOF){
```

```
    npoints++;
    k = 1+(int)((x-minvalue)/epsilon);
    l = 1+(int)((y-minvalue)/epsilon);
    grid[k][l]++;
  }
  printf("Broj tocaka u fajlu je %d\n",npoints);
  for(i=1;i<=nbox;i++)
    for(j=1;j<=nbox;j++)
      if (grid[i][j] != 0) n++;
  free_imatrix(grid,1,nbox,1,nbox);
  return log((double) n)/log(2.0);
}

void main(void)
{
  int i;
  double eps,t,t1=-7.0,t2=-2.0,step;
  char ime[11]="pcr330.dat";
  FILE *fopen(),*macke;

  macke=fopen("capa03.dat","w");
  step=fabs(t2-t1)/60.0;
  t=t1;

  for(i=1;i<=60;i++){
    eps=exp(t*log(2.0));
    fprintf(macke,"%f %f\n",-log(eps)/log(2.0),capacity(ime,Pi,-Pi,eps));
    printf("eps=%lf\n",eps);
```

```
    t += step;
  }
  fclose(macke);
}
```

A.8 Program for Calculating Information Dimension

```
#include <stdio.h>
#include <math.h>
#include "nr.h"
#include "nrutil.h"

#define Pi 3.1415927

double information(char ime[], float maxvalue, float minvalue,float epsilon)
{
  int i,j,k,l,n=0,**grid,npoints=0;
  long nbox;
  float x, y;
  double S=0.0,p;
  FILE *fopen(),*tocke;

  nbox = 1+(int)((maxvalue-minvalue)/epsilon);
  printf("nbox=%ld\n",nbox);

  grid=imatrix(1,nbox,1,nbox);
  tocke=fopen(ime,"r");

  for(i=1;i<=nbox;i++)
    for(j=1;j<=nbox;j++)
      grid[i][j]=0;

  while(fscanf(tocke,"%f %f",&x,&y) != EOF){
```

```
    npoints++;
    k = 1+(int)((x-minvalue)/epsilon);
    l = 1+(int)((y-minvalue)/epsilon);
    grid[k][l]++;
  }
  printf("Broj tocaka u fajlu je %d\n",npoints);
  for(i=1;i<=nbox;i++)
    for(j=1;j<=nbox;j++)
      if (grid[i][j] != 0){
p = grid[i][j]/((double) npoints);
S -= p*log(p)/log(2.0);
      }
  free_imatrix(grid,1,nbox,1,nbox);
  return S;
}

void main(void)
{
  int i;
  double eps,d,t,t1=-7.0,t2=-2.0,step;
  char ime[11]="pcr330.dat";
  FILE *fopen(),*macke;

  macke=fopen("info03.dat","w");
  step=(t2-t1)/60.0;
  t=t1;

  for(i=1;i<=60;i++){
```

```
    eps=exp(t*log(2.0));
    fprintf(macke,"%f %f\n",-log(eps)/log(2.0),information(ime,Pi,-Pi,eps));
    t += step;
  }
  fclose(macke);
}
```

A.9 Program for Calculating Correlation Dimension

```
#include <stdio.h>
#include <math.h>
#include "nr.h"
#include "nrutil.h"

#define N 20000

float *x,*y;

double correlation(double epsilon, long int NPoints)
{
  long int n=0;
  int i,j;
  float u,v;

  for(i=1;i<=NPoints;i++){
    j=0;
    while(++j < i)
      if (sqrt(SQR(x[i]-x[j])+SQR(y[i]-y[j])) <= epsilon) n++;
  }
  printf("n=%d\n",n);
  return -log((double) n/(((NPoints-1.0)*NPoints)/2.0))/log(2.0);
}

int main(void)
{
```

```
int i;
long int NPoints;
float u,v;
double eps,t,t1=-7.0,t2=-2.0,step;
FILE *fopen(),*macke, *tocke;

tocke=fopen("pcr330.dat","r");
macke=fopen("corr.dat","w");
x=vector(1,N);
y=vector(1,N);

while(fscanf(tocke,"%f %f",&u,&v) != EOF){
  NPoints++;
  x[NPoints]=u;
  y[NPoints]=v;
}
printf("Broj tacaka u fajlu je: %d\n",NPoints);


step=fabs(t2-t1)/30.0;
t=t1;

for(i=1;i<=30;i++){
  eps=exp(t*log(2.0));
  printf("eps=%lf\n",eps);
  fprintf(macke,"%f %f\n",-log(eps)/log(2.0),correlation(eps,NPoints));
  t += step;
}
```

```
  free_vector(x,1,N);
  free_vector(y,1,N);
  fclose(macke);
  fclose(tocke);
  return 0;
}
```